Theses and Dissertations | 1. Thesis and Dissertation Collection, all items

1985-03

Use of the Wavenumber Technique with the Lloyds Mirror for an Acoustic Doublet.

King, Portia Baird

Monterey, California. Naval Postgraduate School

http://hdl.handle.net/10945/21610

NAVAL POSTGRADUATE SCHOOL
Monterey, California

THESIS

USE OF THE WAVENUMBER TECHNIQUE
WITH THE LLOYDS MIRROR
FOR AN ACOUSTIC DOUBLET

by

Portia Baird King

March 1985

Thesis Advisors: A. B. Coppens
                                    C. R. Dunlap

T222199

SECURITY CLASSIFICATION OF THIS PAGE (When Data Entered)

REPORT DOCUMENTATION PAGE		READ INSTRUCTIONS BEFORE COMPLETING FORM
1. REPORT NUMBER	2. GOVT ACCESSION NO.	3. RECIPIENT'S CATALOG NUMBER

4. TITLE (and Subtitle)	5. TYPE OF REPORT & PERIOD COVERED
Use of the Wavenumber Technique With the Lloyds Mirror For an Acoustic Doublet	Master's Thesis March 1985
	6. PERFORMING ORG. REPORT NUMBER

7. AUTHOR(s)	8. CONTRACT OR GRANT NUMBER(s)
Portia Baird King	

9. PERFORMING ORGANIZATION NAME AND ADDRESS	10. PROGRAM ELEMENT, PROJECT, TASK AREA & WORK UNIT NUMBERS
Naval Postgraduate School Monterey, California 93943	

11. CONTROLLING OFFICE NAME AND ADDRESS	12. REPORT DATE
Naval Postgraduate School Monterey, California 93943	March 1985
	13. NUMBER OF PAGES
	112

14. MONITORING AGENCY NAME & ADDRESS(If different from Controlling Office)	15. SECURITY CLASS. (of this report)
	15a. DECLASSIFICATION/DOWNGRADING SCHEDULE

16. DISTRIBUTION STATEMENT (of this Report)

Approved for Public Release; Distribution is Unlimited.

17. DISTRIBUTION STATEMENT (of the abstract entered in Block 20, if different from Report)

18. SUPPLEMENTARY NOTES

19. KEY WORDS (Continue on reverse side if necessary and identify by block number)

Lloyds Mirror, Underwater Acoustics, Fast Fourier Transform, Wavenumber Technique, Pressure Spectrum, Source Depth Determination, Acoustic Propagation, ASW, Isospeed Environment

20. ABSTRACT (Continue on reverse side if necessary and identify by block number)

This thesis examines a method to determine the depth of a point source in an isospeed ocean environment. Using the Fourier Transform on the acoustic pressure field in the range domain results in the attainment of the acoustic pressure spectrum in the wavenumber domain and a characteristic nodal spacing unique to the source-receiver depths. Quantitative examination of a magnitude plot of the spectrum and use of simple mathematical formulae yield the source depth. The debilitative effects of narrowband

DD FORM 1473 EDITION OF 1 NOV 65 IS OBSOLETE
1 JAN 73
S/N 0102-LF-014-6601

SECURITY CLASSIFICATION OF THIS PAGE (When Data Entered)

noise and surface roughness on the pressure spectrum are also examined. The pressure spectrum is recognizable in noise after the pressure field in the range domain has been lost in the noise field. The effect of surface gravity waves on the pressure spectrum is similar to that on the pressure field in the range domain: the characteristic nodal spacing is suppressed as the height of the surface waves increases.

Use of the Wavenumber Technique
With the Lloyds Mirror
For an Acoustic Doublet

by

Portia B. King
Lieutenant Commander, United States Navy
B.S., Louisiana State University in New Orleans, 1971

Submitted in partial fulfillment of the
requirements for the degree of

MASTER OF SCIENCE IN SYSTEMS TECHNOLOGY
(Antisubmarine Warfare)

from the

NAVAL POSTGRADUATE SCHOOL
March 1985

ABSTRACT

This thesis examines a method to determine the depth of
a point source in an isospeed ocean environment. Using the
Fourier Transform on the acoustic pressure field in the
range domain results in the attainment of the acoustic pres-
sure spectrum in the wavenumber domain and a characteristic
nodal spacing unique to the source-receiver depths.
Quantitative examination of a magnitude plot of the spectrum
and use of simple mathematical formulae yield the source
depth. The debilitative effects of narrowband noise and
surface roughness on the pressure spectrum are also exam-
ined. The pressure spectrum is recognizable in noise after
the pressure field in the range domain has been lost in the
noise field. The effect of surface gravity waves on the
pressure spectrum is similar to that on the pressure field
in the range domain: the characteristic nodal spacing is
suppressed as the height of the surface waves increases.

TABLE OF CONTENTS

LIST OF TABLES

6

LIST OF FIGURES

LIST OF SYMBOLS

A	Amplitude
c	Sound Speed
e	2.718281828...
FFT	Fast Fourier Transform
FFT^{-1}	Inverse Fast Fourier Transform
f	Frequency
$\underset{\sim}{f}(r)$	Generic Function of Range
$\underset{\sim}{g}(\gamma)$	Spectral Density of $\underset{\sim}{f}(r)$
H_0	Hankel Function
i	Square Root of -1
J_0	Bessel Function of the First Kind
k	Wavenumber
M	Surface Roughness Factor
m	Index of Calculations or Null Number in the Range Domain
N	Number of Points in the Wavenumber Spectrum

n	Index of Calculations or Null Number in the Wavenumber Spectrum
$\underset{\sim}{n}$	Complex Narrowband Noise Field
$\underset{\sim}{P}$	Time Independent Factor of Complex Pressure
$\underset{\sim}{P}_s$	Complex Pressure of the Source
$\underset{\sim}{P}_i$	Complex Pressure of the Reflection
$\underset{\sim}{P}_N$	Complex Pressure in the Presence of Noise
$\underset{\sim}{P}(k)$	Pressure Field in the Wavenumber Spectrum
$\underset{\sim}{p}$	Time Dependent Factor of Complex Pressure
R_1	Distance of the Direct Wave Path
R_2	Distance to the Image (Reflected Path)
RCVR	Receiver
r	Range Between Source and Receiver
SRC	Source
t	time factor
W	Hanning Window
Y_0	Bessel Function of the Second Kind
Z_s	Source Depth

11

Symbol	Definition
z_r	Receiver Depth
Δr	Range Increment
β	Vertical Component of the Wavenumber
$\Delta \beta$	Vertical Wavenumber Increment
γ	Horizontal Component of the Wavenumber
$\Delta \gamma$	Horizontal Wavenumber Increment
θ	Angle of Grazing Incidence at the Surface
λ	Wavelength
π	3.14159265...
φ	Phase Angle
ψ_R	Surface Reflection Coefficient
ω	Angular Frequency
$\sqrt{}$	Square Root Operator
$\int$	Integration Operator

ACKNOWLEDGEMENTS

I. HISTORY AND INTRODUCTION

This thesis is the third in a series of investigations into a proposal put forth by R. Lauer of Naval Underwater Systems Center, New London, CT, in 1979. In his memorandum [Ref. 1], Lauer describes a "new" way to analyze sound propagation in the ocean and two applications of the method, which he named the "Wavenumber Technique," or W.T. In his proposal, Lauer stated that a source of sound in the ocean could be pinpointed in both depth and range by a single omnidirectional hydrophone provided the source is generating a continuous wave tone.

The W.T. was initially described by F. DiNapoli [Ref. 2] as an intermediary step in his development of a speedier computer algorithm used in analyzing sound propagation as a function of range. DiNapoli and Lauer proposed converting the pressure as a function of range $\underset{\sim}{P}(r)$ to the pressure spectrum as a function of the wavenumber $\underset{\sim}{P}(k)$. The conversion is accomplished by taking a weighted Fourier transform of the pressure field $\underset{\sim}{P}(r)$. Once the pressure spectrum is obtained, analysis of the pressure field can be accomplished in a manner analogous to that presently used in signal processing.

Lauer proposed two uses for his "Wavenumber Technique:"
1. determination of the depth of the acoustic source, an ability which has obvious tactical applications;
2. use of the W.T. to evaluate the accuracy of existing, and future, acoustic models such as P.E. and F.A.C.T., by breaking the generated pressure field down into ray path "families," such as bottom-bounce, refracted-surface-reflected, and surface-ducted families, thus giving a quantitative read-out of what

proportion of the total acoustic energy is being channelled through the various ray paths. For both uses, a knowledge of the acoustic environment is necessary.

It is the intended purpose of this thesis to investigate the validity of the first application of Lauer's wavenumber technique by using it in conjunction with an acoustic phenomenon that is well-known and for which accurate results can be calculated with precision; this phenomenon is the LLoyds Mirror for an Acoustic Doublet. Using several source/receiver combinations, this investigator intends to compare actual source depth with that predicted by the W.T. If Lauer's technique is cogent, the source depths calculated via the two methods should be equal, or very close within a statistically acceptable degree.

As mentioned in the beginning of this thesis, two prior investigators, B. Stamey and J. Blanchard, looked into applying the W.T. to determining source depth. Stamey's investigation [Ref. 3] utilized a parabolic equation computer model developed by H.K. Brock, the Split Step Fast Fourier Transform, or SSFFT, to generate the pressure fields. He qualitatively compared the model to a Normal Mode model and a P. E. Finite Difference model, both range dependent, and to DiNapoli's Fast Field Program model, a range independent model. Stamey concluded that the W.T. showed promise as an analysis tool and that further investigations were warranted.

J. Blanchard carried Stamey's researches one step further [Ref. 4]. Using two Parabolic Equation computer algorithms, Brock's Split Step Fast Fourier Transform and Jaeger's Implicit Finite Difference, as his pressure field generators, he examined the use of the spacing between nulls of the pressure spectrum to determine source depth. His results are interesting and support the need for further investigation.

15

The author was not satisfied with Stamey's and Blanchard's findings. Both individuals acknowledged shortcomings in their respective studies, especially with regard to the mutual presence of the "U-shaped phenomenon" encountered in the pressure spectrum. One should remember, however, that their theses were preliminary studies only and were produced within a highly restricted time frame. Also, they used existing computer algorithms specifically designed to approximate acoustic propagation in a velocity-variant medium. However, the environmental settings used by both gentlemen were that of the Lloyds Mirror for an Acoustic Doublet which requires a constant sound speed throughout the water column; thus, the approximations, assumptions and "fudge factors" used by these models make their results for an isospeed medium highly artificial and somewhat suspect. Fortunately, however, there exists for the Lloyds Mirror a simple, geometric solution specifically designed for an isospeed environment [Ref. 5]. Since the pressure fields for varying source and receiver depths and, therefore, the corresponding pressure spectra, can be precisely calculated, it was thought this model would be a good check on the operational applicability of Lauer's proposed technique.

Secondary considerations of this study were to examine what effect, if any, the introductions of, firstly, surface waves and, secondly, noise would have on the pressure spectrum. The first objective was simulated by use of mathematical formulae given in reference 5; for the second objective, it was thought that complex noise, random in both amplitude and phase and similar to a Rician distribution [Ref. 6: p. 189], would provide a simple but reasonable approximation of an ocean noise field. This investigator intends to gradually intensify the surface waves and the noise field, separately, until the original pressure spectrum is no longer recognizable. In this manner, it should

be possible to make a qualitative assessment of their respective debilitating effects under the carefully controlled conditions found in the Lloyds Mirror phenomenon.

Section II sets forth in more detail the theoretical development of each point described in this introduction. Section III summarizes the investigator's results and the conclusions drawn from those results. Section IV contains a listing of the computer algorithms utilized.

II. THEORY

This chapter presents the mathematical basis of the wavenumber technique.

A. THE LLOYDS MIRROR PHENOMENON

A diverging monofrequency spherical pressure wave [Ref. 5: p. 112] can be written in complex form as

$$p(R,t) = P(R)e^{-i\omega t} = \frac{A}{R}e^{i(kR-\omega t)} \qquad \text{(eqn 2.1)}$$

where $P(R)$ is the spatial factor. Referring to Figure 2.1, R_1 is the range from the source to the receiver and R_2 is the range from the image to the receiver. For convenience in all that follows, we shall set A to unit magnitude. The following equations apply to the acoustic waves propagating directly out from the source P_s and from the apparent image P_i (which is actually the wave reflected from the surface):

$$P_s(R,t) = P_s(R)e^{-i\omega t} = \frac{1}{R_1}e^{i(kR_1-\omega t)}$$

$$P_i(R,t) = P_i(R)e^{-i\omega t} = \frac{-1}{R_2}e^{i(kR_2-\omega t)} \qquad \text{(eqn 2.2)}$$

where P, P_s, and P_i are complex functions of horizontal range r, vertical depth Z and time t; the minus sign in the equation for P_i is derived from the surface reflection coefficient, $\psi_R = -1$, for a smooth surface. Inspection of Figure 2.1 reveals that

$$R_1 = \sqrt{(z_r - z_s)^2 + r^2} \quad , \quad R_2 = \sqrt{(z_r + z_s)^2 + r^2} \quad ,$$

18

and $\Delta r = \left| R - R_{1,2} \right|$

And so the total field can be written as

$$\underset{\sim}{P_s} - \underset{\sim}{P_i} = \underset{\sim}{P(R)} e^{-i\omega t} = \frac{e^{i(kR_1 - \omega t)}}{R_1} - \frac{e^{i(kR_2 - \omega t)}}{R_2} \qquad \text{(eqn 2.3)}$$

Since $\underset{\sim}{P_s}$ and $\underset{\sim}{P_i}$ both have the same time factor, $\exp(-i\omega t)$, we can retain just the spatial factors and equations 2.3 reduce to

$$\underset{\sim}{P(R)} = \left[\frac{e^{ikR_1}}{R_1} - \frac{e^{ikR_2}}{R_2} \right] \qquad \text{(eqn 2.4)}$$

Equation 2.4 is a form of the complex pressure as a function of range used in the computer algorithm shown in Appendix I.

Inspection of Figure 2.1 reveals that, for $R \gg Z_s$ and θ very small,

$$r \approx R$$

or

$$\sin \theta \approx \frac{Z_r}{R}$$

or

$$\Delta r \approx \frac{Z_r Z_s}{R} \qquad \text{(eqn 2.5)}$$

and the pressure amplitude can be approximated by

$$\underset{\sim}{P(R)} \approx \frac{2}{R} \left| \sin\left(\frac{k Z_r Z_s}{R} \right) \right| \qquad \text{(eqn 2.6)}$$

Looking at just the formula for the pressure amplitude, we can see that as

$$\left(\frac{k\,z_r z_s}{R}\right) \longrightarrow n\pi \, , \quad n = 0,1,2,3,\ldots \qquad \text{(eqn 2.7)}$$

the pressure amplitude goes to zero, producing the classic $|P(R)|$ vs R curve shown in Figure 2.2

B. THE RELATIONSHIP BETWEEN K, γ, AND β

In his description of the Wavenumber Technique [Ref. 1: p. 5-6], Lauer utilizes the horizontal and vertical components of the wavenumber, k. The general relationship amoung these three terms is illustrated in Figure 2.3 and can be written mathematically as

   k = the wavenumber = $2\pi f/c$

   γ = the horizontal component of k = k $\cos\varphi$

   β = the vertical component of k = k $\sin\varphi$

or

$$k = \sqrt{\gamma^2 + \beta^2} \qquad \text{(eqn 2.8)}$$

C. THE WAVENUMBER TECHNIQUE AND THE LLOYDS MIRROR

Given a point source in free space, the monofrequency pressure field at the receiver, $\underset{\sim}{P}(R)$, can be expressed as a spherical wave (time factor suppressed),

20

$$\mathcal{P}(R) = \frac{e^{ikR}}{R}. \qquad \text{(eqn 2.9)}$$

where, from Figure 2.1,

$$R^2 = r^2 + Z_r^2 \;,\; \text{for } Z_r > Z_s$$

or

$$R^2 = r^2 + Z_s^2 \;,\; \text{for } Z_r < Z_s \qquad \text{(eqn 2.10)}$$

In integral form, $\mathcal{P}(R)$ can be written as [Ref. 7: p. 127]

$$\mathcal{P}(R) = \frac{e^{ikR}}{R} = \int_0^\infty \frac{J_0(\gamma r)\, e^{\pm i\beta|Z_r - Z_s|}}{i\beta} \, \gamma \, d\gamma \qquad \text{(eqn 2.11)}$$

which is taken from the Fourier-Bessel Transform Pair [Ref. 7: p. 126],

$$\underline{f}(r) = \int_0^\infty \underline{g}(\gamma)\, J_0(\gamma r)\, \gamma \, d\gamma$$

$$\underline{g}(\gamma) = \int_0^\infty \underline{f}(r)\, J_0(\gamma r)\, r \, dr \qquad \text{(eqn 2.12)}$$

where $\underline{f}(r)$ represents the acoustic pressure function in the range domain, and $\underline{g}(\gamma)$ is the acoustic pressure spectrum in the wavenumber domain. The sign of the exponential function in the integral is based on which of Z_s and Z_r is greater. For the case of receiver depth being greater than source depth so that waves from both image and source are travelling downward at the receiver depth, the total pressure at the receiver can be expressed as

$$\mathcal{P}(R) = \int_0^\infty \frac{e^{i\beta(z_r - z_s)} - e^{i\beta(z_r + z_s)}}{i\beta} \, J_0(\gamma r)\, \gamma \, d\gamma \qquad \text{(eqn 2.13)}$$

Use of Euler's Identity reduces Equation 2.13 to

21

$$\mathcal{P}(R) = -2 \int_0^\infty \frac{e^{i\beta z_r} \sin(\beta z_s)}{\beta} J_o(\gamma r) \gamma \, d\gamma \qquad \text{(eqn 2.14)}$$

Using the relationship between the Hankel functions [Ref. 5: p. 449],

$$H_o^{(1)}(\gamma r) = J_o(\gamma r) + i Y_o(\gamma r)$$

and

$$H_o^{(2)}(\gamma r) = J_o(\gamma r) - Y_o(\gamma r)$$

$$\text{(eqn 2.15)}$$

one can re-write the Bessel function in equation 2.14 as

$$J_o(\gamma r) = \frac{1}{2} \left[H_o^{(1)}(\gamma r) + H_o^{(2)}(\gamma r) \right] \qquad \text{(eqn 2.16)}$$

so that

$$2 g(\gamma) = \int_0^\infty f(r) H_o^{(1)}(\gamma r) r \, dr \; + \; \int_0^\infty f(r) H_o^{(2)}(\gamma r) r \, dr \qquad \text{(eqn 2.17)}$$

Letting r' = -r and looking at the second term on the right hand side of equation 2.17,

$$\int_0^{-\infty} f(-r') H_o^{(2)}(-\gamma r') r' \, dr' = \int_{-\infty}^0 f(-r) H_o^{(1)}(\gamma r) r \, dr \qquad \text{(eqn 2.18)}$$

Now, assuming that $\underset{\sim}{f}(r) = \underset{\sim}{f}(-r)$, then

$$2 g(\gamma) = \int_{-\infty}^\infty f(r) H_o^{(1)}(\gamma r) r \, dr \qquad \text{(eqn 2.19)}$$

Therefore,

22

$$P(R) = -\int_{-\infty}^{\infty} \frac{\gamma H_{o}^{(1)}(\gamma r)}{\beta} \, e^{i\beta z_r} \sin(\beta z_s) \, d\gamma \qquad \text{(eqn 2.20)}$$

For $\gamma r > 2\pi$, the asymptotic approximation of the Hankel function for large argument can be used:

$$H_{o}^{(1)}(\gamma r) \approx \sqrt{\frac{2}{\pi \gamma r}} \, e^{i(\gamma r - \frac{\pi}{4})} \qquad \text{(eqn 2.21)}$$

assuming $|r \underset{\sim}{f}(r)|$ goes to zero faster than (ln r),

$$P(R) \approx -\sqrt{\frac{2}{\pi r}} \, e^{-i\frac{\pi}{4}} \int_{-\infty}^{\infty} \left[\frac{\sqrt{\gamma}}{\beta} \, e^{i\beta z_r} \sin(\beta z_s) \right] e^{i\gamma r} d\gamma \quad \text{(eqn 2.22)}$$

Let the terms inside the brackets in equation 2.22 be defined as $g(\gamma)$, then

$$P(R) = -\sqrt{\frac{2}{\pi r}} \, e^{-i\frac{\pi}{4}} \int_{-\infty}^{\infty} g(\gamma) \, e^{i\gamma r} d\gamma$$

and

$$\int_{-\infty}^{\infty} g(\gamma) e^{i\gamma r} d\gamma = -\sqrt{\frac{\pi r}{2}} \sqrt{r} \, P(R) \qquad \text{(eqn 2.23)}$$

or, using equation 2.12,

$$g(\gamma) = -\left[e^{i\frac{\pi}{4}} \right] \sqrt{\frac{\pi}{2}} \frac{1}{2\pi} \int_{-\infty}^{\infty} \sqrt{r} \, P(R) e^{-i\gamma r} dr \qquad \text{(eqn 2.24)}$$

Note that equation 2.24 has the form of the Fourier transform of the pressure function if we define

$$\underset{\sim}{f}(r) \equiv \sqrt{r} \, P(R) \qquad \text{(eqn 2.25)}$$

so that $\sqrt{r}\ \underline{p}(R)$ and $\underline{g}(\gamma)$ are Fourier Transform pairs. This equation can be easily evaluated [Ref. 8],

$$\underline{g}(\gamma) = -\left[e^{i\frac{\pi}{4}}\right]\frac{1}{\sqrt{2\pi}}\left[\frac{\sqrt{\gamma}}{\beta}\ e^{i\beta z_r}\ sin(\beta z_s)\right]$$

(eqn 2.26)

for $z_r > z_s$. And the magnitude of $\underline{g}(\gamma)$ is

$$\left|g(\gamma)\right| = \frac{\sqrt{\gamma}}{\beta}\ sin(\beta z_s)$$

(eqn 2.27)

For the case where $z_s > z_r$; it can be shown that

$$g(\gamma) = -\frac{e^{i\frac{\pi}{4}}}{\sqrt{2\pi}}\left[\frac{\sqrt{\gamma}}{\beta}\ e^{i\beta z_s}\ sin\left(\beta z_r\right)\right]$$

(eqn 2.28)

and the magnitude of $\underline{g}(\gamma)$ is

$$\left|g(\gamma)\right| = \frac{\sqrt{\gamma}}{\beta}\ sin(\beta z_r)$$

(eqn 2.29)

A close look at the magnitude of the pressure spectrum function in equation 2.27 reveals that nodes occur for values of

$$\beta z_s = n\pi \quad , \quad n = 0,1,2,3,\ldots$$

(eqn 2.30)

24

If the magnitude of the pressure spectrum is plotted as a function of the vertical wavenumber then the spacing between nodes $\Delta\beta$ is uniform and the depth of the source can be derived from the relationship given by

$$Z_s = \frac{\pi}{\Delta\beta} \qquad\qquad \text{(eqn 2.31)}$$

In the event the source is deeper than the receiver, looking at equation 2.29, we can see that nodes now occur for values of

$$\beta Z_r = n\pi \quad , \quad n = 0,1,2,3,\ldots \qquad \text{(eqn 2.32)}$$

Plotting equation 2.29 as a function of the vertical wavenumber, the spacing between nodes will now reveal the receiver depth based on

$$Z_r = \frac{\pi}{\Delta\beta} \qquad\qquad \text{(eqn 2.33)}$$

Notice in equations 2.31 and 2.33 the exchange of source and receiver depths. By placing the receiver at a shallower depth than the source, no new information (namely the source depth) is to be found.

In summary, there is a way to calculate the complex pressure amplitude as a function of range using the complex pressure spectrum. Conversely, if the complex pressure $\underset{\sim}{P}(r)$ has been measured at the receiver, then the complex pressure spectrum $\underset{\sim}{P}(k)$ can be derived by making use of the relationship between the Fourier-Bessel Transform Pairs (see equation 2.12), and the depth of the source can be found from the magnitude of that spectrum (see equation 2.31).

25

The foregoing is the mathematics involved in deriving the theoretical pressure spectrum. One purpose of this thesis was to compare the theoretical value of the pressure spectrum as derived with the Fourier-Bessel Transform with the pressure spectrum obtained by use of the computerized Discrete Fourier Transform (DFT), otherwise known as the Fast Fourier Transform, or FFT. At this point, it will be helpful to review what happens in the FFT.

Starting with the Fourier-Bessel transform pair shown in equation 2.12, $\underset{\sim}{f}(r)$ and $\underset{\sim}{g}(\gamma)$ can be re-written in terms of a discrete sum as is done in the DFT:

$$FFT^{-1}\left\{\underset{\sim}{g}(\gamma)\right\} = \sum_{n=0}^{N-1} g(n\Delta\gamma) e^{i\frac{2\pi mn}{N}} = f(m\Delta r) \qquad \text{(eqn 2.34)}$$

where $N = 1,2,3,\ldots$, up to some large positive integer, and represents the number of transform points, and

$$\gamma r = (n\Delta\gamma)(m\Delta r) = \frac{2\pi mn}{N} \qquad \text{(eqn 2.35)}$$

based on the relationship between Δr and $\Delta \gamma$ as described in sampling theory [Ref. 2: p. 2],

$$\Delta\gamma\Delta r = \frac{2\pi}{N}$$

or

$$\Delta r = \frac{2\pi}{N\Delta r} \qquad \text{(eqn 2.36)}$$

By convention, the sign of the exponential function in equation 2.34 is taken as negative when performing the "forward" transform,

$$FFT\left\{\underset{\sim}{f}(m\Delta r)\right\} = g(n\Delta\gamma) \qquad \text{(eqn 2.37)}$$

and is taken as positive when performing the "inverse" transform,

$$FFT^{-1}\left\{ g(n\Delta\gamma)\right\} = f(m\Delta r)$$

(eqn 2.38)

Then,

$$\int_{-\infty}^{\infty} g(\gamma)\, e^{i\gamma r} d\gamma \approx \left[\sum_{n=1}^{N-1} g(n\Delta\gamma)\, e^{i\frac{2\pi mn}{N}}\right]\Delta\gamma$$

where

$$g(n\Delta\gamma) = \frac{\sqrt{\gamma}}{\beta}\, e^{i\beta z_r} \sin(\beta z_s)$$

Therefore

and

$$P(m\Delta r) = -\sqrt{\frac{2}{\pi r}}\, e^{-i\frac{\pi}{4}}\left[\Delta\gamma\, FFT^{-1}\left\{ g(n\Delta\gamma)\right\}\right]$$

$$\left| g(n\Delta\gamma)\right| = \frac{\sqrt{\gamma}}{\beta}\, \sin(\beta z_s)$$

(eqn 2.39)

D. THE EFFECTS OF SURFACE ROUGHNESS

Surface roughness [Ref. 5: p.409] reduces the Lloyds Mirror effect. The rougher the surface, the greater the effect for angles increasingly closer to grazing incidence. If M represents the surface roughness factor, then equation 2.3 can be re-written as

$$P(R) = \frac{e^{ikR}}{R} - e^{-M^2}\,\frac{e^{ikR}}{R}$$

where

$$M \equiv \frac{4H\,\sin\phi}{\lambda}$$

(eqn 2.40)

27

ϕ is the grazing angle of incidence, H is the average height of the surface gravity waves, and λ is the wavelength of the narrowband continuous wave acoustic signal. When M is less than 1, the surface is said to be smooth; when M is greater than 1, the surface is said to be rough.

Looking at Figure 2.1, we can see that the overall effect of increasing surface roughness is to reduce the contribution of the surface reflection or "image" to the interference pattern at the receiver. In other words, as H increases, the energy detected by the receiver is increasingly only the energy coming directly from the source. When the effect of surface roughness is a maximum such that the contribution to the pressure field of the "image" is completely suppressed, then

$$g_s(\gamma) = \int_0^\infty \frac{e^{ikR_1}}{R_1} J_0(\gamma r) r \, dr$$

$$= \frac{e^{i\beta|z_s - z_r|}}{i\beta} \qquad \text{(eqn 2.41)}$$

and the magnitude of the spectrum is

$$|g(\gamma)| = \frac{1}{\beta} \qquad \text{(eqn 2.42)}$$

E. THE EFFECT OF ADDING NOISE

In an effort to simulate a realistic ocean environment, a normally distributed narrowband noise field based on a Rician distribution [Ref. 6: p. 189] was adapted. The resulting acoustic pressure field can be expressed as

28

$$\mathcal{P}_N(R) = \mathcal{P}(R) + \underset{\sim}{n} \qquad\qquad \text{(eqn 2.43)}$$

where $\underset{\sim}{n}$ is a normally-distributed random function with a mean of zero, a standard deviation of one and possesses both amplitude and phase. The noise operates independently on both the amplitude and phase components of the pressure field. Since $\underset{\sim}{n}$ is independent of range and wavenumber, it is treated as a constant by the Fourier Transform.

A fourth intention of this thesis was to discover the degree to which noise degrades the wavenumber spectrum compared with the corresponding degradation of the range domain. To produce the random noise fields used in this research, the routine listed as "GGNML" in the IMSL library [Ref. 9] was called upon twice to generate independent, pseudo-random functions which interact separately and simultaneously with both the amplitude and phase components of $\underset{\sim}{P}(R)$. While not an elaborate scheme, owing to time and resource constraints, it was felt that this modest simulacrum of narrowband noise would give a fairly accurate, first cut "feel" for the effects of noise on the wavenumber spectrum. The reader should be aware, however, that no direct consideration of coherency along the range path was taken into account by this method.
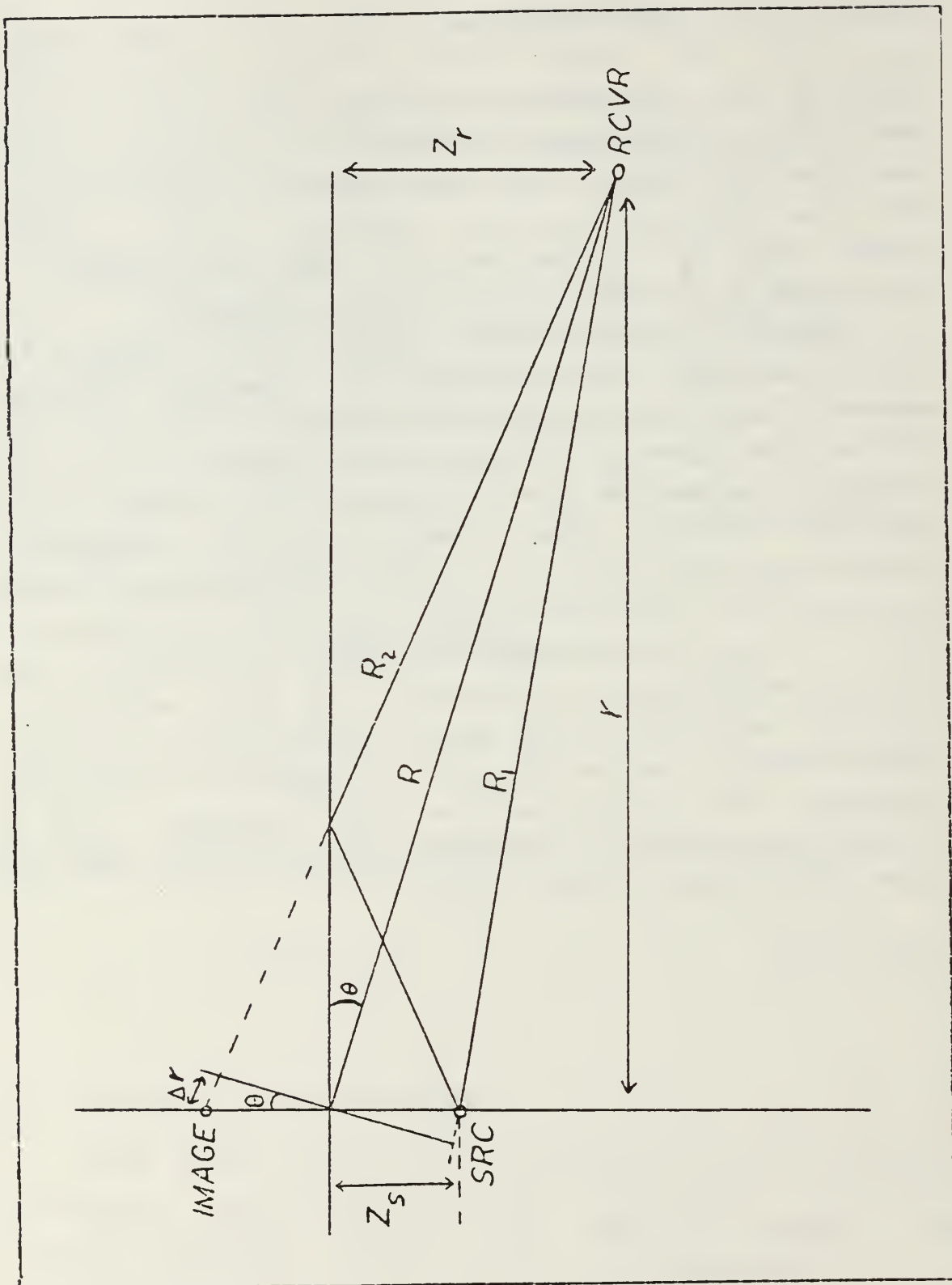
Figure 2.1   The Geometry of the Lloyds Mirror Effect
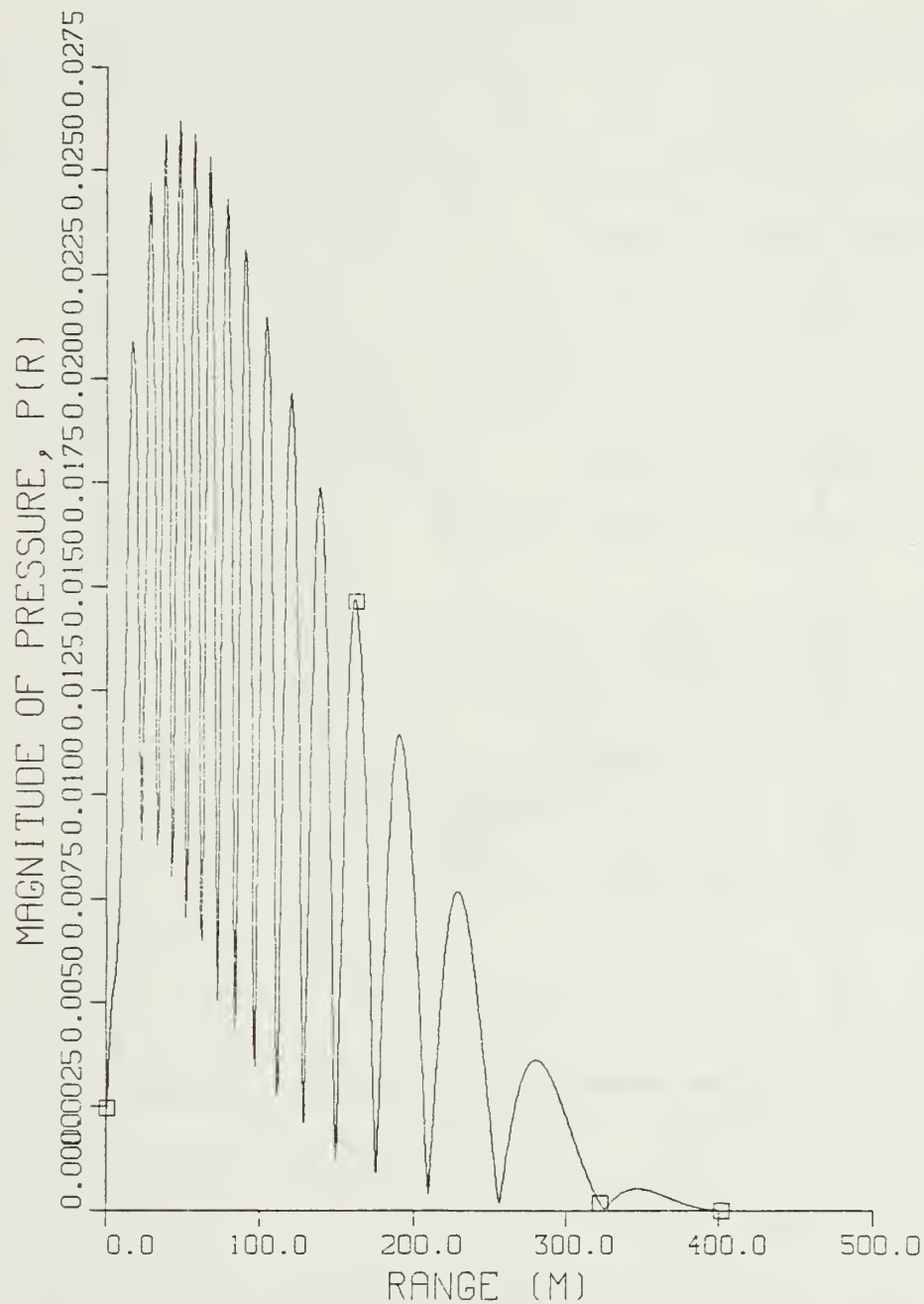
Figure 2.2   A Classic $|P(R)|$ vs. R Curve
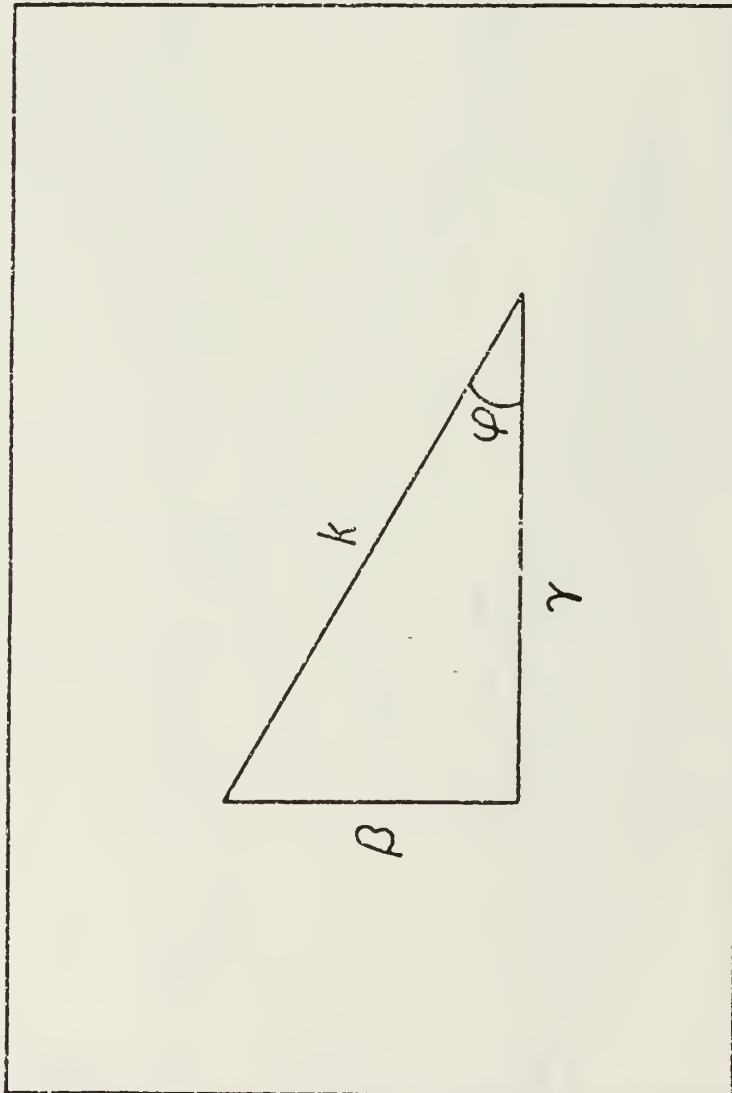
Figure 2.3   The Relationship Between K, γ and β

32

III. <u>RESULTS</u> <u>AND</u> <u>CONCLUSIONS</u>

A. THE FFT ALGORITHM

The research for this thesis was conducted entirely with
computer algorithms to model the Lloyds Mirror, the Fast
Fourier Transform, the range windows, waves, and the narrow-
band noise. This was necessary since the Lloyds Mirror is
an idealized representation of a situation that occurs only
rarely in nature, and at that is limited to isospeed surface
ducts. Also, time and money constraints were such that the
use of computer models was an absolute necessity. For these
reasons and because the FFT is the heart of the Wavenumber
Technique, finding a reliable, easy-to-use computer algo-
rithm to perform the FFT on the complex pressure function
was deemed very important.

Initially, the IMSL library routines, FFT2C and FFTCC
[Ref. 9: p. 232], were used to generate the pressure
spectra. Although the author was unable to ascertain just
how Stamey performed the FFT on his data, it is highly prob-
able that he used an IMSL library routine. While in his
thesis, Blanchard stated that he used the FFTCC routine.
The magnitude of a typical spectrum generated by the routine
FFT2C is shown in Figure 3.1.

The same scenario used to generate Figure 3.1 was used
to produce the spectrum shown in Figure 3.2, but the routine
FFTCC was utilized. As can be seen, the resulting graphs of
the pressure spectrum magnitude are practically identical.
Indeed, the set-up of the pressure fields for insertion into
each routine differ only in that FFT2C requires a data set
consisting of an integral power of two number of points,
whereas FFTCC will handle any number of points. And, when

33

the Cooley-Tukey FFT listed in Appendix I was used to trans-
form the same pressure field as was utilized to produce
Figures 3.1 and 3.2, Figure 3.3 was the result. This algo-
rithm differs somewhat from the IMSL routines by the manner
in which the pressure field data is treated. Both FFT2C and
FFTCC are designed to handle a complex array. The
Cooley-Tukey FFT, on the other hand, is designed to trans-
form real data; but the pressure field is complex. To get
around this apparent conundrum, the pressure data is defined
as either real or imaginary by its placement in the array.
As can be seen, the resultant graph of the spectrum magni-
tude is almost indistinguishable from that produced by
either IMSL routine. In conclusion, it does not matter
which FFT routine is used to generate the pressure spectrum,
as long as the pressure field in the range domain is
"fitted" into the array in a manner suitable to the
particular algorithm used.

TABLE I
Critical Values Used in the Research

K (m^{-1})	N	r (m)	(m^{-1})
3.0	1024	0.524	1.172×10^{-2}
2.0	1024	0.785	7.816×10^{-3}
1.0	1024	1.571	3.906×10^{-3}

It is important to note four things about the FFT at
this point.
   1. Since the FFT is given only a finite sample of a
      function while the theoretical Fourier Transform

looks at the complete function, the computer algorithm is designed to overcome this necessary shortcoming by assuming the submitted finite sample repeats its pattern an infinite number of times. This can present problems. If the right hand side of one pattern does not flow smoothly into the left hand side of the next repetition, as is shown in Figure 3.4, then high frequency oscillations known as the Gibbs Phenomenon can be introduced into the spectrum. (See Figure 3.5) This is a very real danger where accustic pressure fields are concerned. For example: if the sample size does not include the entire pattern (i.e., the pressure magnitude has not been completely attenuated prior to the endpoints of the sample), this unwanted "jitter" in the spectrum can result. To avoid this situation, not only was a pressure field symmetric about the origin (the source) used, but also a Hanning Window was constructed to reduce both the amplitude and the phase components of the pressure field to zero at the endpoints, thus avoiding the Gibbs Phenomenon. Figure 3.6 shows the same pressure field depicted in Figure 3.4 combined with a Hanning Window. Its spectrum is shown in Figure 3.7. The Gibbs Phenomenon is absent. The form of the window is given below. The reader's attention is directed to Appendix I for a view of the manner in which it is combined with the pressure field.

The Hanning Window:

$$W = 0.5\left[1 + \cos\left(\frac{(I-1)\pi}{NPTS}\right)\right] \qquad \text{(eqn 3.1)}$$

35

where "NPTS" is the number of data points,
and I = 1,2,3,...,NPTS.

The Hanning Window does not affect the acoustic pres-
sure field in any other way; the interference pattern
in the range domain characteristic of the Lloyds
Mirror for an Acoustic Doublet remains the same
except for its amplitude near the end points. As
shall be shown later in this chapter, it is the
pattern of the entire pressure field, not simply the
amplitude of the pattern, on which the W.T. performs
its legerdemain.

2. Because the vertical wavenumber beta is real and has
physical meaning for values of the horizontal
wavenumber less than k, only those values of the
magnitude of the acoustic pressure spectrum corre-
sponding to $\gamma < k$ were retained.

3. In the Wavenumber Technique, the relationship between
the horizontal range step size $\triangle r$ and the hori-
zontal wavenumber step size $\triangle \gamma$ is extremely
important. Recalling equation 2.36,

$$\triangle \gamma \triangle r = \frac{2\pi}{N}$$ (eqn 3.2)

for a given "N," the term on the right hand side,
$2\pi/N$, is a constant. Consequently,

$$\triangle r \propto (\triangle \gamma)^{-1}$$ (eqn 3.3)

Simultaneously, in accordance with sampling theory,
in order to prevent aliasing in the pressure spec-
trum, there is an upper limit on the size of $\triangle r$:

$$\Delta r \leq \frac{\lambda}{2} \qquad \text{(eqn 3.4)}$$

Normally, Δr is chosen such that it is much less than half a wavelength; specifically, $\Delta r < \lambda/5$ or $\lambda/6$, thus a good sample of the range domain is ensured. However, from equation 2.36, the smaller Δr becomes, the larger $\Delta \gamma$ becomes and the coarser the sample sizes of the spectrum become. Also, to ensure adequate samples in the spectrum, examination of equations 2.25 and 2.36 and [Ref. 10] reveals that

$$\Delta \gamma \leq \frac{1}{2k}\left(\frac{\pi}{z}\right)^2 \qquad \text{(eqn 3.5)}$$

where Z is the deeper of the two depths, whether source or receiver. So there is a delicate balance to maintain between the sizes of Δr and $\Delta \gamma$. In the spirit of compromise, the investigator chose to use a range step size equal to a quarter of a wavelength where

$$\lambda \equiv \frac{2\pi}{k} \qquad \text{(eqn 3.6)}$$

For most cases investigated, values for k, N, Δr and $\Delta \gamma$ are summarized in Table I. As can be seen, using these values and equation 3.5, for a "Z" value of 25 wavelengths, the maximum size $\Delta \gamma$ can assume and still ensure an adequate sample size is $\Delta \gamma = 0.0004$ /m. Clearly the sizes of $\Delta \gamma$ shown in Table I are too coarse by a factor of approximately 20. Only by increasing N, the number of sample points, can this discrepancy be corrected.

However, as mentioned earlier, computer resources were limited. The effect on the research results is not significant; nevertheless, it is recommended the reader bear this limitation in mind during the succeeding pages.

4. Looking again at Figures 3.1 through 3.3, the FFT is the curve marked by the solid line, while the theoretical Fourier Transform is the curve marked by the dotted line. Notice the large discrepancy between the theoretical values and the actual values in the region corresponding to small vertical wavenumbers. This happens to correspond to a region of the spectrum characterized by more rapid fluctuations in the spectrum. However, the size of beta is constant. Consequently, fewer samples of this region of the spectrum are available as compared with that region corresponding to high beta values. Since the plotting routine utilized is interpolating between sampled points of the spectrum, the graph at this end is less smooth and results in a marked difference between the curves. Where the curves are determined by more points and are smoother, the discrepancy between theory and computerized reality is much less noticeable.

B. SOURCE DEPTH DETERMINATION

Theory predicts that, for a source shallower than the receiver, when the magnitude of the pressure spectrum is plotted as a function of the vertical wavenumber, the resultant nodal spacing can be used to determine source depth by either consulting a chart (see Figure 3.8) or by performing a simple calculation (see equation 2.31). To test this prediction, several scenarios were designed. Figures 3.9

38

through 3.11 are typical of the many cases run. In each, source depth is less than receiver depth. For each case, careful measurement of the $\triangle\beta$ spacing coupled with use of equation 2.31 yielded the (already known) source depth with less than a two per cent error, which can be attributed to human error in the measurement of $\triangle\beta$.

TABLE II

Results of Source Depth Determination Runs

Figure Nr.	ZS (m)	ZR (M)	(Meas'd)	Z(Calc'd)
3.9	21.998	47.124	0.14 m^{-1}	22.4 m
3.10	31.416	47.124	0.10 "	31.4 "
3.11	15.708	47.124	0.20 "	15.7 "
3.12	47.124	21.998	0.14 "	22.4 "
3.13	47.124	31.416	0.10 "	31.4 "
3.14	47.124	15.708	0.20 "	15.7 "

To test what happens when the receiver depth is shallower than the source depth, the cases depicted in Figures 3.12 through 3.14 were run. The scenario is the same as for Figures 3.9 through 3.11; only the source and receiver depths have been exchanged. As can be seen, the $\triangle\beta$ spacing corresponds with the receiver depth. This is again as predicted by theory. Table II summarizes the findings of Figures 3.9 through 3.14.

The scenarios shown in Figures 3.9 through 3.14 all start with a pressure field measured horizontally from the source; i.e., the exact range to the source is known. What if the range to the source is not known, or only minimal information concerning the range is known? In this case, only a portion of the pressure field starting at some initial range P_0 can be sampled. What is the effect on the spectrum?

To answer these questions, a range window was constructed and placed at varying initial ranges from the source. As Figure 2.2 illustrates, as range from the source increases, the nodes of the Lloyds Mirror interference pattern in the range domain become more widely spaced. Given fewer nodes to sample, will the spectrum be the same? In accordance with theory, the spectrum is independent of range (see equation 2.39) and so should be the same wherever the window is placed.

Figures 3.15 through 3.17 illustrate that the spectrum is not entirely independent of range. The figures utilize the same scenario as was used above, differing only in the range from the source at which the sampling of the pressure field begins. As can be seen, beginning at the right hand side which corresponds to high vertical wavenumber values, or the low horizontal wavenumber values (see equation 2.8), a "washing out" of the spectrum occurs, increasing as the range window is moved further from the source. Again, the theoretical curve is marked by the dotted line.

When the magnitude of the pressure spectrum is plotted as a function of the vertical wavenumber, the useful portion of the resulting graph is the last two-thirds of the beta range. For $K = 2.0/m$, this is the range $0.67/m < \beta < 2.0/m$. This phenomenon is explained more fully in Section III A 4. With this caveat in mind and based upon multiple source, receiver, range window

40

combinations run through the model, the following criterion
was established: the nodal spacing of the spectral plots
was no longer determinable once the initial range R_0 was
increased to approximately three times the source depth. In
other words, minimum knowledge of the range from receiver to
source must be available to ensure adequate sampling of the
acoustic pressure field in the range domain. This, in turn,
will produce a pressure spectrum of such a quality that
source depth determination can be made.

What causes this not entirely unexpected result? As the
range window is moved further from the source, for
$Z_s \neq Z_r$, those samples of the pressure field corresponding
to low gamma values are lost to the spectrum first. Low
gamma values correspond to waves arriving at high angles
with respect to the horizontal. At greater receiver ranges,
R more closely approximates r and the arrival angles become
closer to the horizontal (see Figure 2.1).

As the window is moved further from the source and fewer
nodes of the interference pattern are encountered, if a
wider window were used, could this "washing out" effect in
the spectrum be minimized or even eliminated? In the
author's opinion, it would be minimized; because of the
reasoning in the preceding paragraph, it probably would not
be eliminated. However, a wider window would require more
sample points; because of equation 2.36, one cannot merely
make $\triangle$r larger. Time and the computer resources available
to this investigator were limited, and the test cases run
were already using the maximum available array sizes, thus
precluding a quantitative illustration of this hypothesis.
Succeeding research into the W.T. might include ways to test
this point.

In conclusion, the Wavenumber Technique has the poten-
tial for being a valuable operational tool in determining
the depth of an acoustic source provided the receiver is at

a greater depth than the source. It is strongly recommended that further research into use of the W.T. in a realistic ocean environment be done.

C. THE EFFECT OF SURFACE ROUGHNESS

This and the succeeding section were purely qualitative portions of the research. Therefore, in the figures the spectra were plotted as functions of the horizontal wavenumber for ease of discussion except where a particular point about the vertical wavenumber was being illustrated, and the theoretical curve was omitted.

As described in Chapter II, the effect of surface roughness is to suppress the contribution of the image to the dipole interference pattern. Moreover, by increasing M, the effect is to suppress the image's contribution to the pressure field in the range domain and reduce the pressure spectrum to the contribution of the direct path wave only (see equation 2.41); the resultant magnitude of the spectrum is inversely proportional to the vertical wavenumber (see equation 2.42). As Figures 3.18 through 3.21 illustrate, this is exactly what happens in the FFT. In Figure 3.21, an inverse beta curve has been manually superimposed onto the actual curve to reflect this point.

Looking at the pressure field in the range domain $\underline{P}(R)$ the effect of surface roughness is inversely proportional to the wavelength of the signal. For longer wavelengths, the Lloyds Mirror effect is more tolerant of surface roughness than it is for shorter wavelengths. Does the same relationship hold for the pressure spectrum? Comparison of the respective sea states in Figures 3.22 and 3.23 with Figures 3.24 and 3.25 illustrate that it does.

This investigator also looked at the effect of varying the range window in the presence of waves. This is similar

42

to what was looked at in Section B of this chapter. Results
should be similar and for the same reasons. For a given sea
state, source and receiver geometry and wavelength, the
range window was moved successively further from the source
(see Figures 3.26 through 3.29). As can be seen, the
"washing out" effect of the spectral nodes begins to effect
the lower horizontal wavenumber values first.

D. THE EFFECT OF NOISE

Random noise was simulated in this research. Being
independent of range and frequency, it was treated as a
constant by both the Fourier Transform and the FFT. The
investigator wished to compare qualitatively the effects of
equal amounts of noise on the pressure field in the range
domain and in the wavenumber domain. To do this, succes-
sively larger values of the "noise factor" were used in
computing $\underset{\sim}{n}$ (see equation 2.43). Values of the noise
factor used in the research were limited to the maximum
amplitude of the pressure field $\underset{\sim}{P}(R)$. Since dipole radia-
tion is predicated, as range from the source increases, the
maxima of the interference pattern decrease as the inverse
square of the range (i.e., R^{-2}). Hence, even small noise
factors can have a devastating effect on the pressure field
as the receiver is stepped out in range. The destructive
effect on the spectrum of successively more intense amounts
of noise at varying wavelengths is illustrated in Figures
3.30 through 3.47

Several conclusions concerning the pressure spectra can
be drawn from these results:

1. For equal amounts of noise, longer wavelengths are
   affected less than shorter wavelengths. Compare
   Figures 3.31 and 3.32 with Figures 3.43 and 3.44, and
   Figures 3.34 and 3.35 with Figures 3.46 and 3.47.

43

This was not a surprising result since the same prin-
ciple holds for the range domain.

2. The spectrum is affected less by noise than is the
    range domain. Compare Figures 3.30 through 3.35 and
    Figures 3.36 through 3.47 for an illustration of this
    point at two different wavelengths and various noise
    levels. This was a rather welcome surprise.

3. If the magnitude of the pressure spectrum is plotted
    as a function of beta, the $\Delta\beta$ spacing can still
    be detected even after the pressure function in the
    range domain has been "swallowed up" by the noise
    field. Compare Figures 3.33 through 3.35 and Figures
    3.42 through 3.44. This was not surprising in view
    of 2. above.

E. SUMMATION

All of the foregoing results are based specifically on
the Lloyds Mirror for an Acoustic Doublet. This is a highly
idealized and artificial environment. Any thought of imme-
diately applying conclusions reached in this paper to a real
world situation is premature. However, the results are
still significant if only for supporting the statement made
by each preceding investigator that the Wavenumber Technique
should be examined very closely for a future operational
role, especially in view of the current trends in source
levels and ambient noise levels.

Certain fundamental conclusions regarding the author's
research into the Wavenumber Technique can now be made
within the confines of the above restriction:

1. Source depth can be determined quickly and easily
    from the acoustic pressure spectrum provided
    a) the receiver is deeper than the source,

b) some knowledge of the range from receiver to
      source is available,and
   c) the magnitude of the pressure spectrum is plotted
      as a function of the vertical wavenumber.
2. Source depth determination in even a noisy environ-
   ment is possible. While the introduction of
   increasing amounts of narrow band noise adversely
   affects both the range domain and the wavenumber
   domain, the pressure spectrum seems able to withstand
   the chaotic destruction longer than does the pressure
   field in the range domain.
3. The ability to determine source depth is adversely
   affected by the height of surface gravity waves since
   surface roughness reduces the Lloyds Mirror as the
   sea state increases.
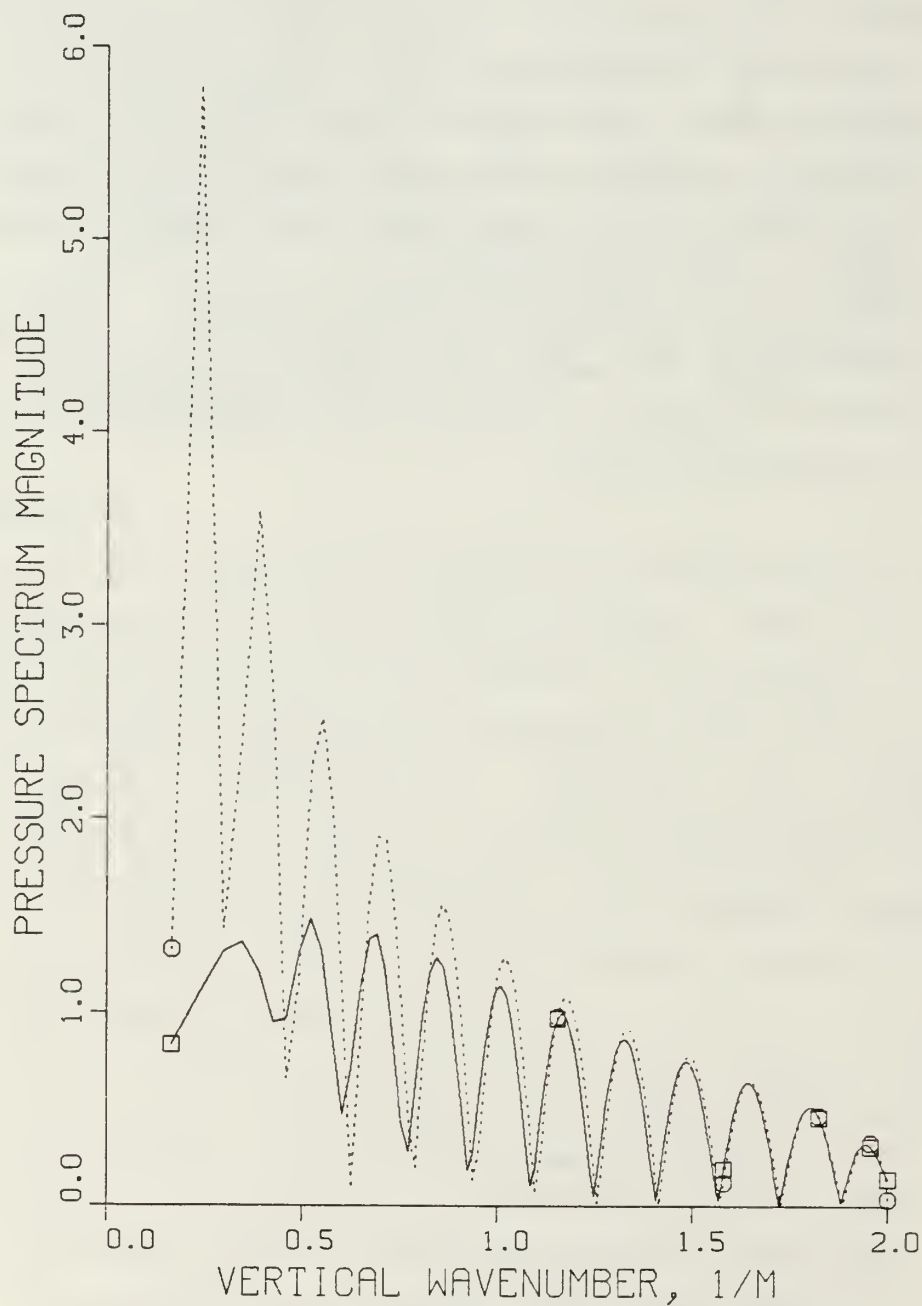
Figure 3.1   Pressure Spectrum Using FFT2C

46
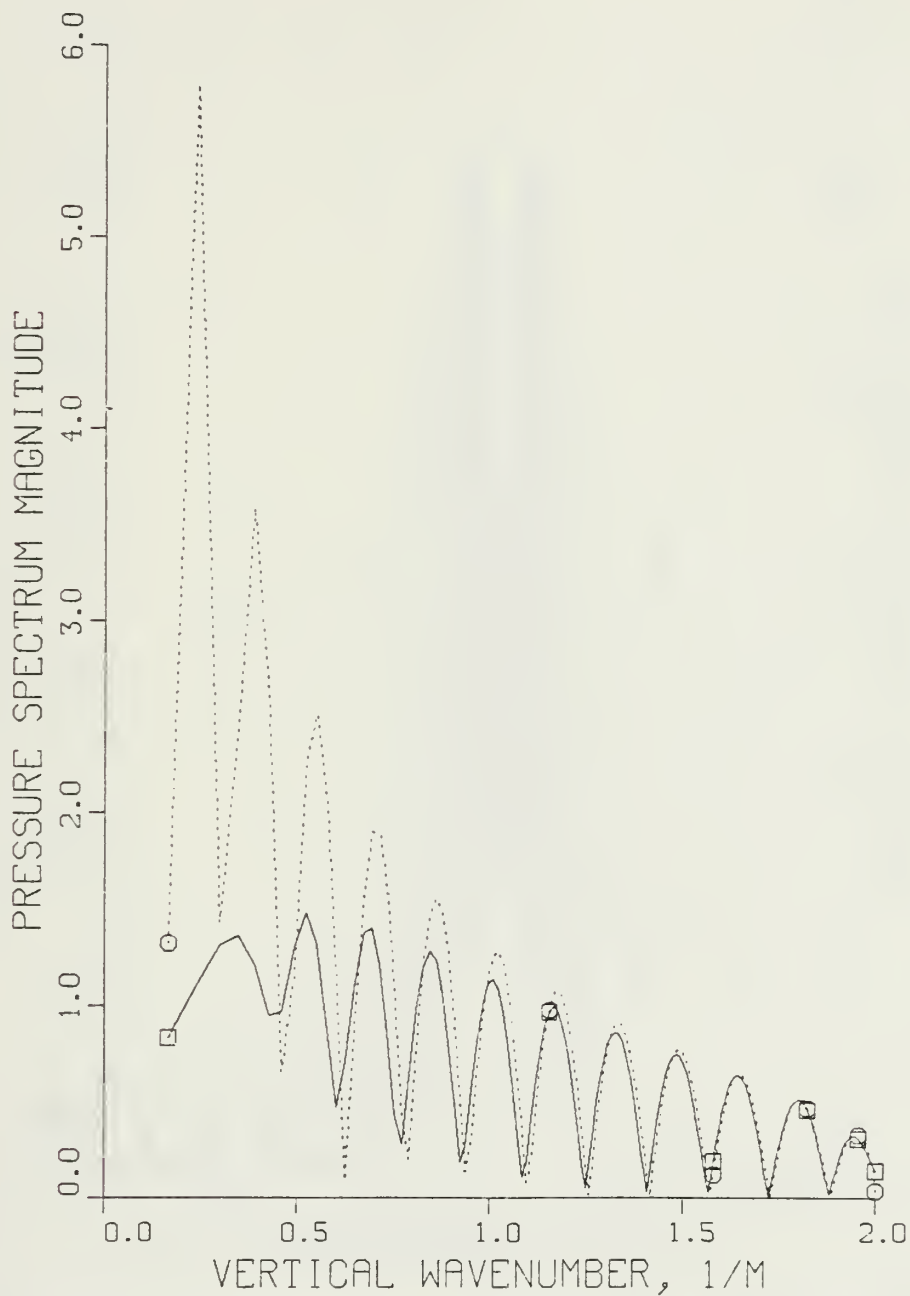
Figure 3.2   Pressure Spectrum Using FFTCC
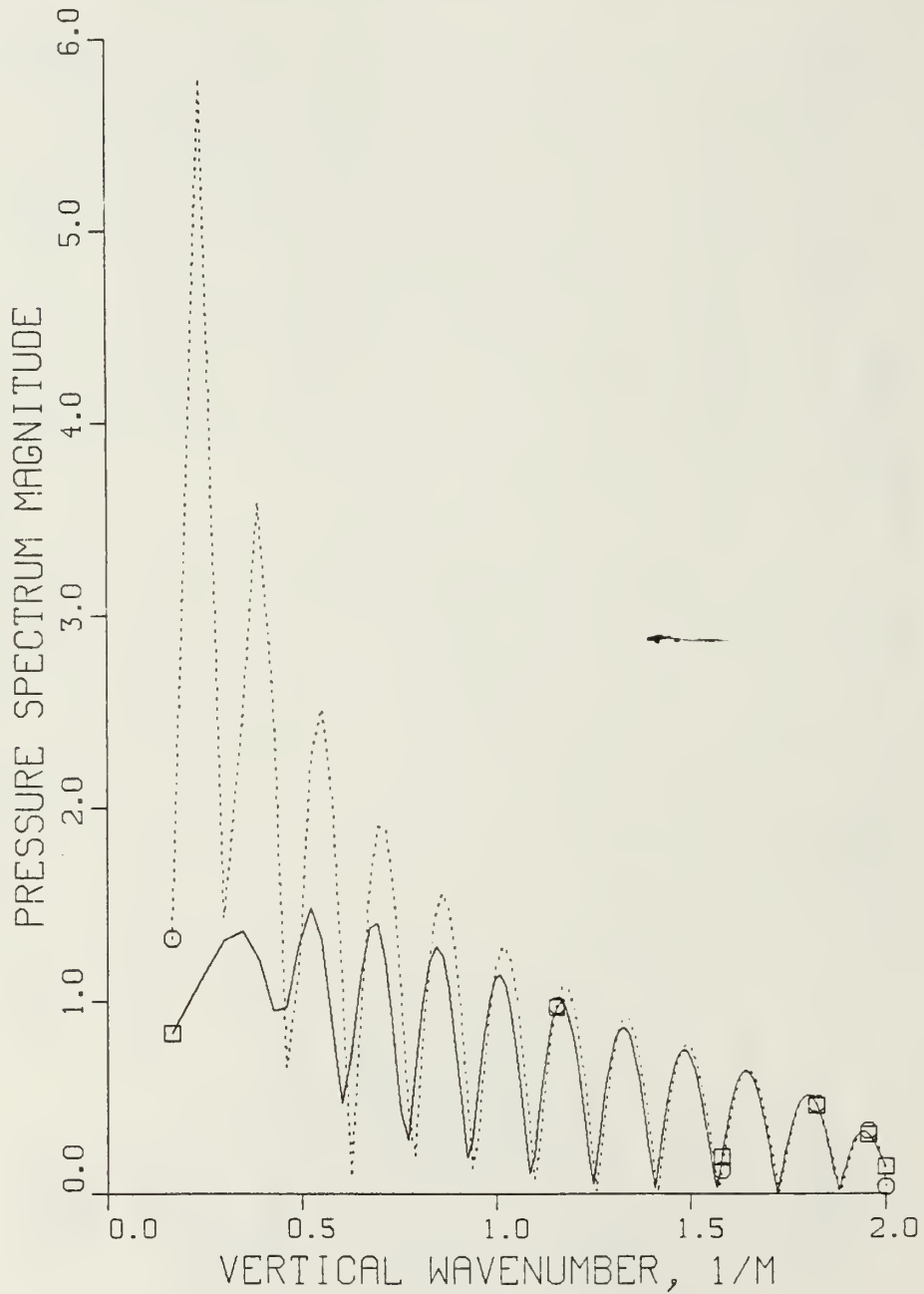
Figure 3.3   Pressure Spectrum Using Cooley-Tukey FFT
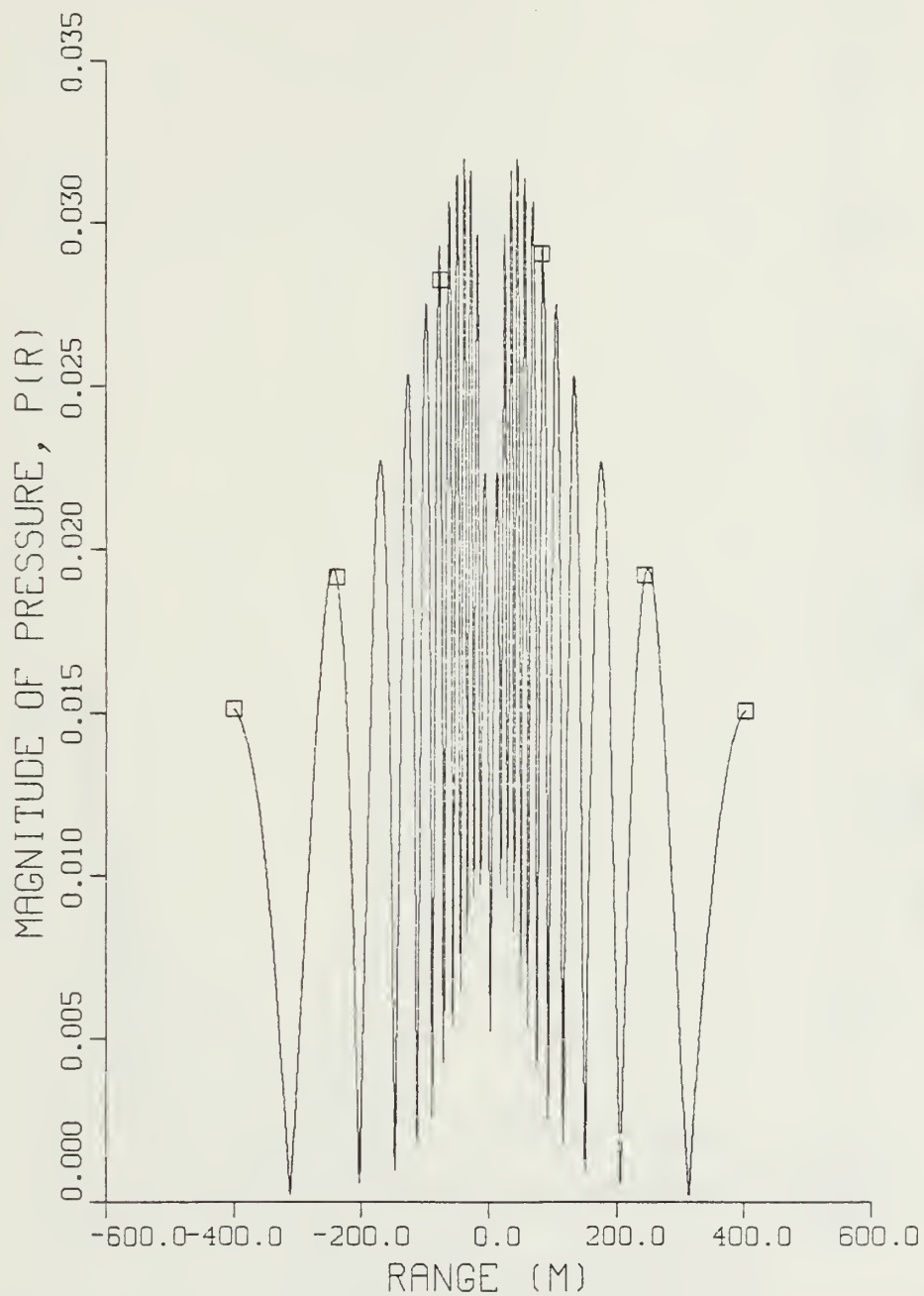
Figure 3.4   Non-smoothed Pressure Field

49
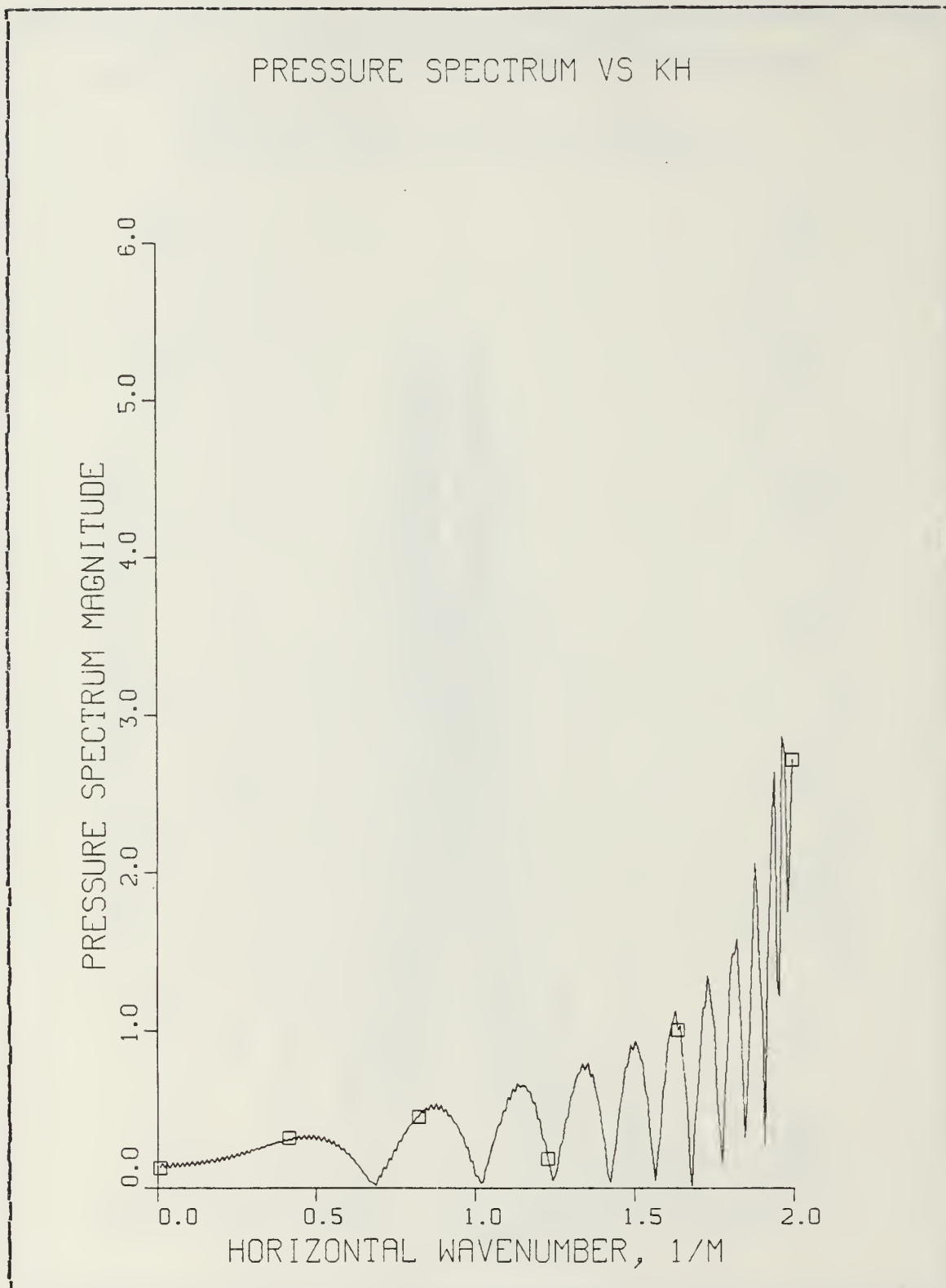
Figure 3.5   Pressure Spectrum Showing Gibbs Phenomenon

50

Figure 3.6   Pressure Field Combined With a Hanning Window
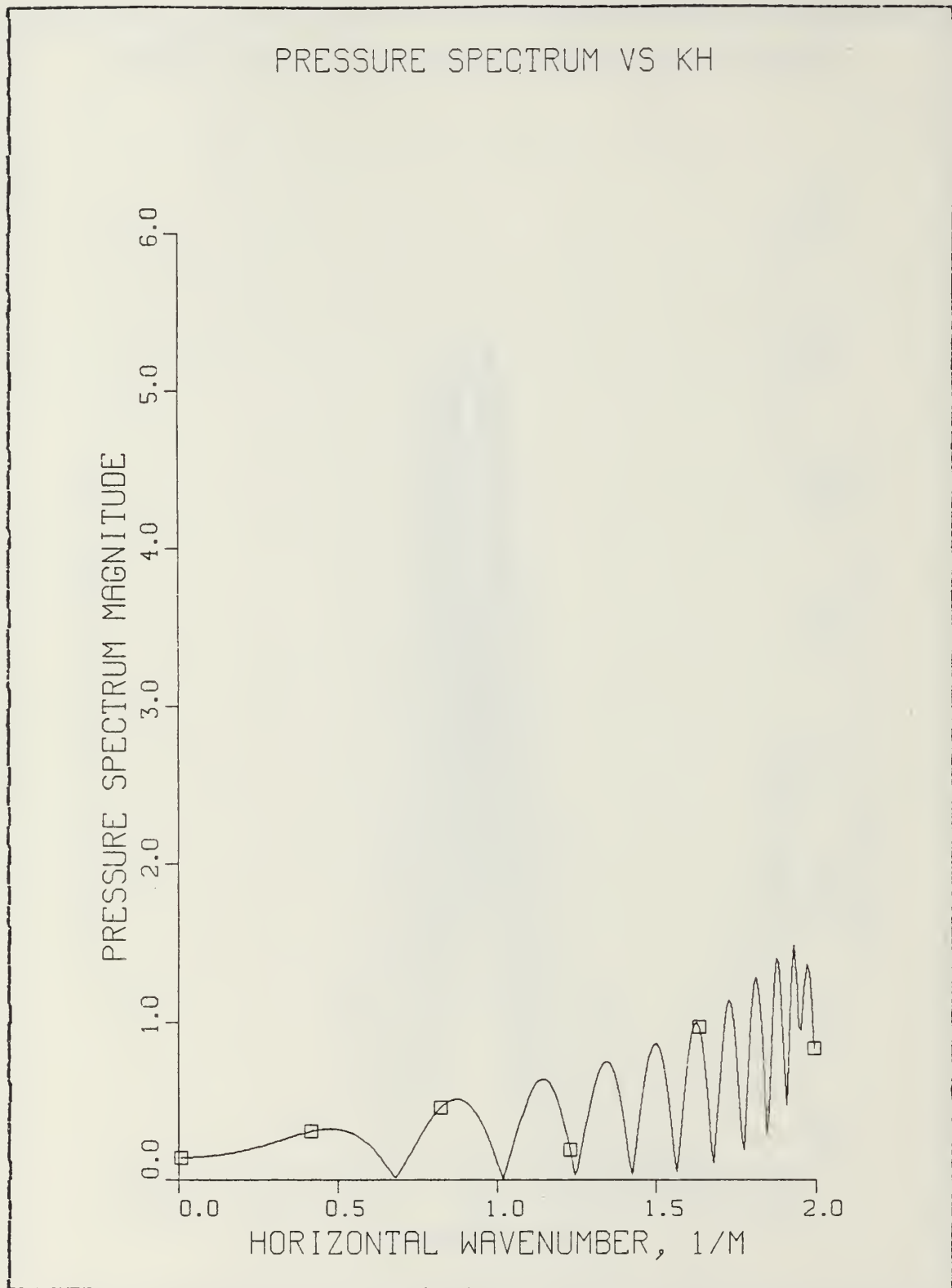
Figure 3.7   Pressure Spectrum Combined With a Hanning Window

Figure 3.8   Theoretical Source Depth Determination Curve

53

Figure 3.9   Graph of Pressure Spectrum,
              Source at 22.0 Meters

54

Figure 3.10   Graph of Pressure Spectrum,
Source at 31.4 Meters

55

PRESSURE SPECTRUM VS KZ

RECEIVER DEPTH = 47.124 M, K = 2.0/M,
N = 1024
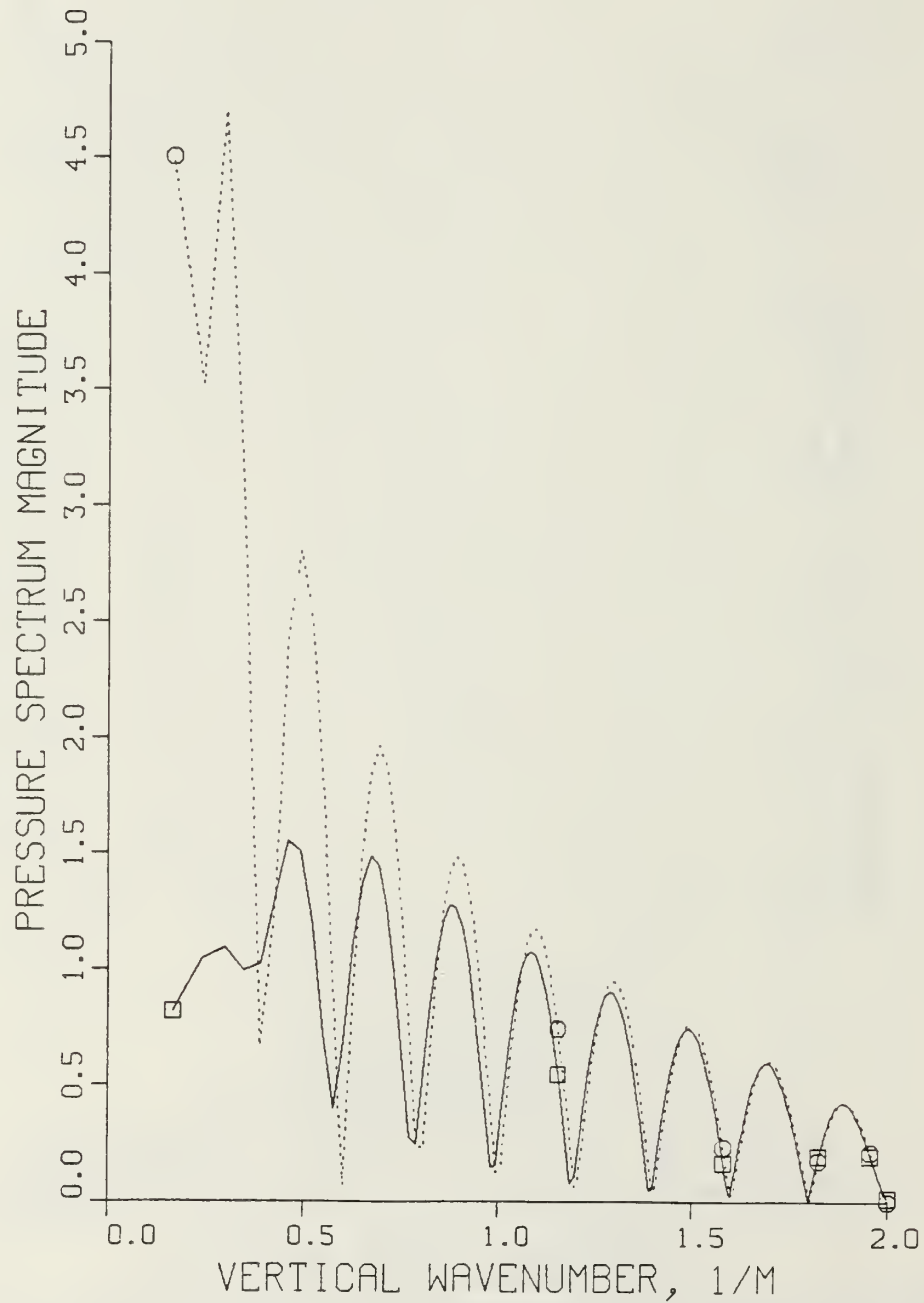
Figure 3.11   Graph of Pressure Spectrum,
Source at 15.7 Meters
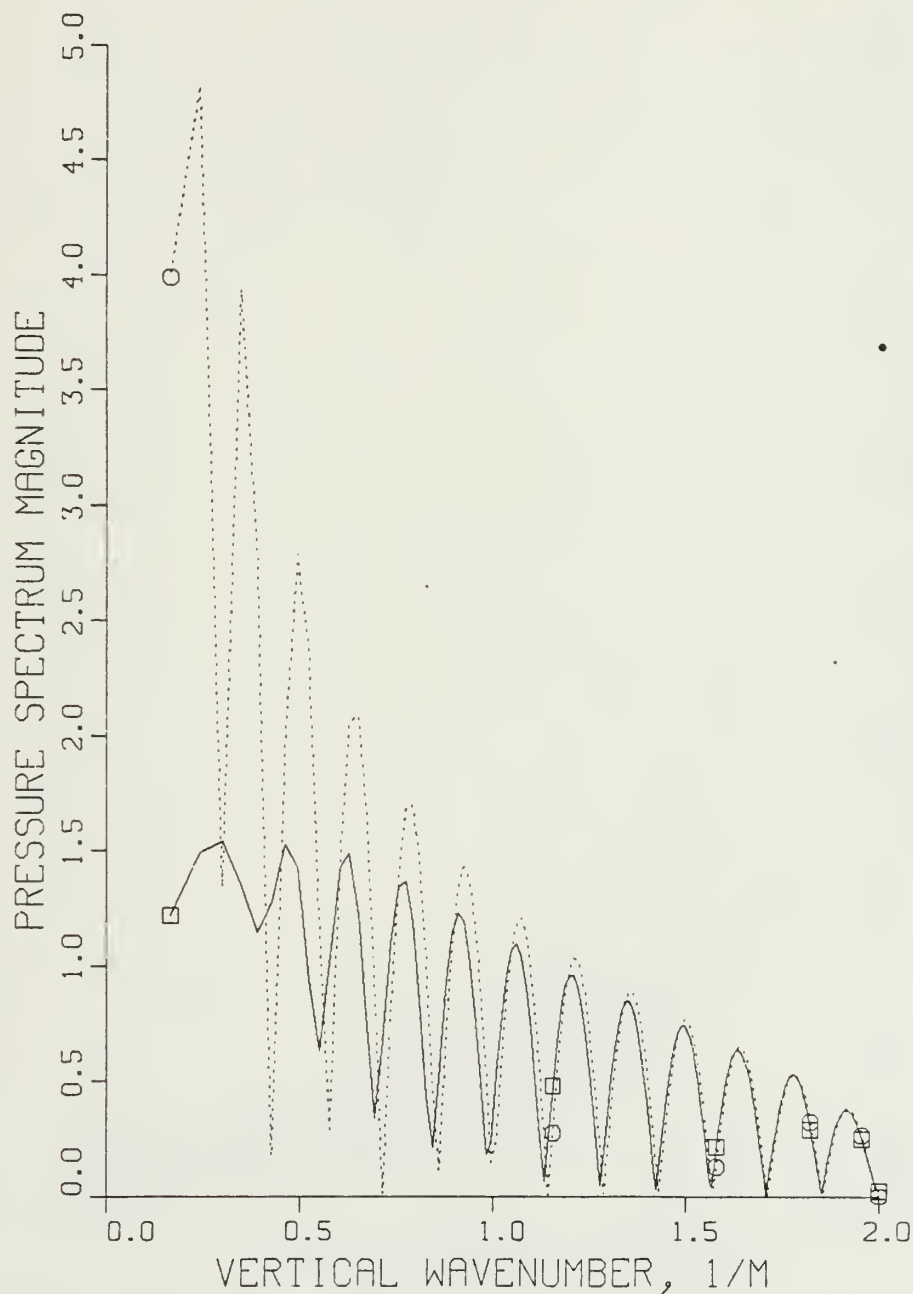
Figure 3.12   Graph of Pressure Spectrum,
Receiver at 22.0 Meters

57
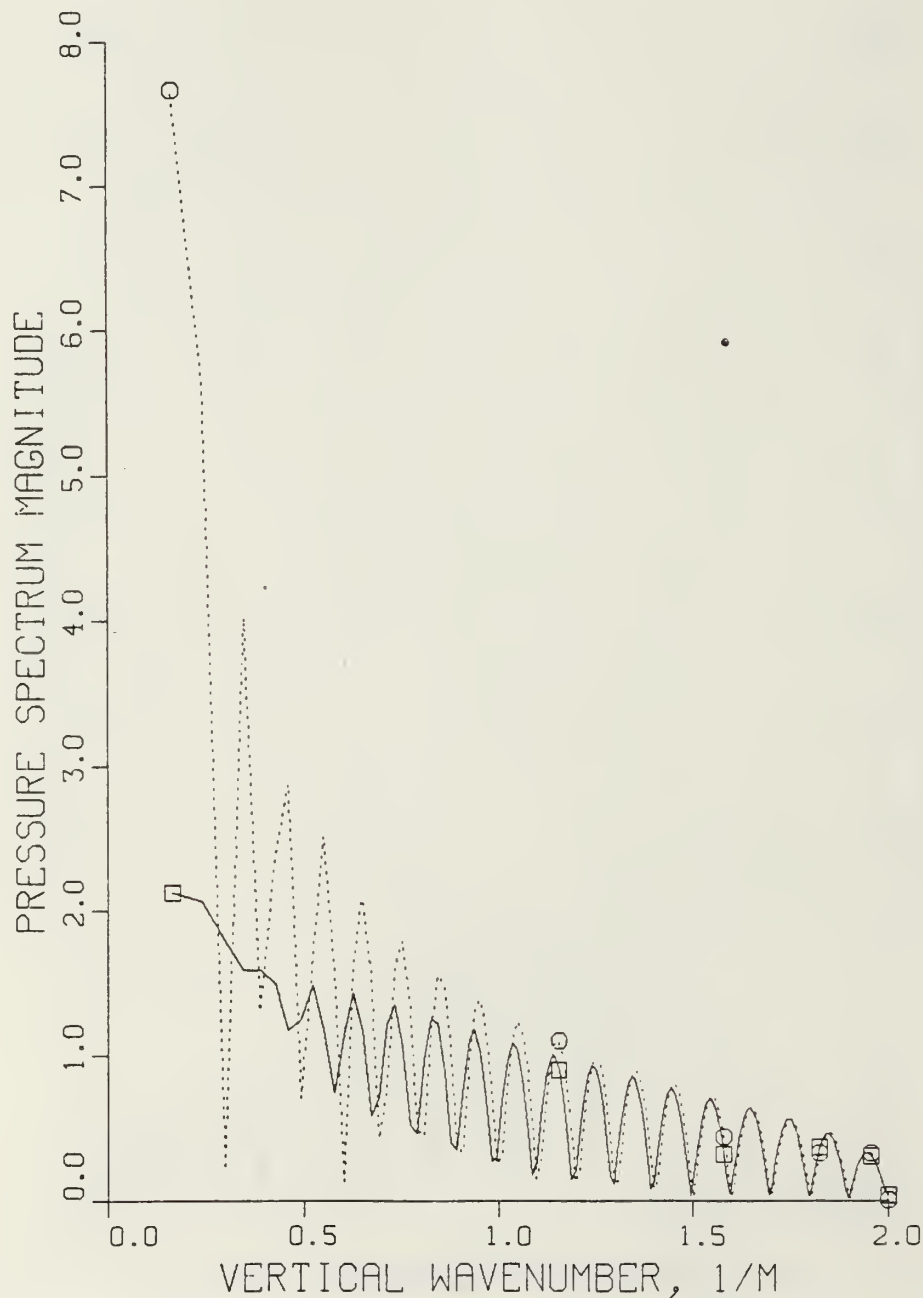
Figure 3.13   Graph of Pressure Spectrum,
Receiver at 31.4 Meters
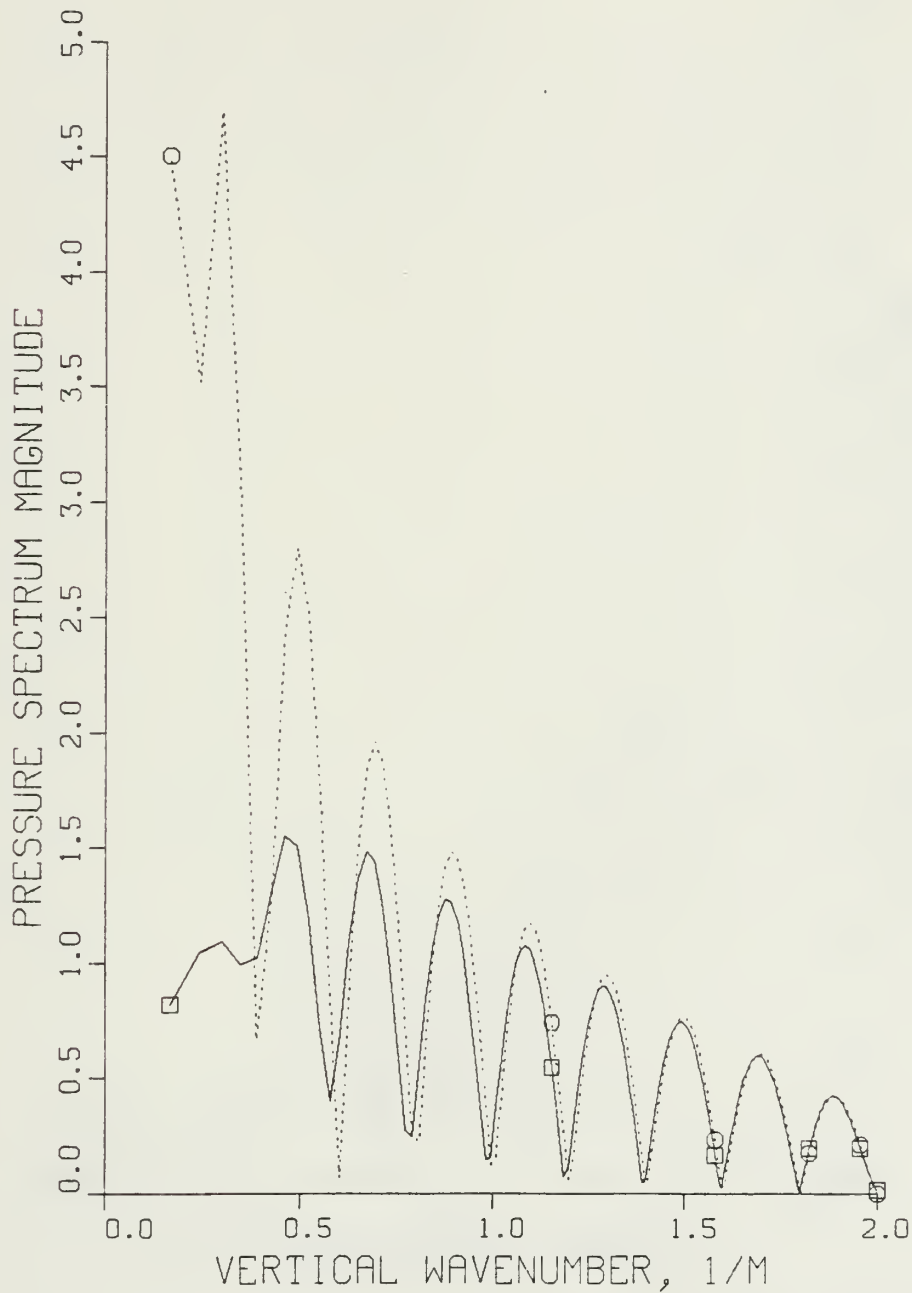
Figure 3.14   Graph of Pressure Spectrum,
Receiver at 15.7 Meters
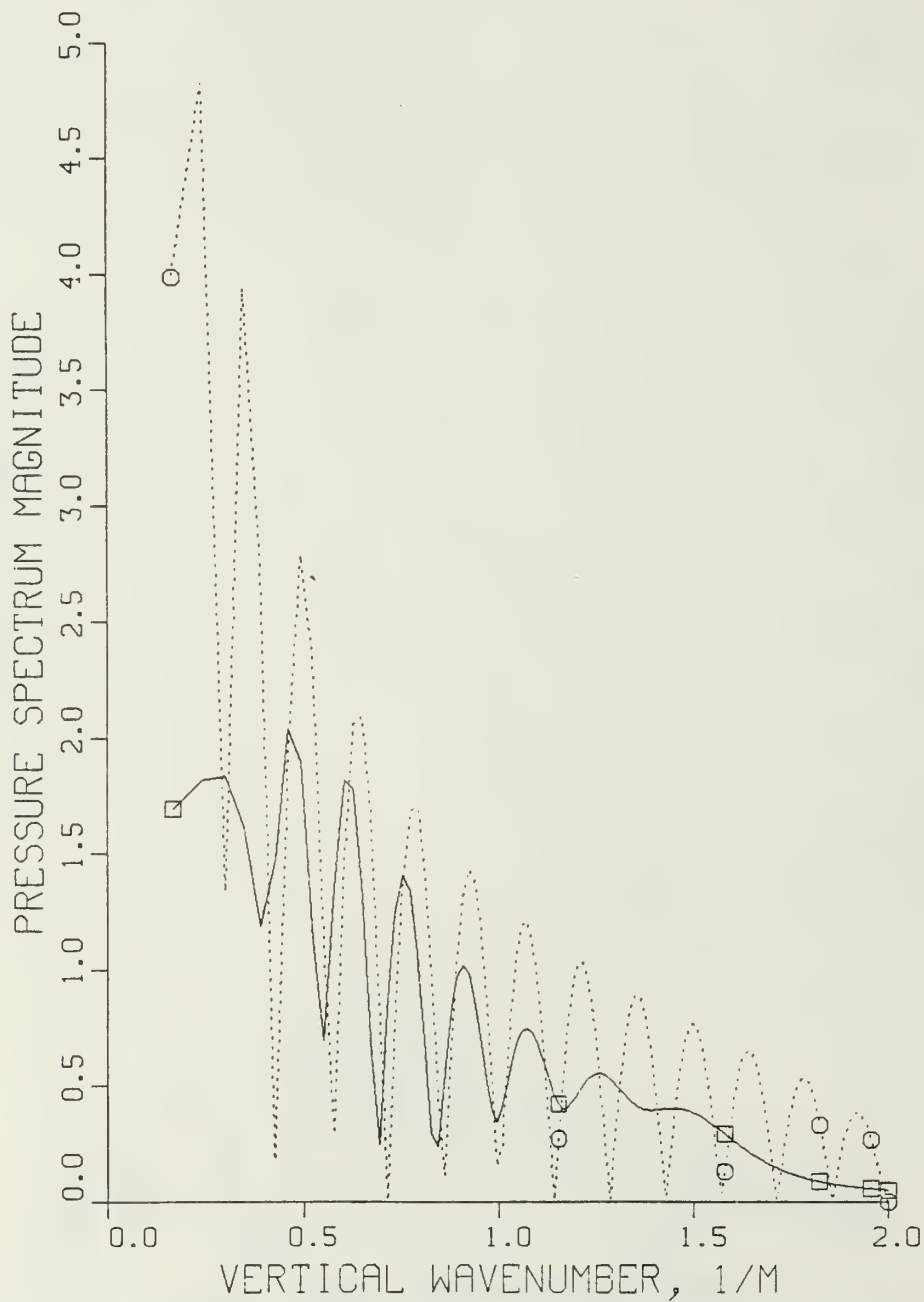
Figure 3.15   Pressure Spectrum,
Range Window Set at 47.1 Meters

60
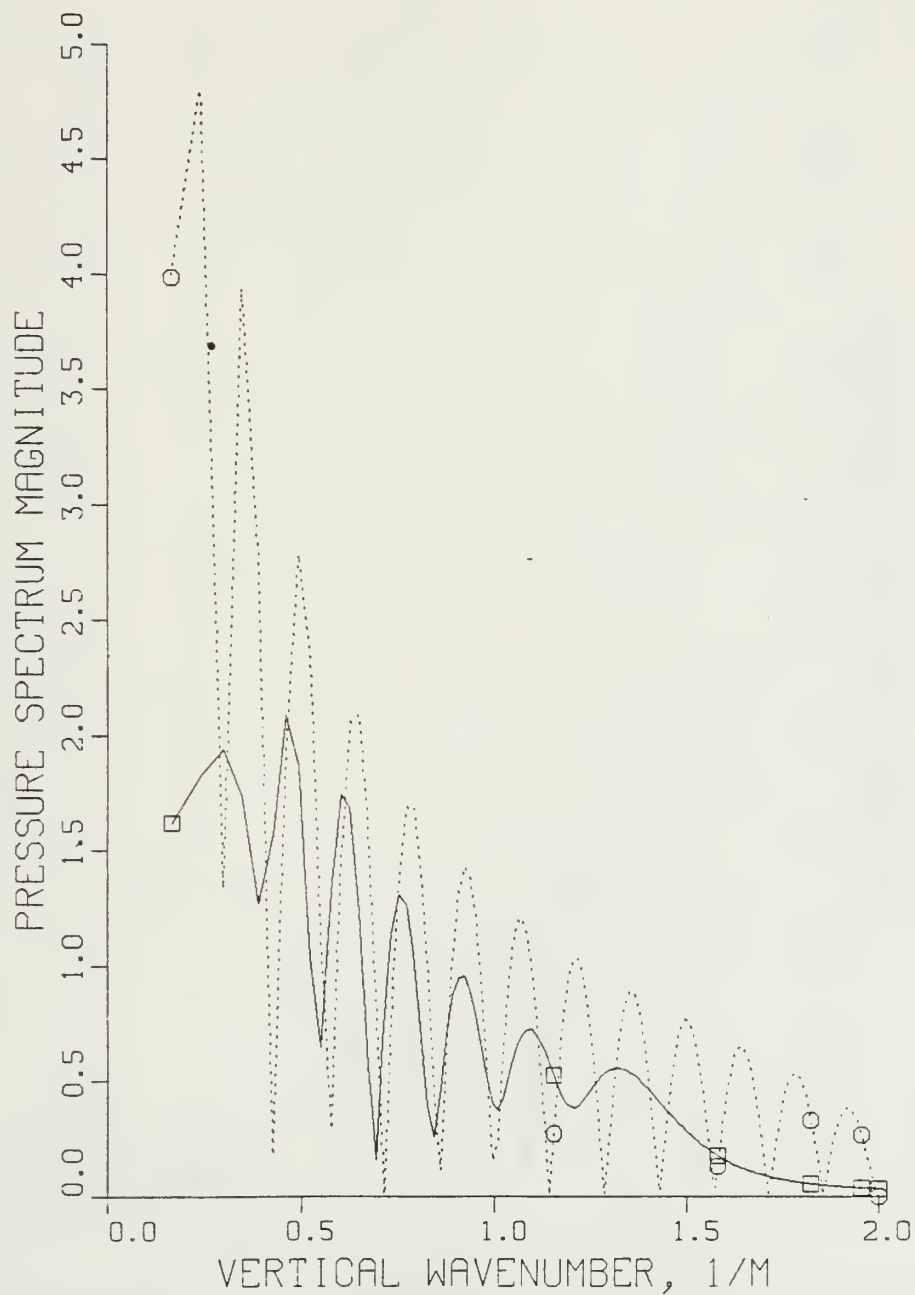
Figure 3.16   Pressure Spectrum,
Range Window Set at 50.3 Meters

61
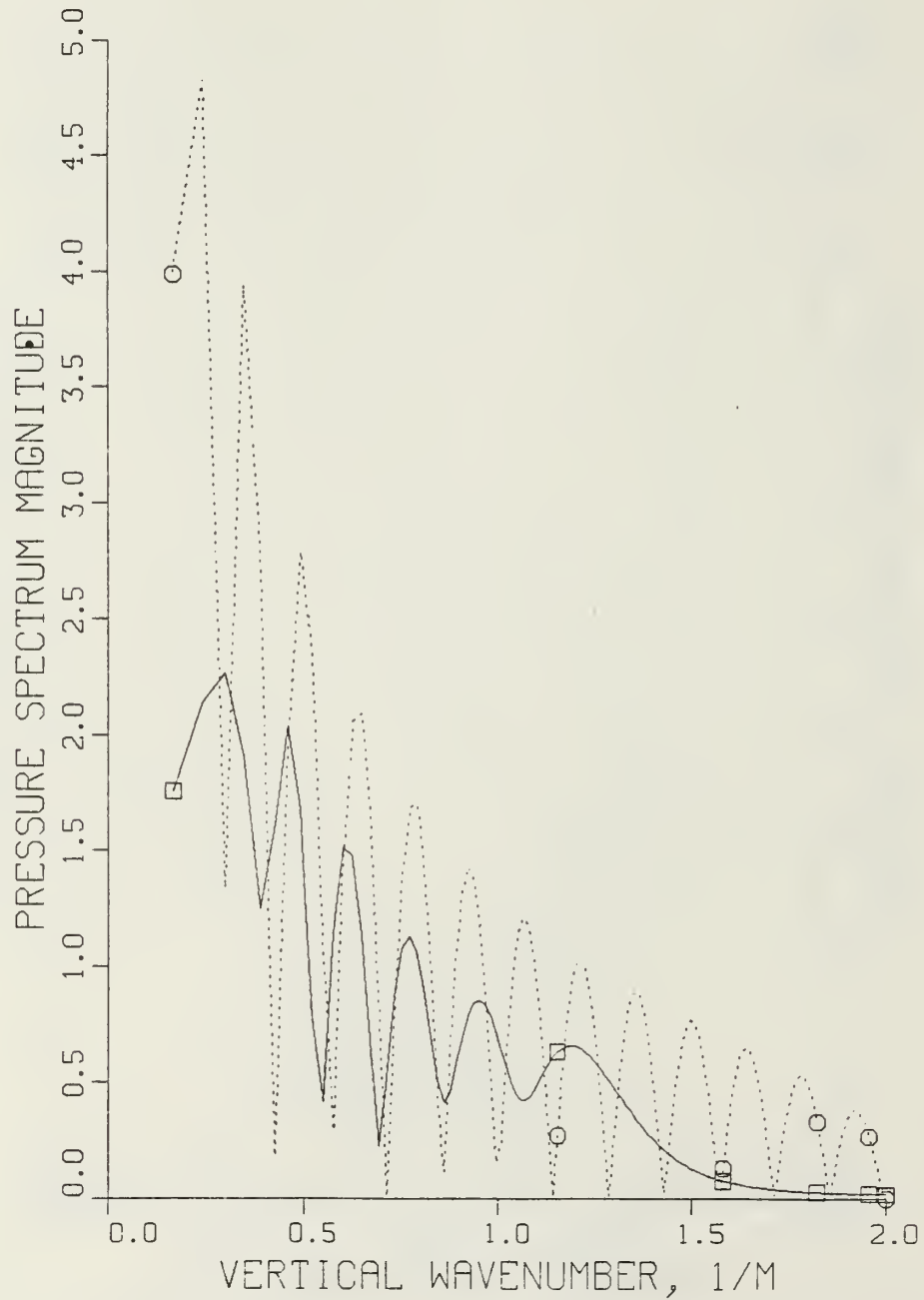
Figure 3.17   Pressure Spectrum,
Range Window Set at 62.8 Meters

62

PRESSURE SPECTRUM VS KZ

SOURCE DEPTH = 21.998 M, K = 2.0/M
RECEIVER DEPTH = 47.124 M, H = 0.0 M
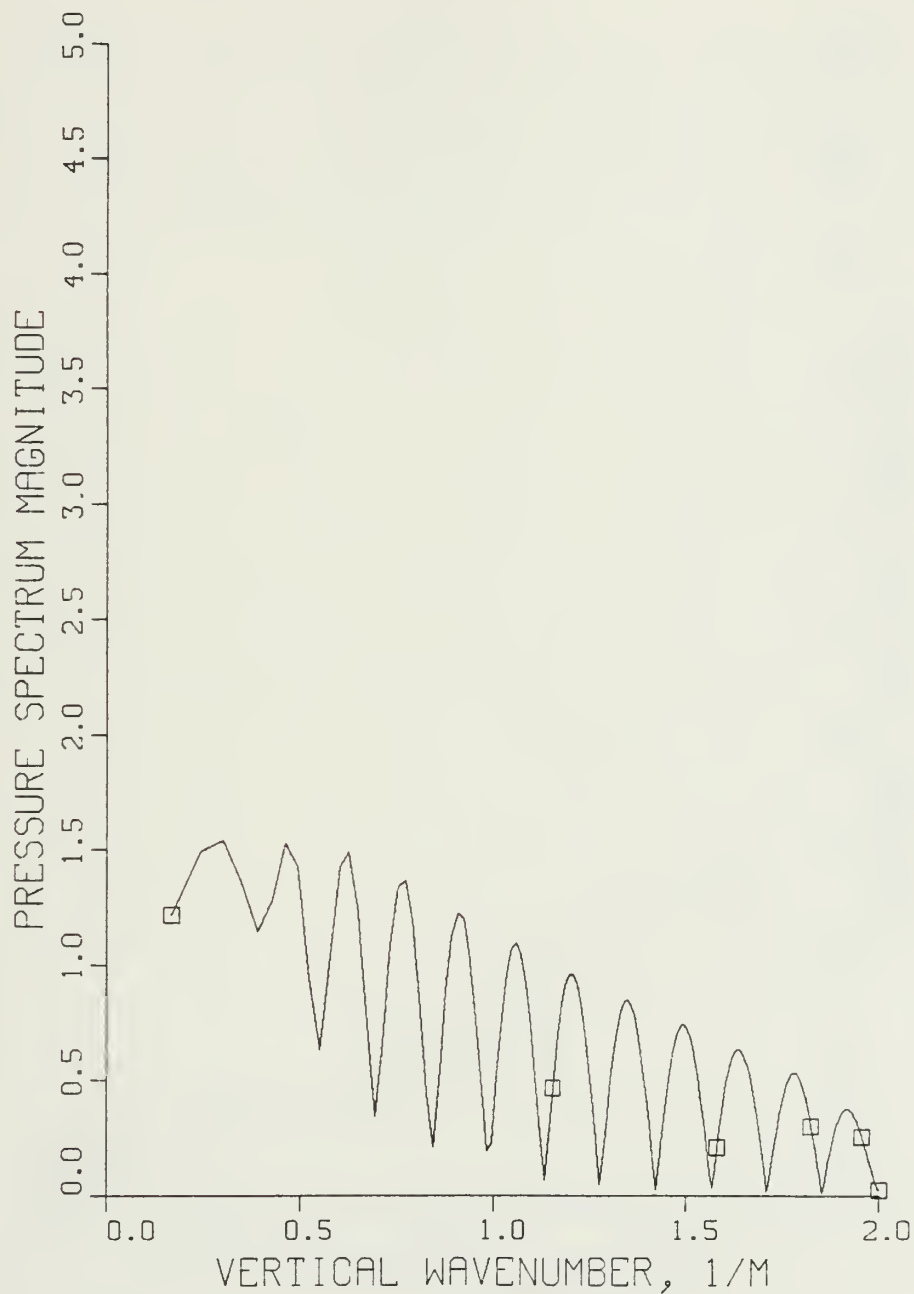
Figure 3.18   Pressure Spectrum, Sea State 0

63
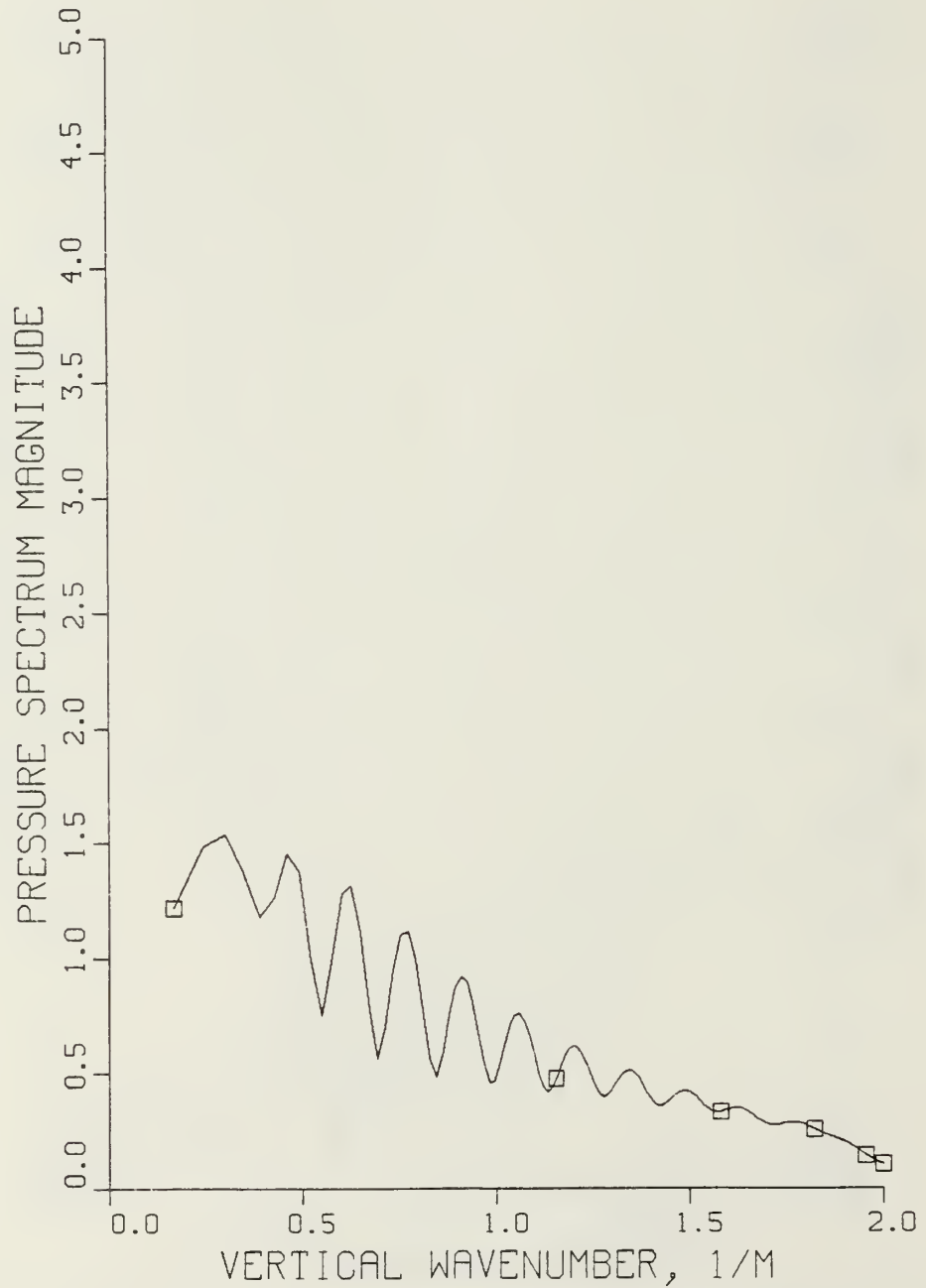
Figure 3.19   Pressure Spectrum, Sea State 2
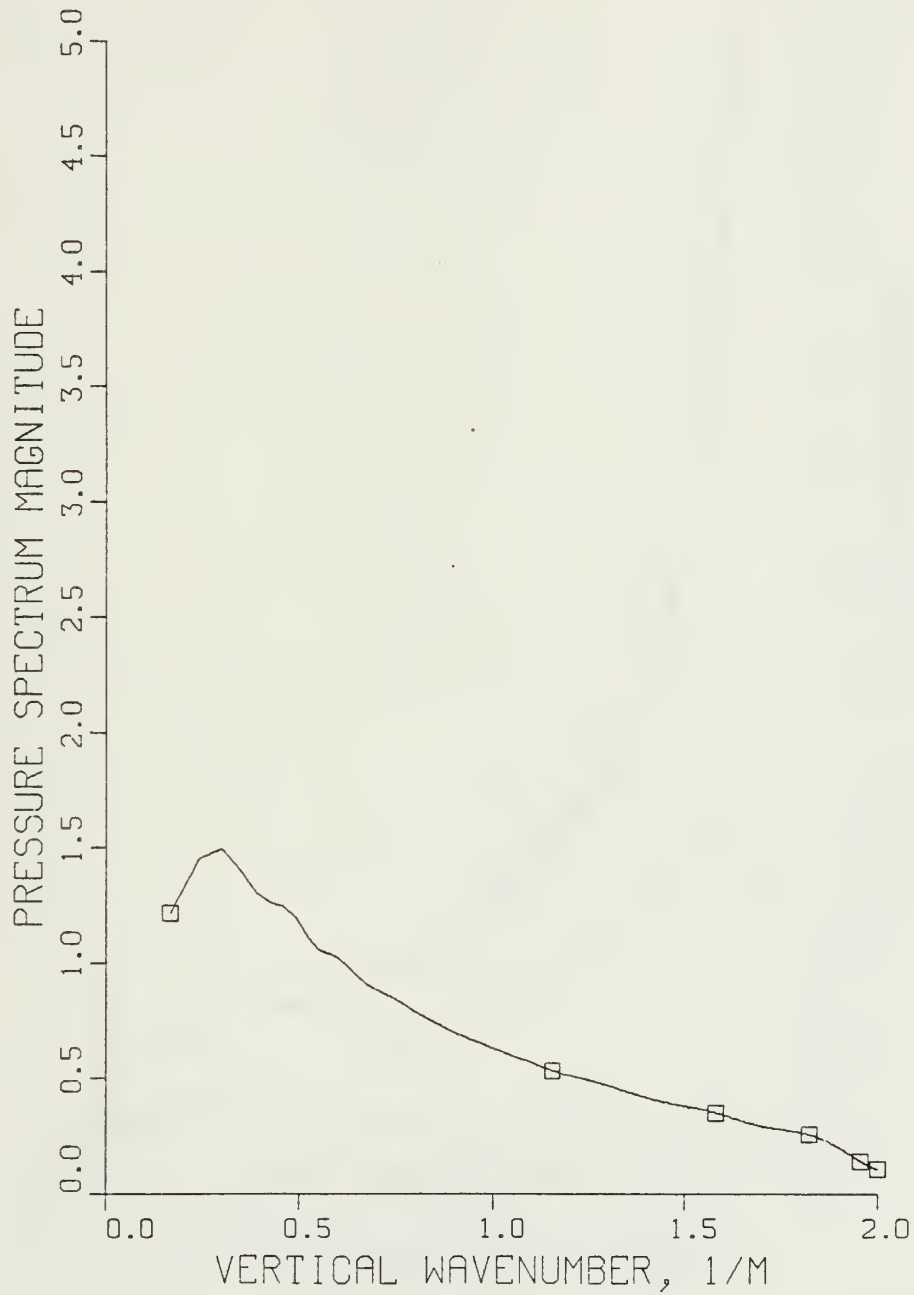
Figure 3.20   Pressure Spectrum, Sea State 3

65
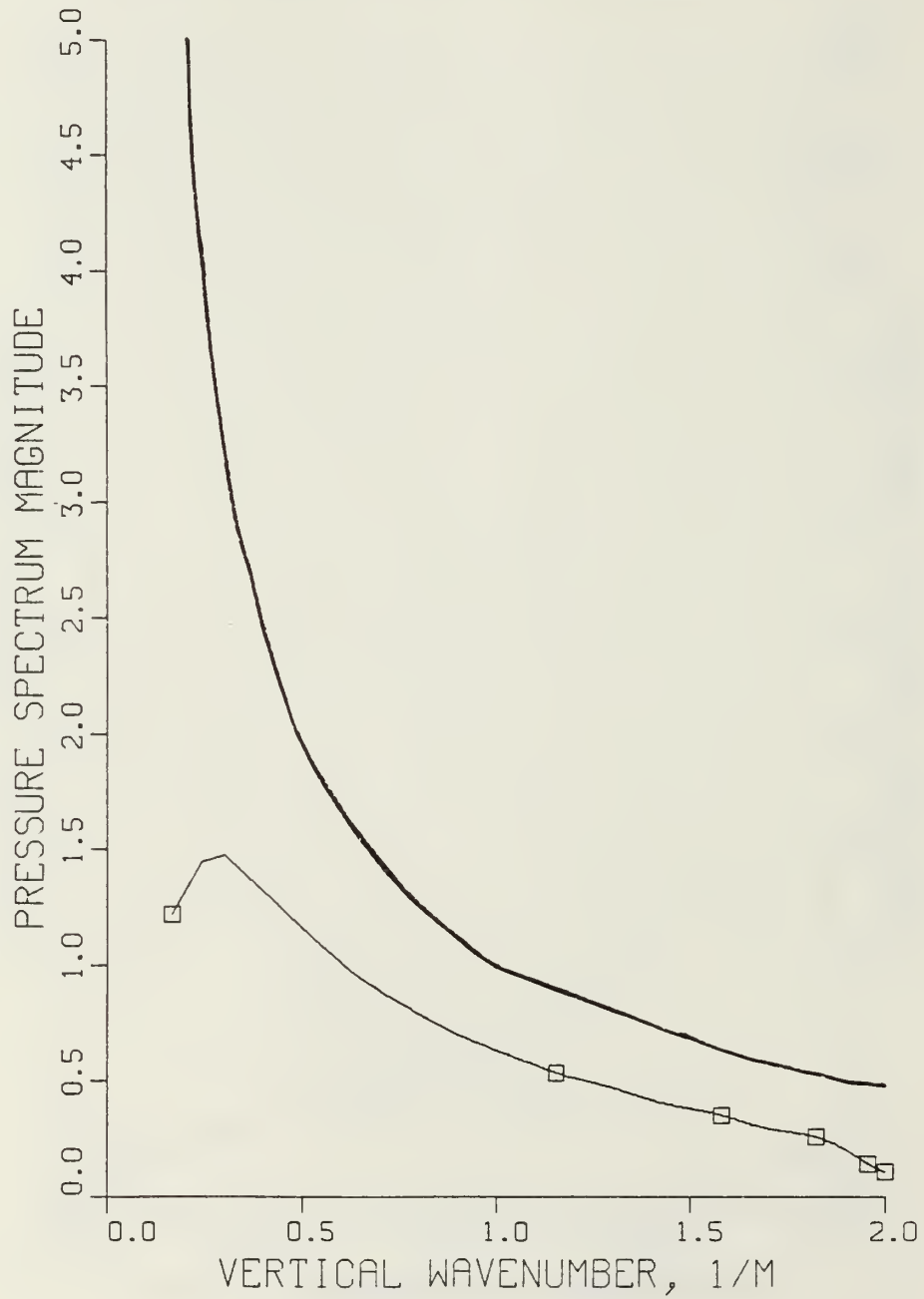
Figure 3.21   Pressure Spectrum, Sea State 5

66

PRESSURE SPECTRUM VS KH

SOURCE DEPTH = 21.998 M, N = 1024

RECEIVER DEPTH = 47.124 M

Figure 3.22   Pressure Spectrum, Sea State 0, K = 1.0

67

Figure 3.23   Pressure Spectrum, Sea State 3, K = 1.0

68

PRESSURE SPECTRUM VS KH

SOURCE DEPTH = 21.998 M, N = 1024

RECEIVER DEPTH = 47.124 M
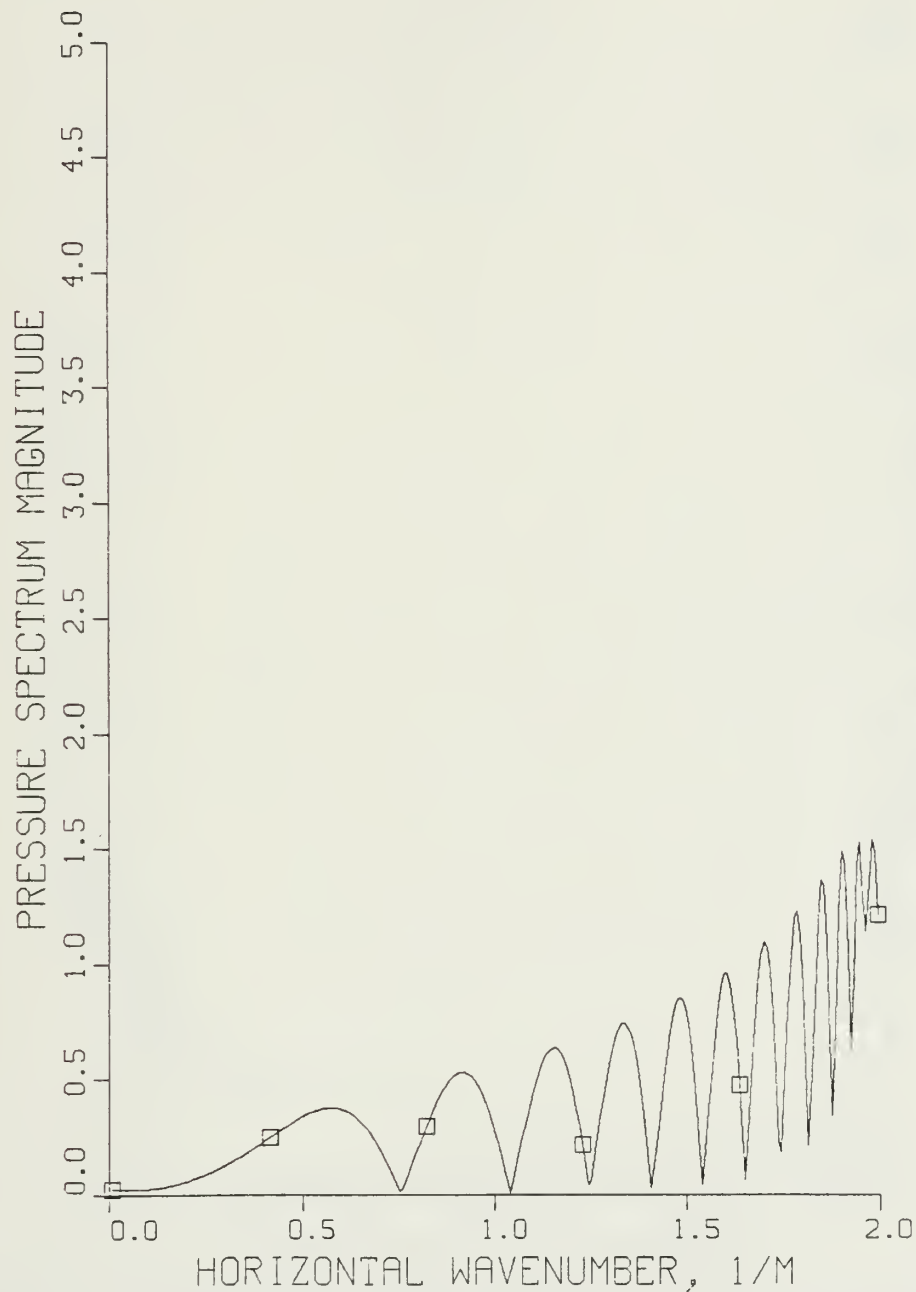
Figure 3.24   Pressure Spectrum, Sea State 0, K = 2.0

69
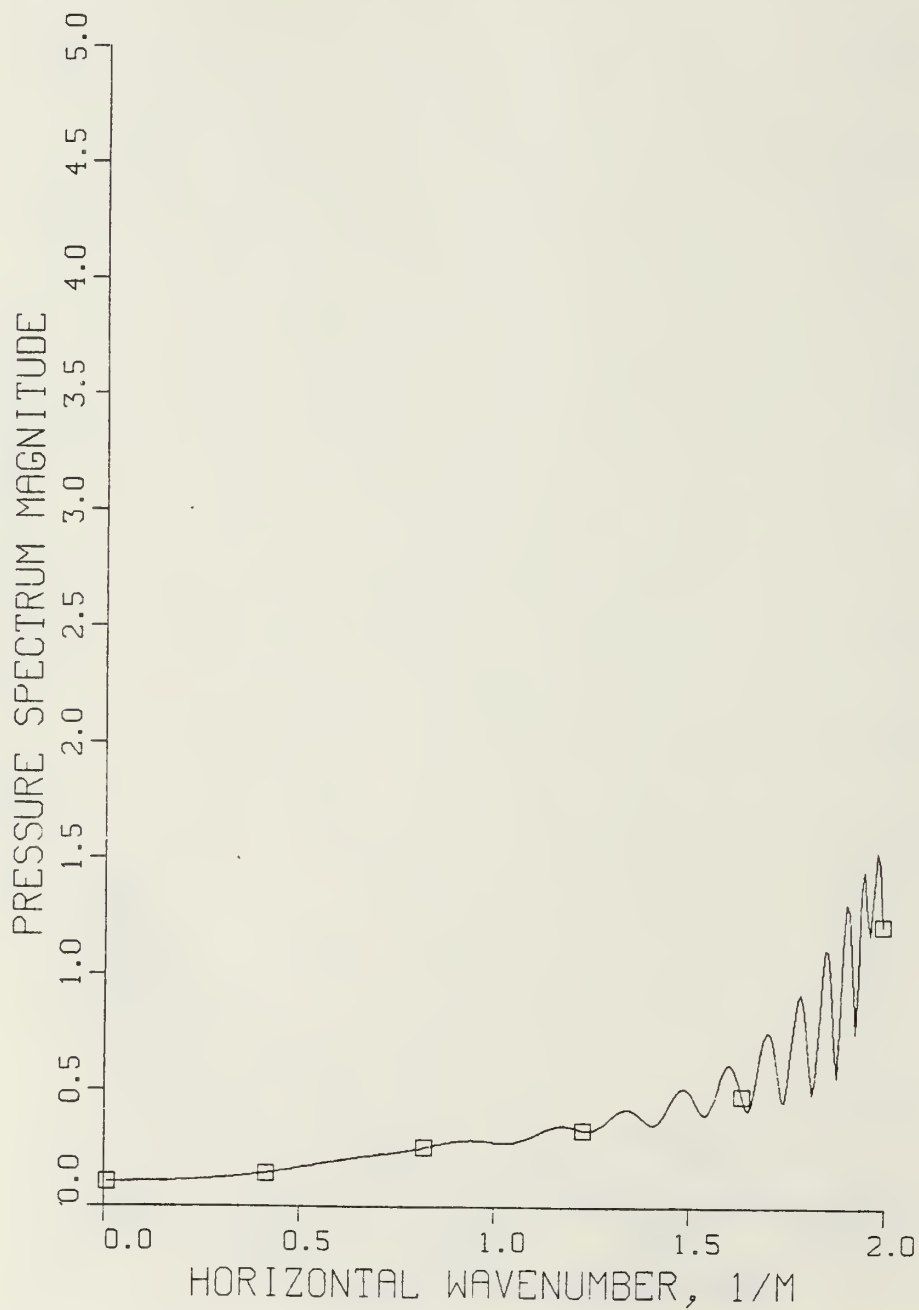
Figure 3.25   Pressure Spectrum, Sea State 3, K = 2.0

70
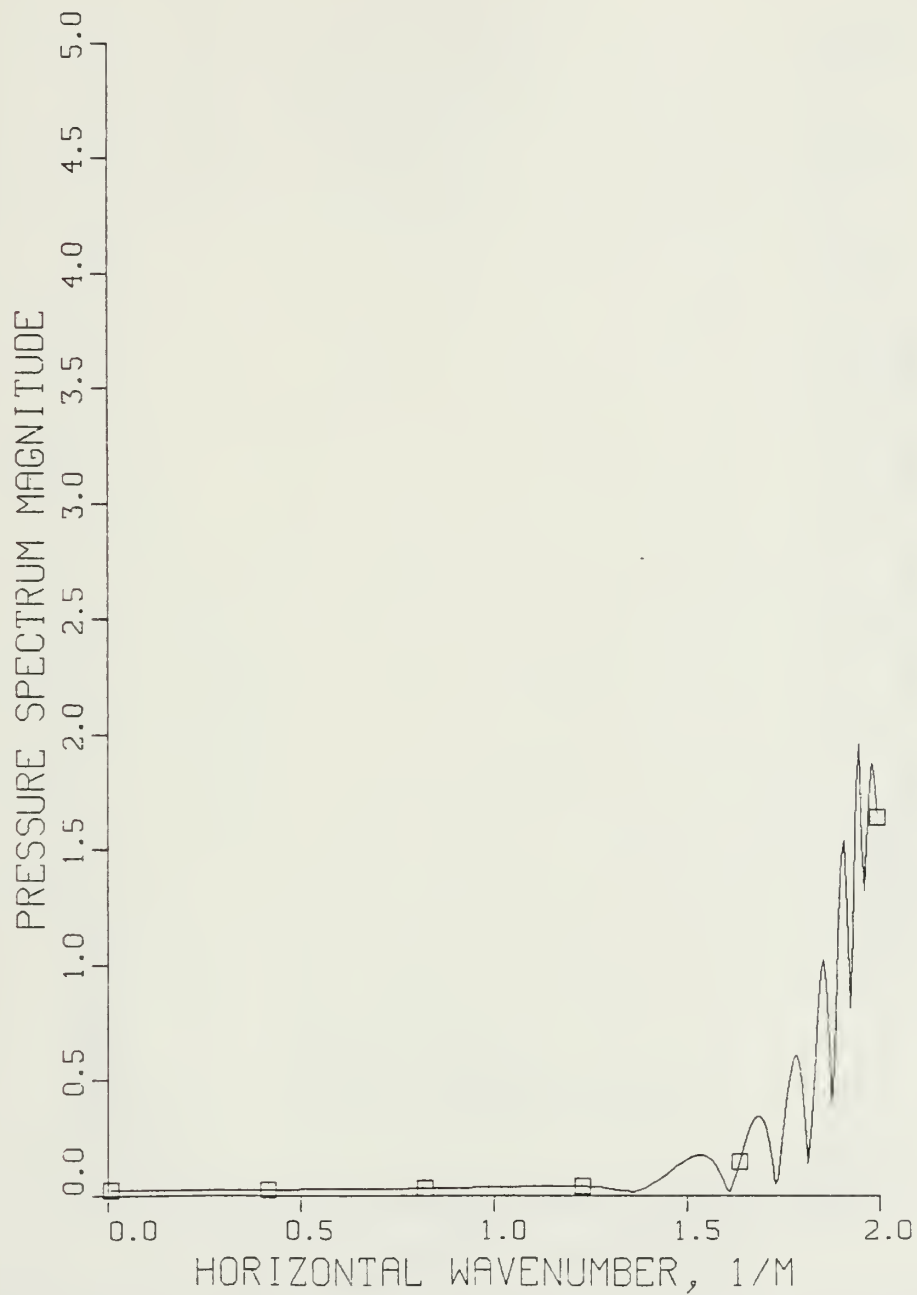
Figure 3.26   Pressure Spectrum,
SS 2, Range Window Set at 50 Meters

71
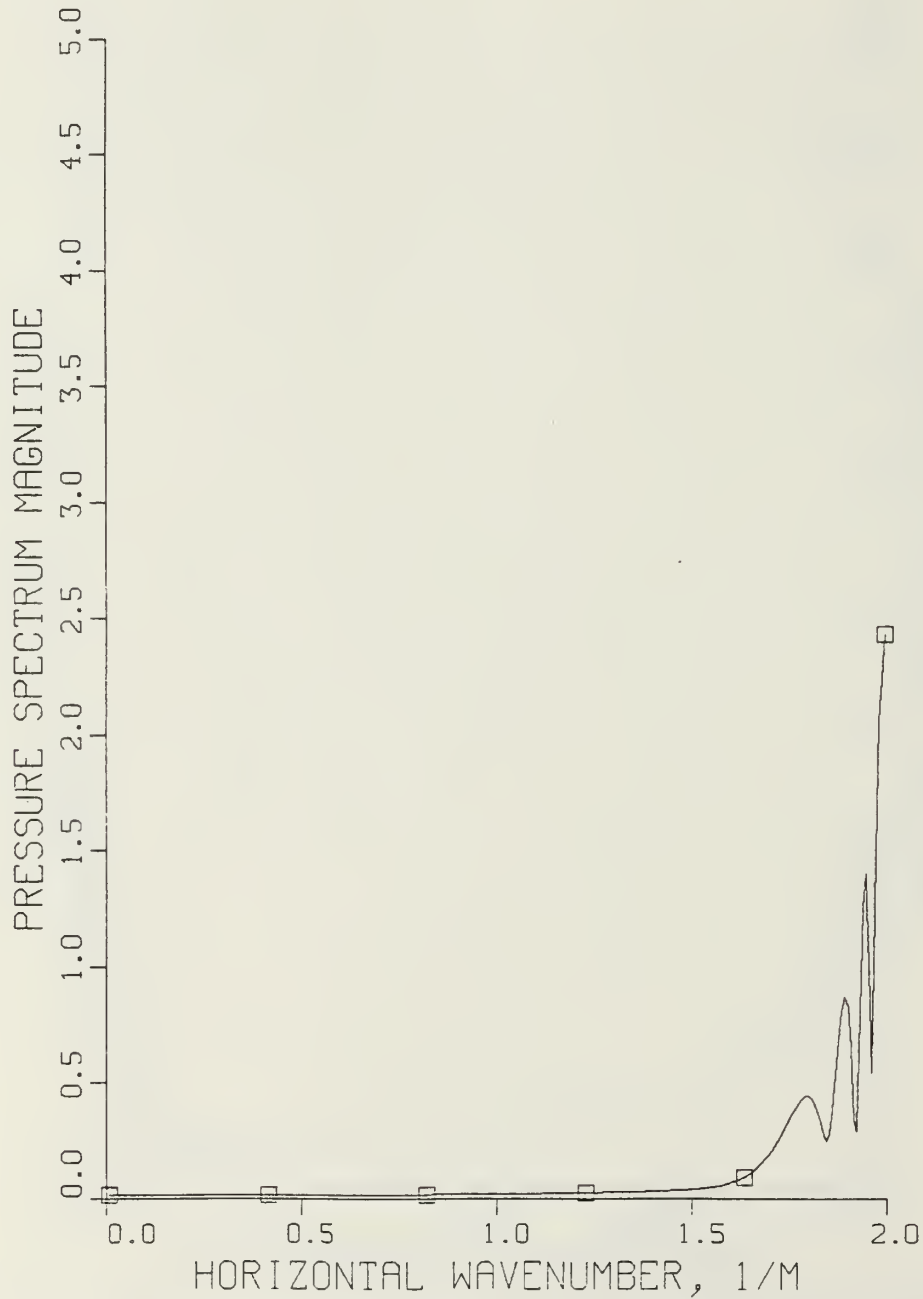
Figure 3.27   Pressure Spectrum,
SS 2, Range Window Set at 100 Meters
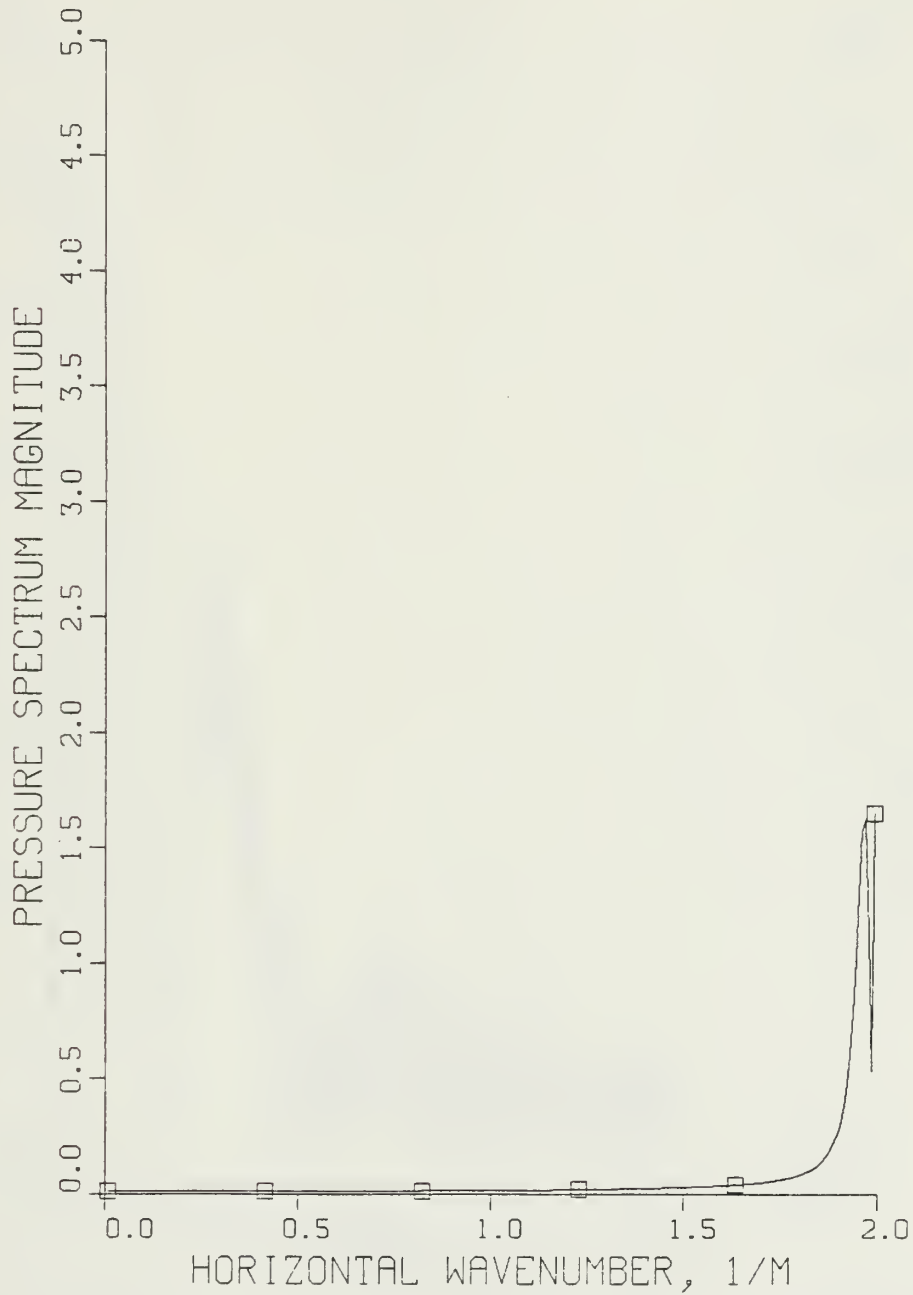
Figure 3.28   Pressure Spectrum,
SS 2, Range Window Set at 200 Meters

73
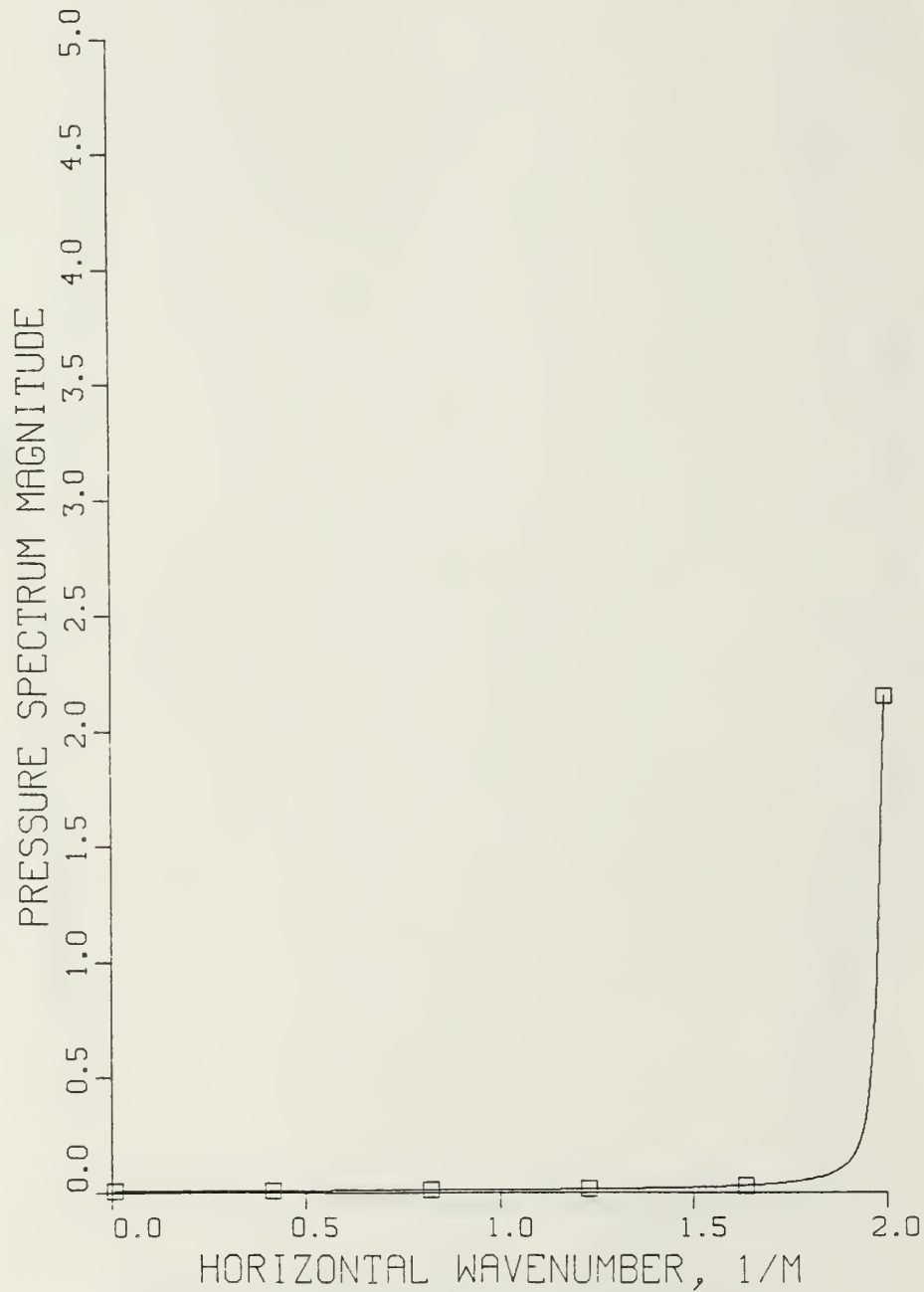
Figure 3.29   Pressure Spectrum,
SS 2, Range Window Set at 300 Meters

74

MAGNITUDE OF PRESSURE AS A FN OF RANGE

SOURCE DEPTH = 21.998 M, RECEIVER DEPTH = 47.124 M,
RANGE STEP SIZE = 1.57 M, N = 1024
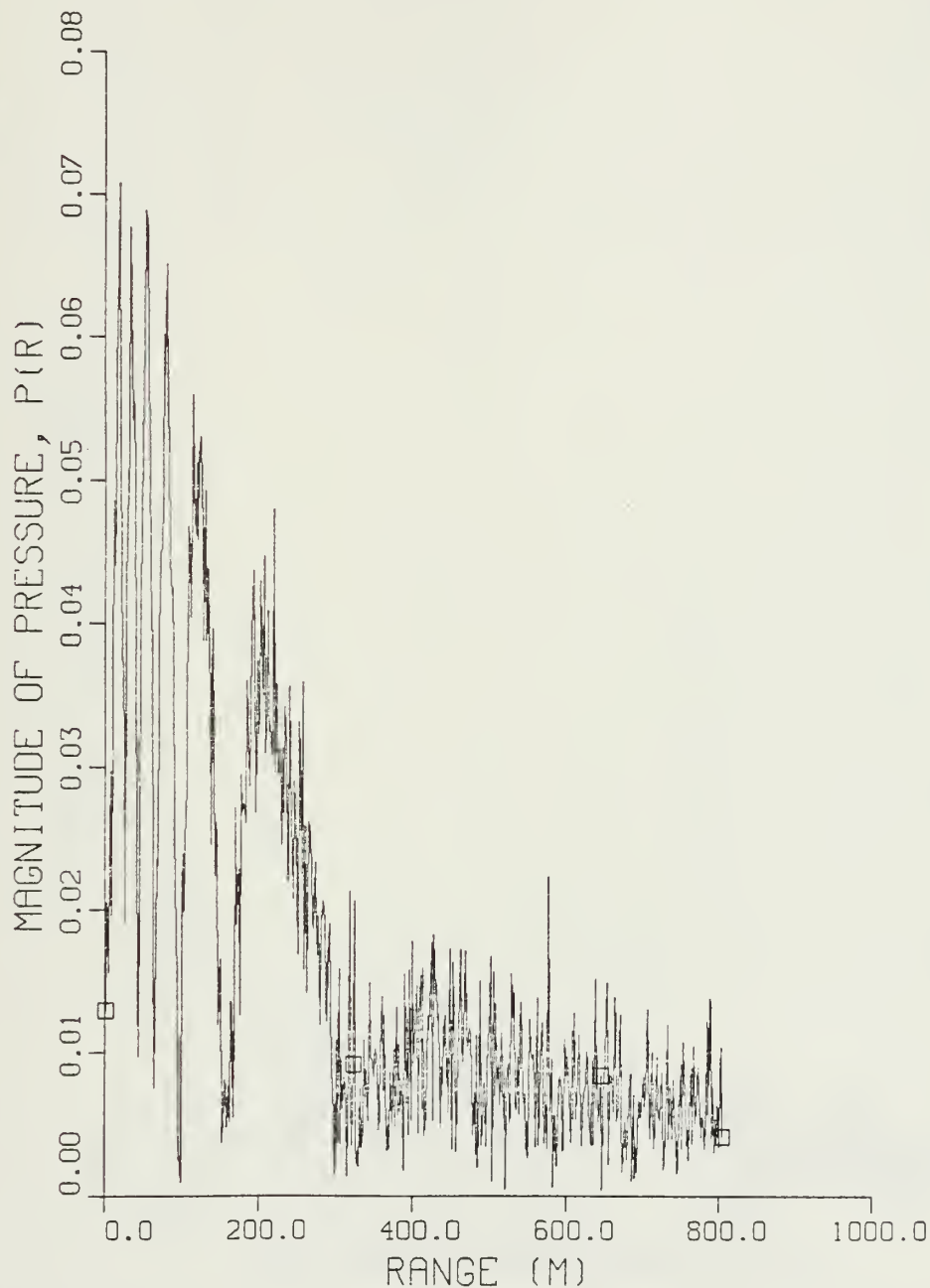
Figure 3.30   Pressure Field, K = 1.0, μ = 0.005

75
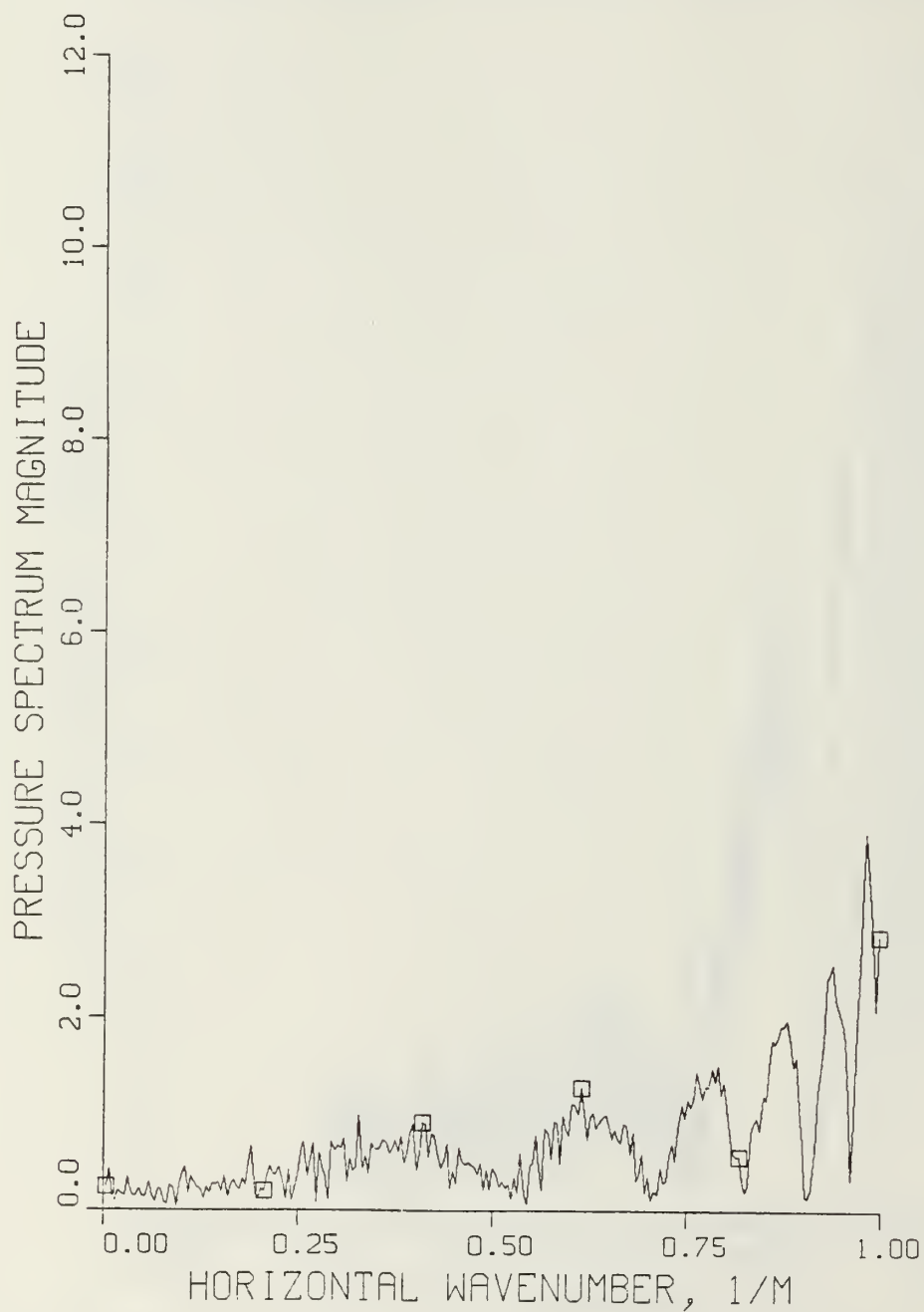
Figure 3.31   Pressure Spectrum vs. Gamma
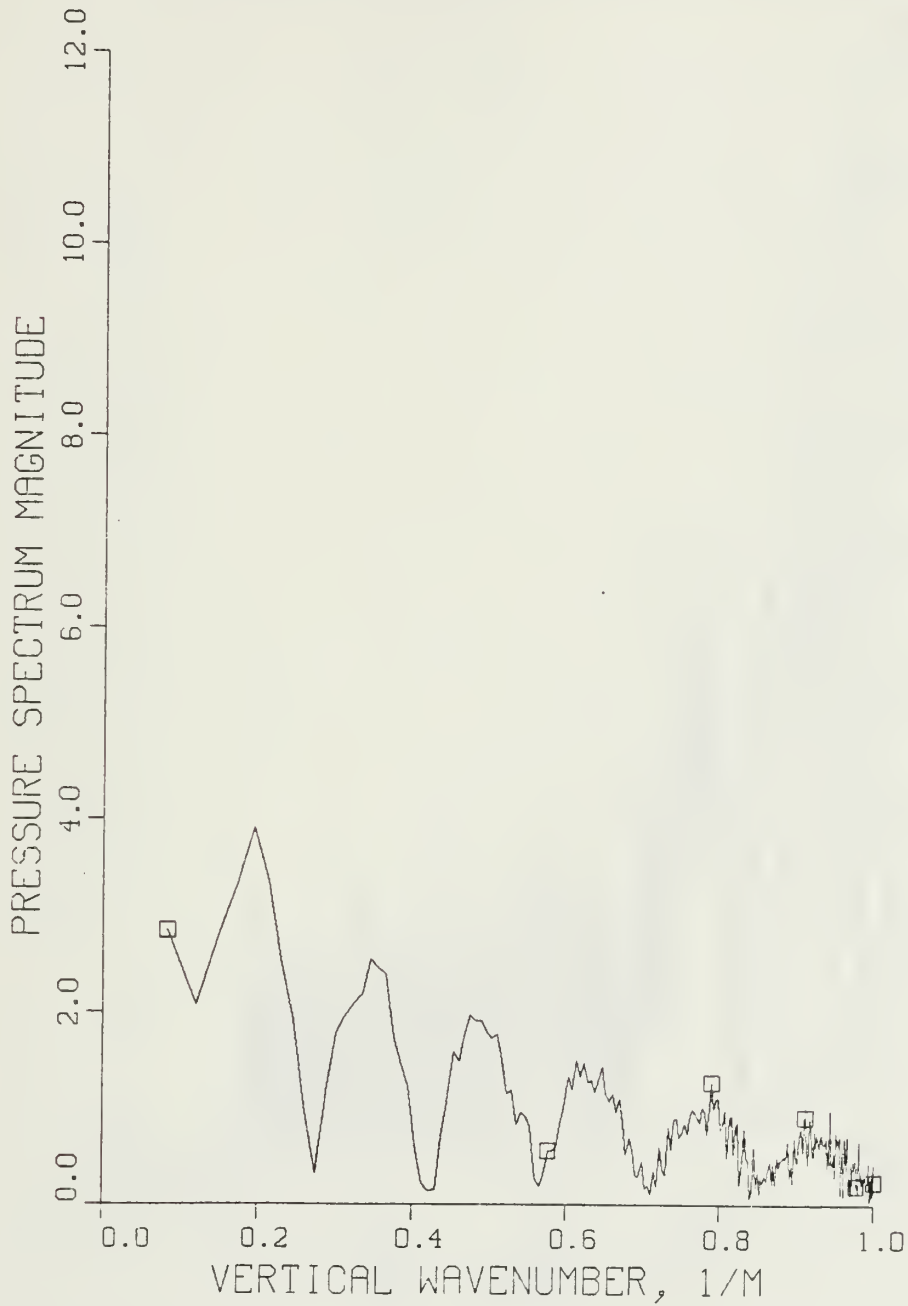
Figure 3.32   Pressure Spectrum vs. Beta

77

MAGNITUDE OF PRESSURE AS A FN OF RANGE

SOURCE DEPTH = 21.998 M, RECEIVER DEPTH = 47.124 M,
RANGE STEP SIZE = 1.57 M, N = 1024
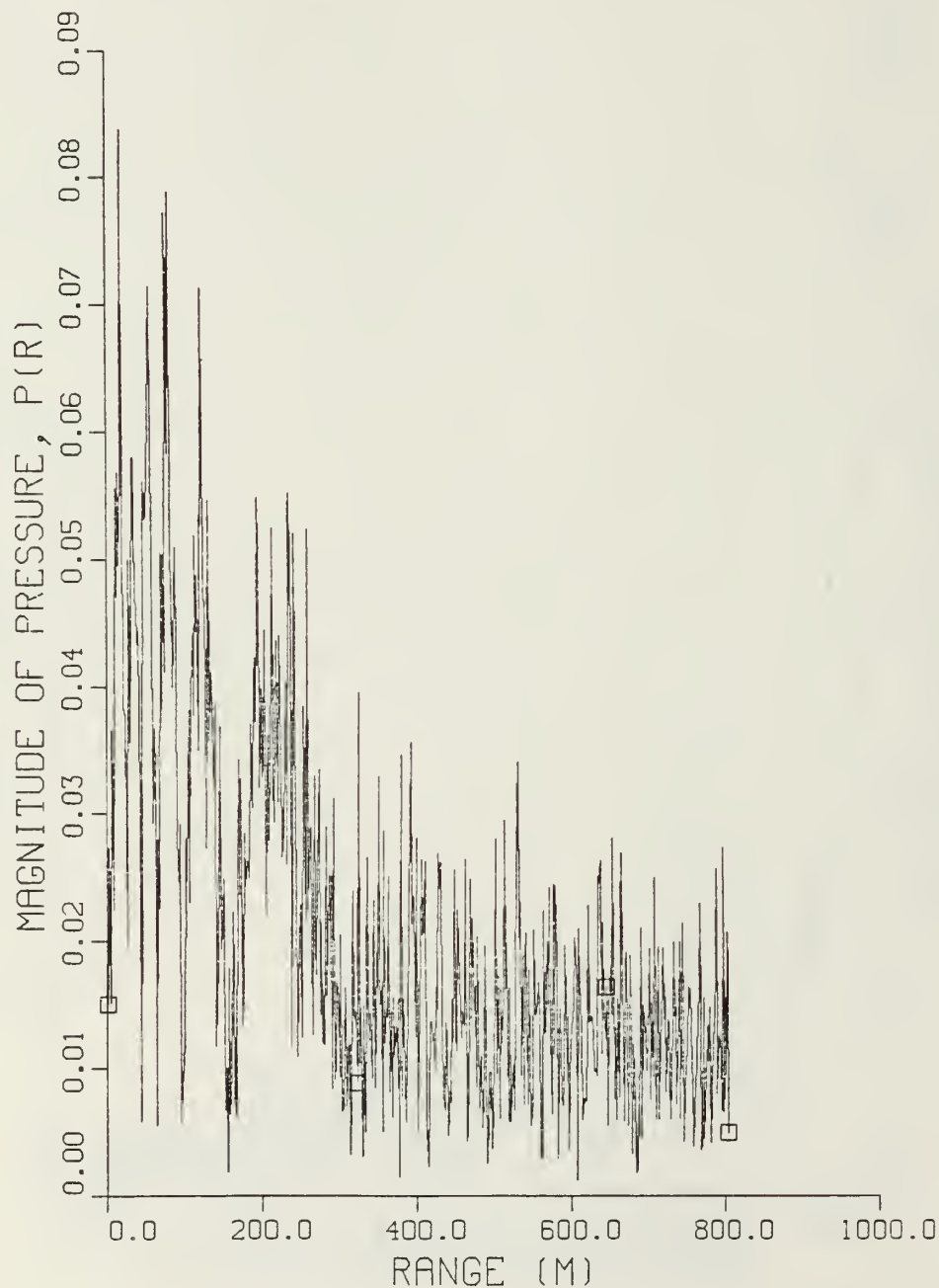
Figure 3.33   Pressure Field, K = 1.0, μ = 0.01

78

Figure 3.34   Pressure Spectrum vs. Gamma

79
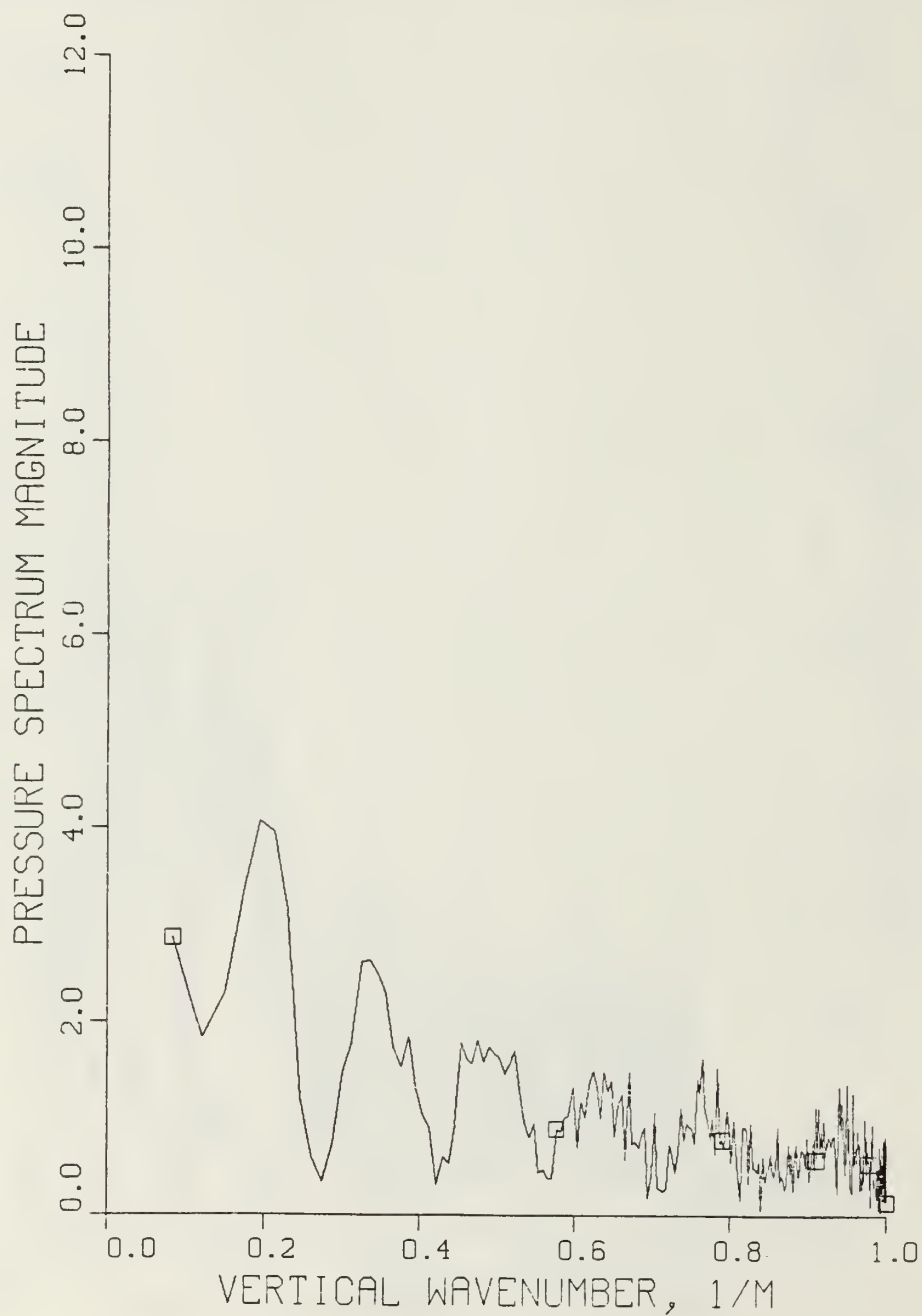
Figure 3.35   Pressure Spectrum vs. Beta
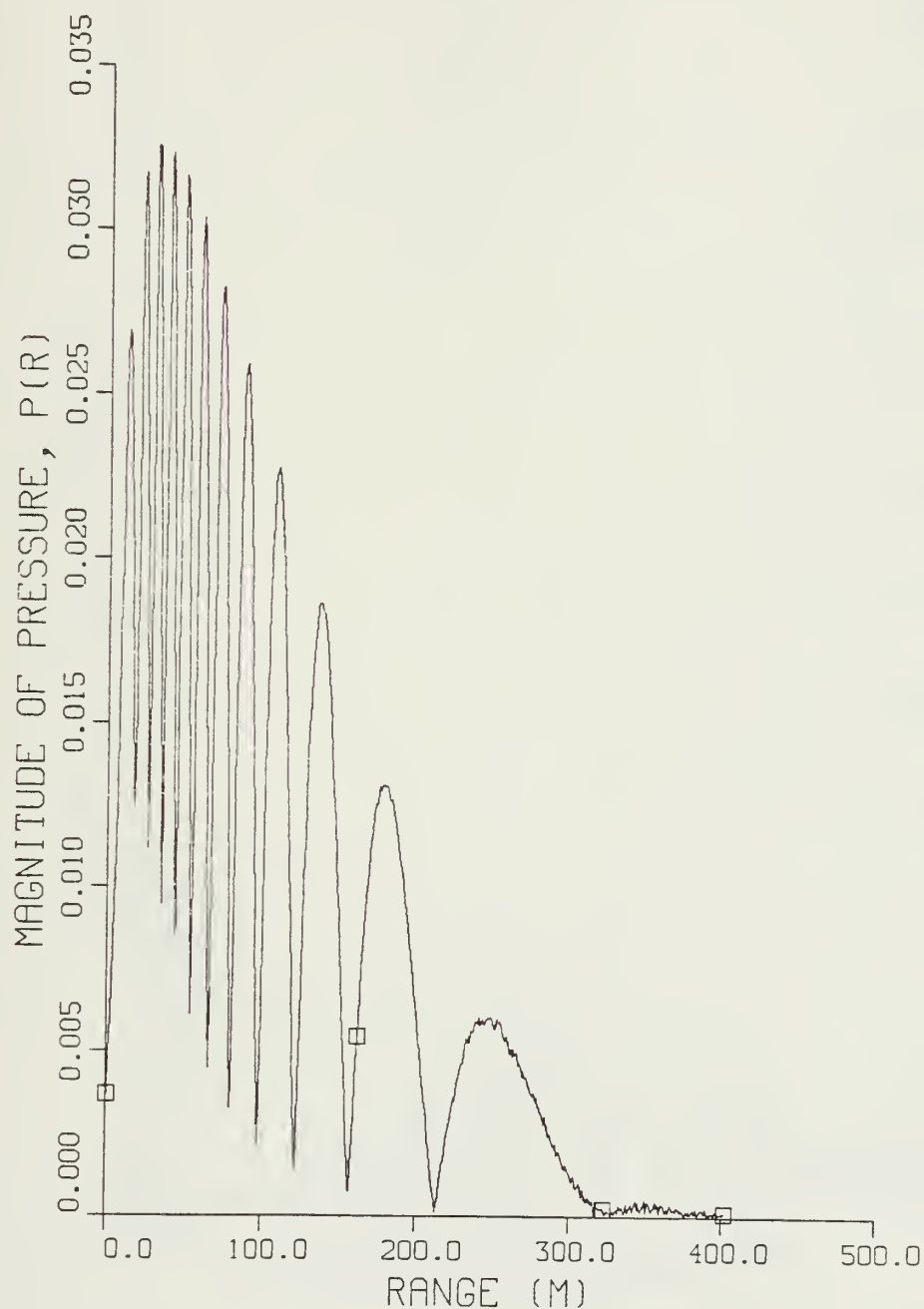
Figure 3.36   Pressure Field, K = 2.0, μ = 0.0001

81
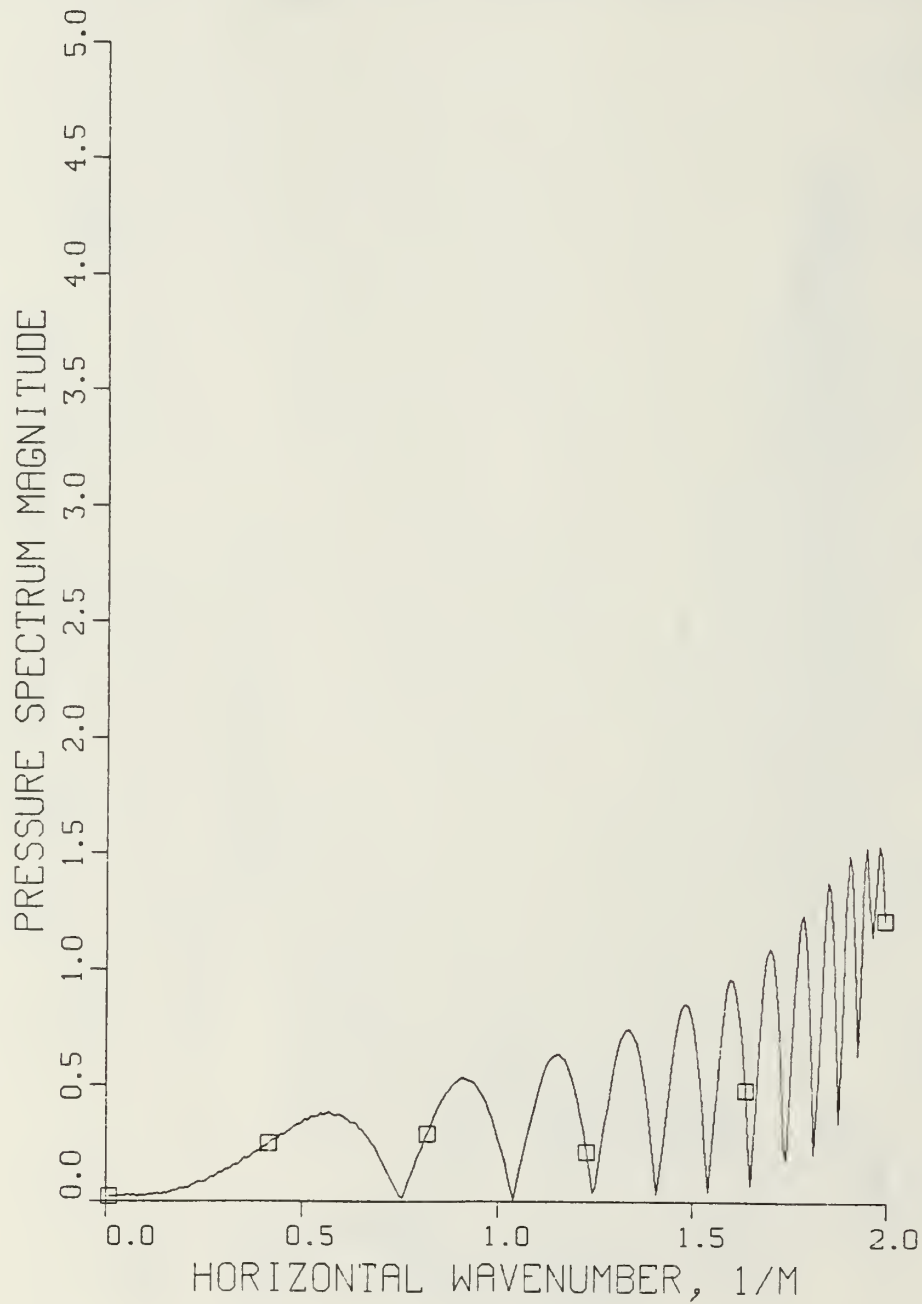
Figure 3.37   Pressure Spectrum vs. Gamma

82
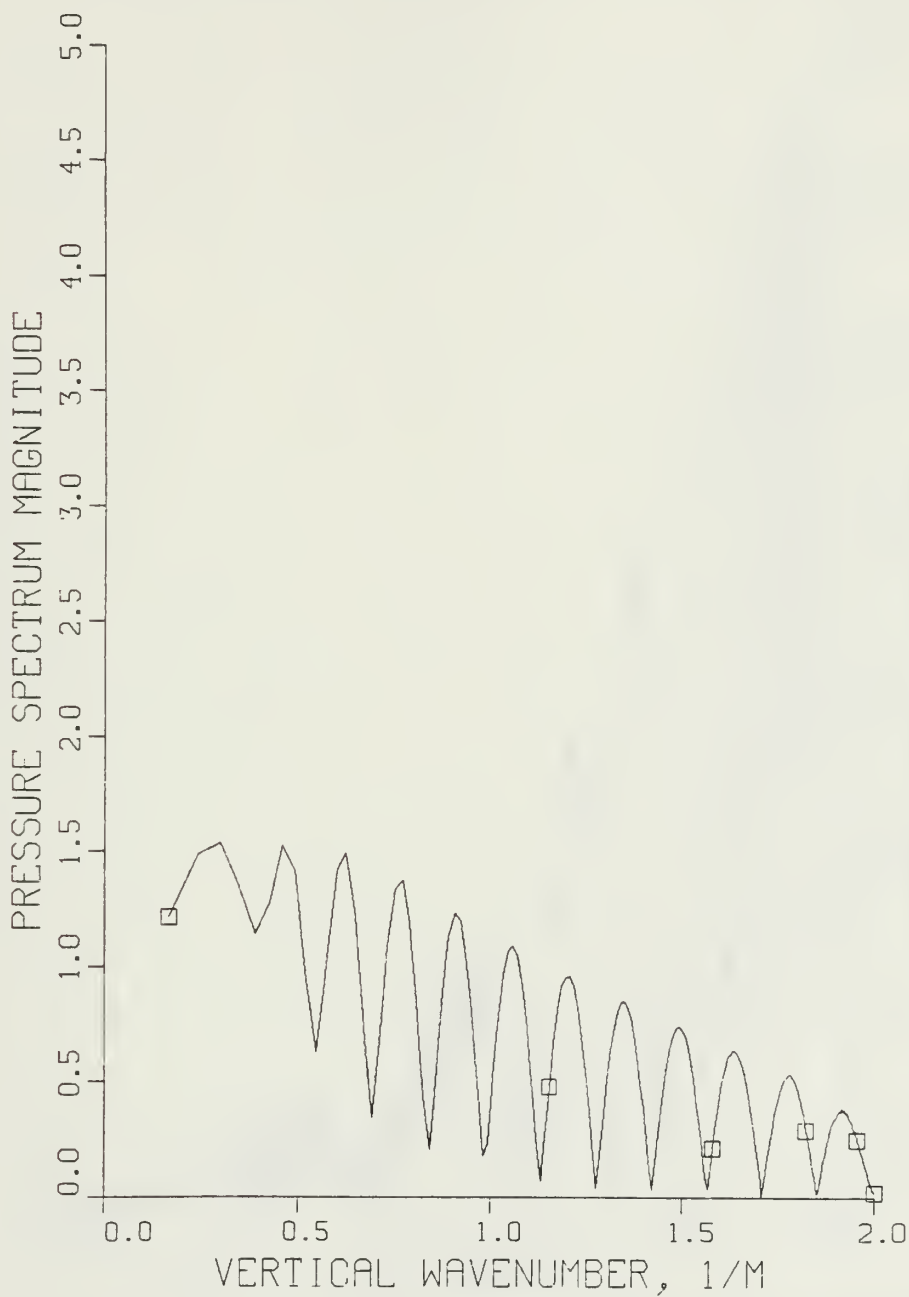
Figure 3.38   Pressure Spectrum vs. Beta

83

MAGNITUDE OF PRESSURE AS A FN OF RANGE

SOURCE DEPTH = 21.998 M, RECEIVER DEPTH = 47.124 M,
RANGE STEP SIZE = 0.785 M, N = 1024
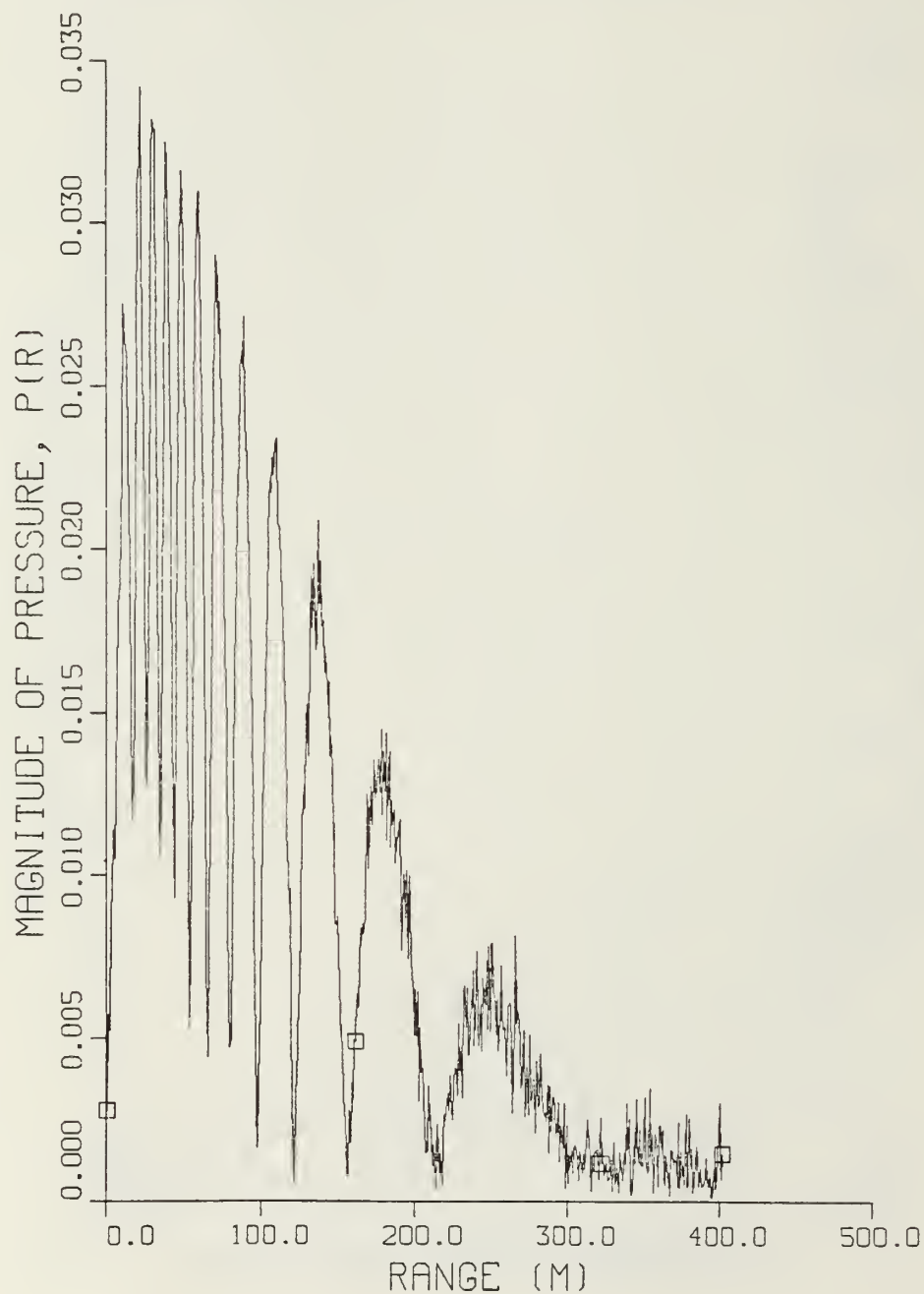
Figure 3.39   Pressure Field, K = 2.0, μ = 0.001

84

PRESSURE SPECTRUM VS KH

SOURCE DEPTH = 21.998 M, K = 2.0/M
RECEIVER DEPTH = 47.124 M, μ = 0.001
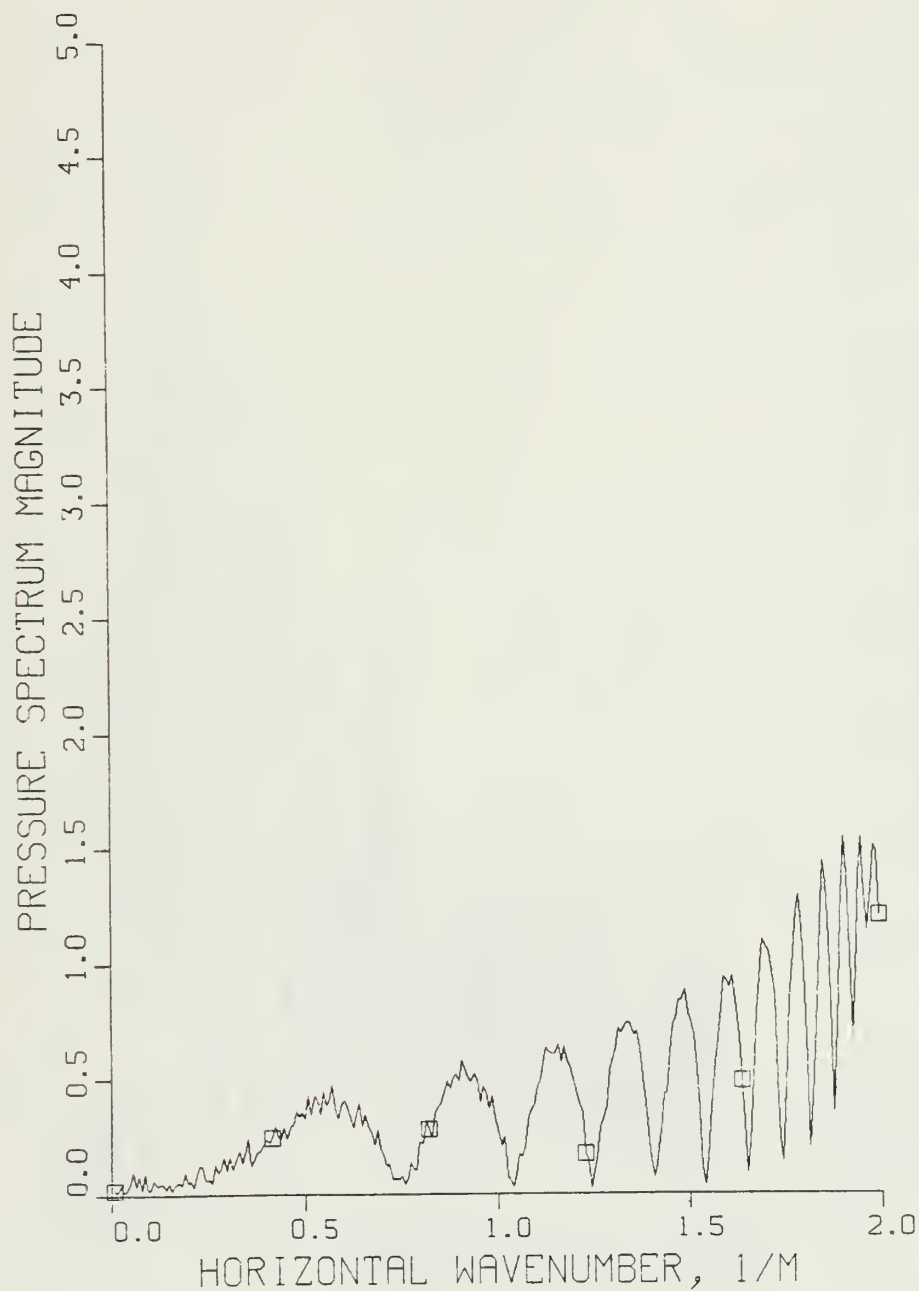
Figure 3.40   Pressure Spectrum vs. Gamma

85
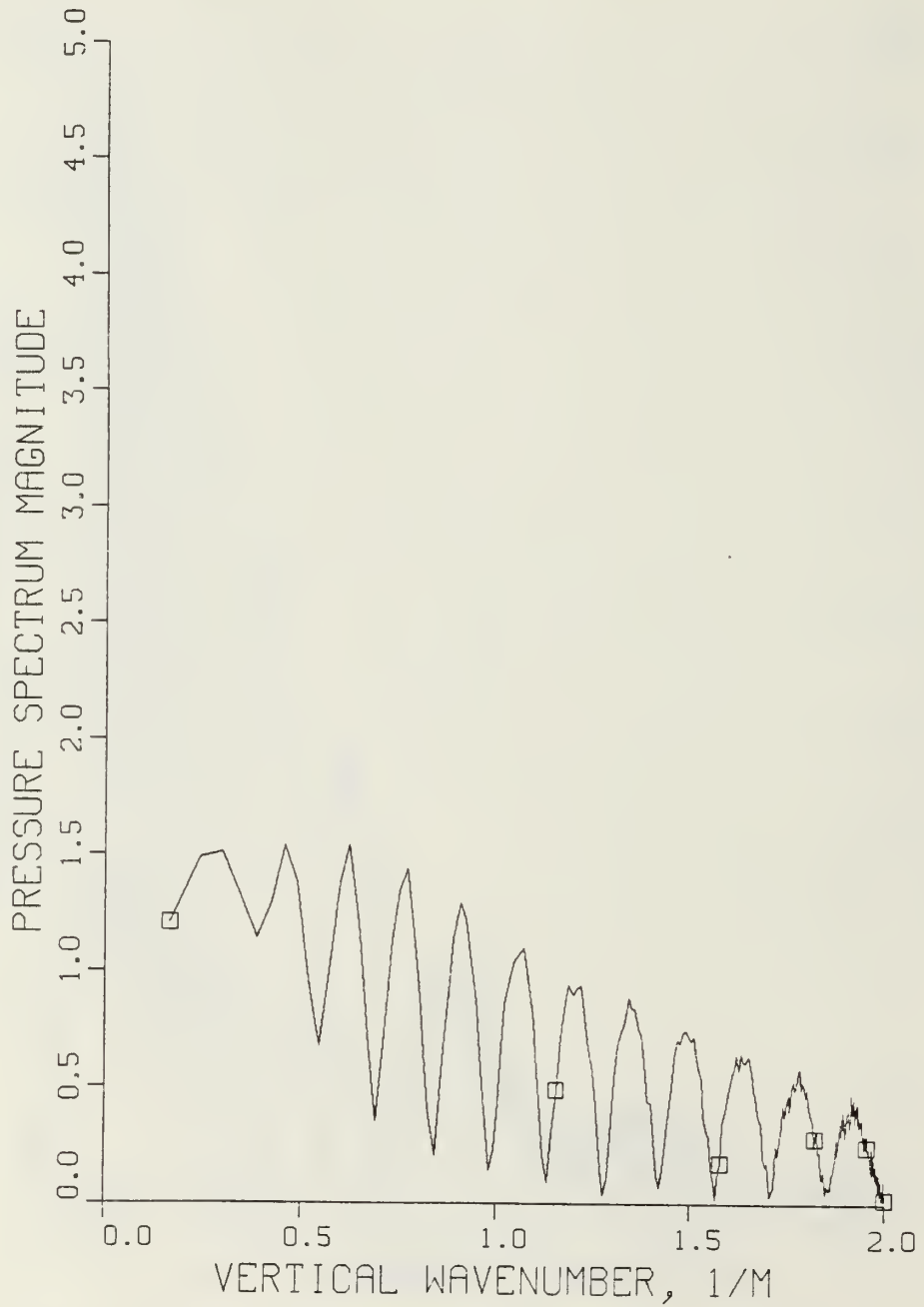
Figure 3.41   Pressure Spectrum vs. Beta
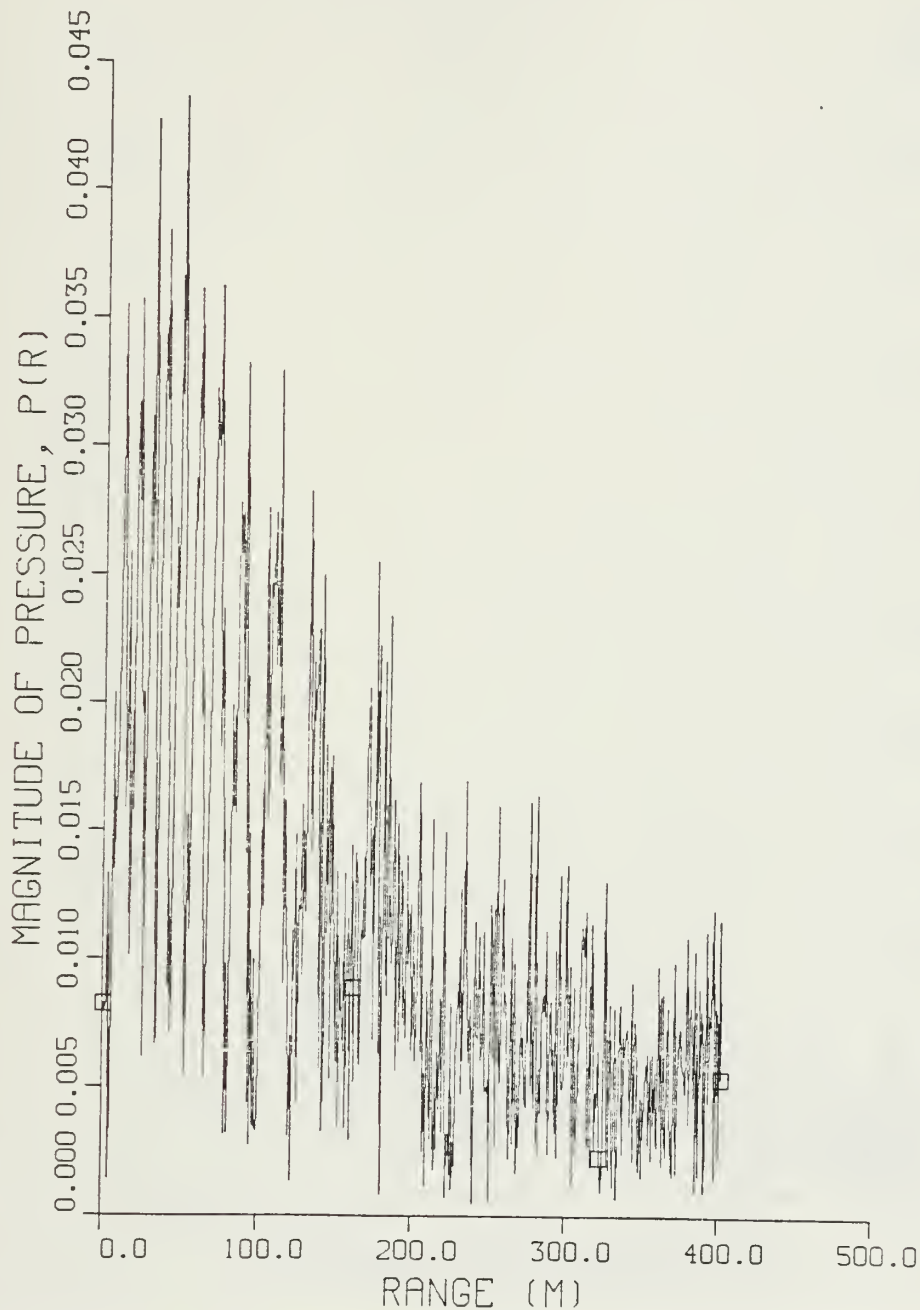
Figure 3.42   Pressure Field, K = 2.0, μ = 0.005

87
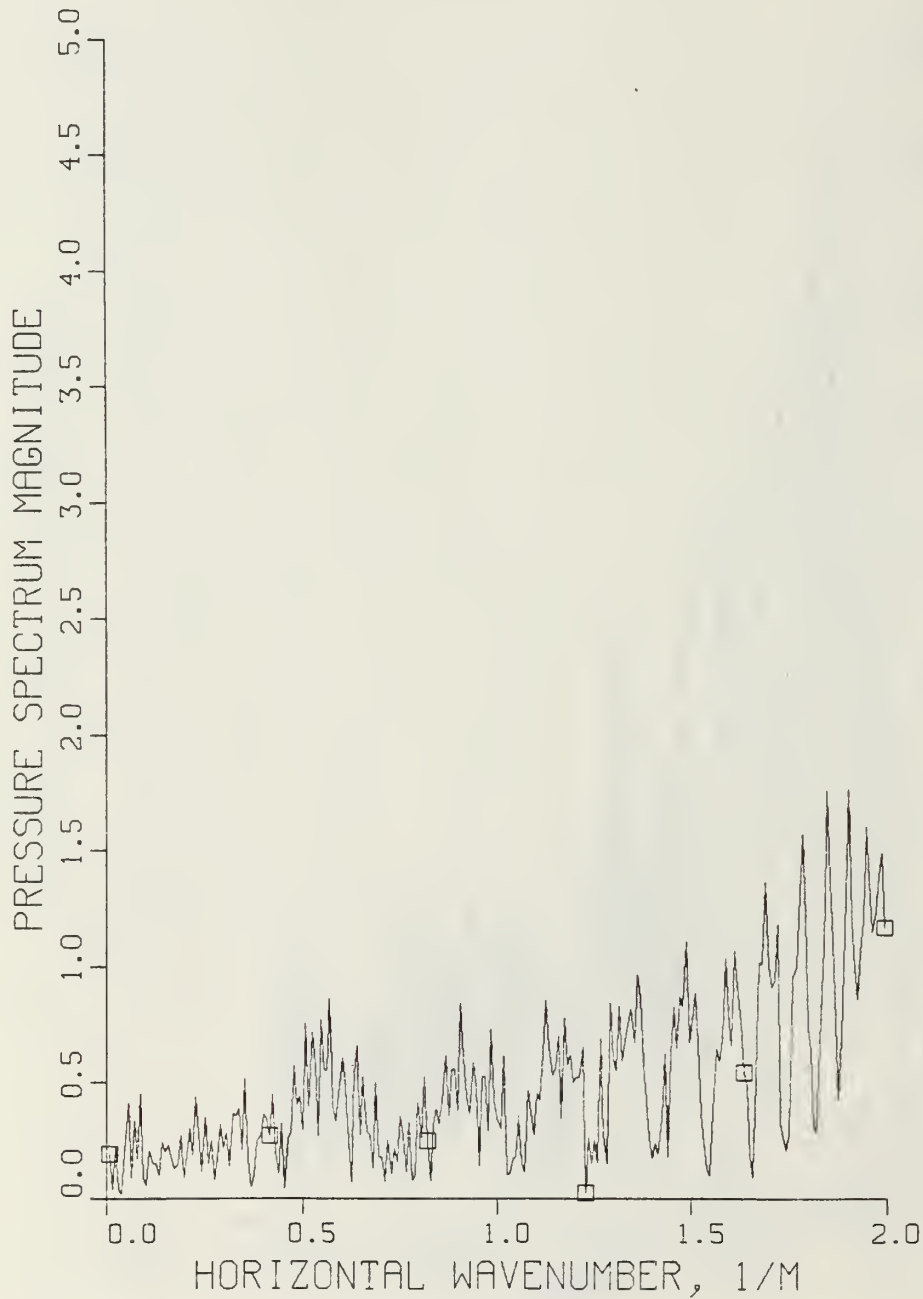
Figure 3.43   Pressure Spectrum vs. Gamma

88
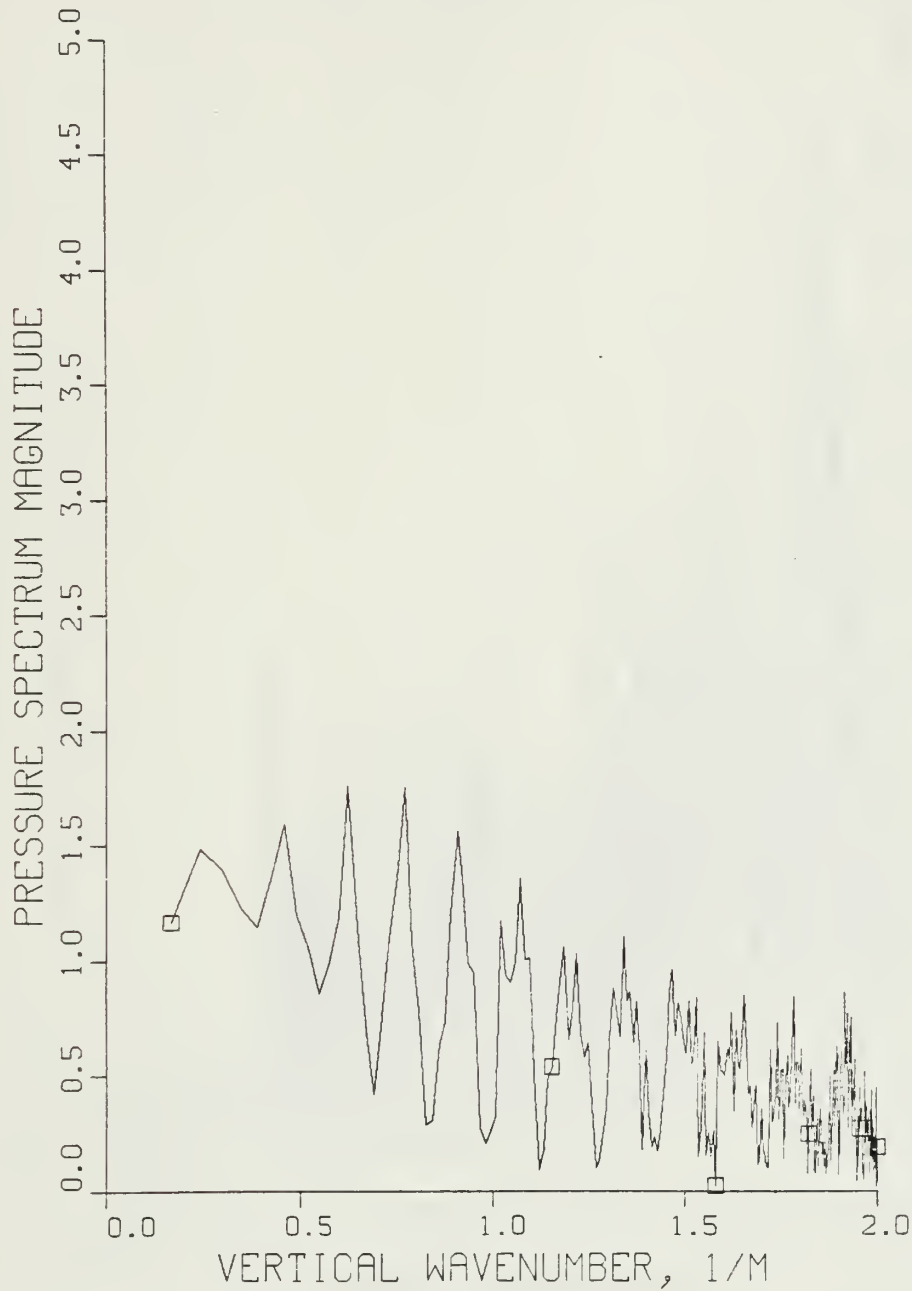
Figure 3.44   Pressure Spectrum vs. Beta

89

MAGNITUDE OF PRESSURE AS A FN OF RANGE

SOURCE DEPTH = 21.998 M, RECEIVER DEPTH = 47.124 M,
RANGE STEP SIZE = 0.785 M, N = 1024
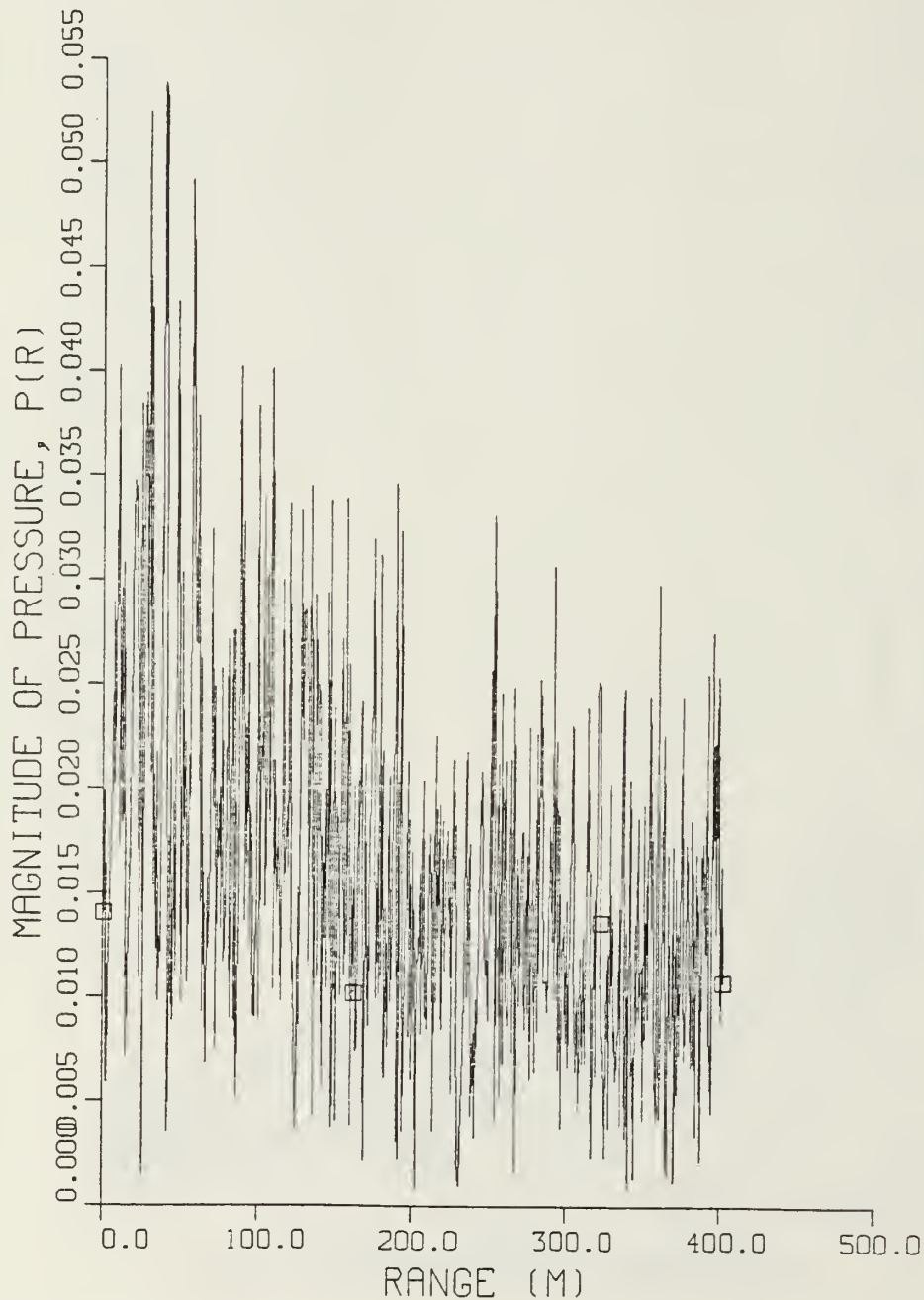
Figure 3.45   Pressure Field, $K = 2.0$, $\mu = 0.01$

90
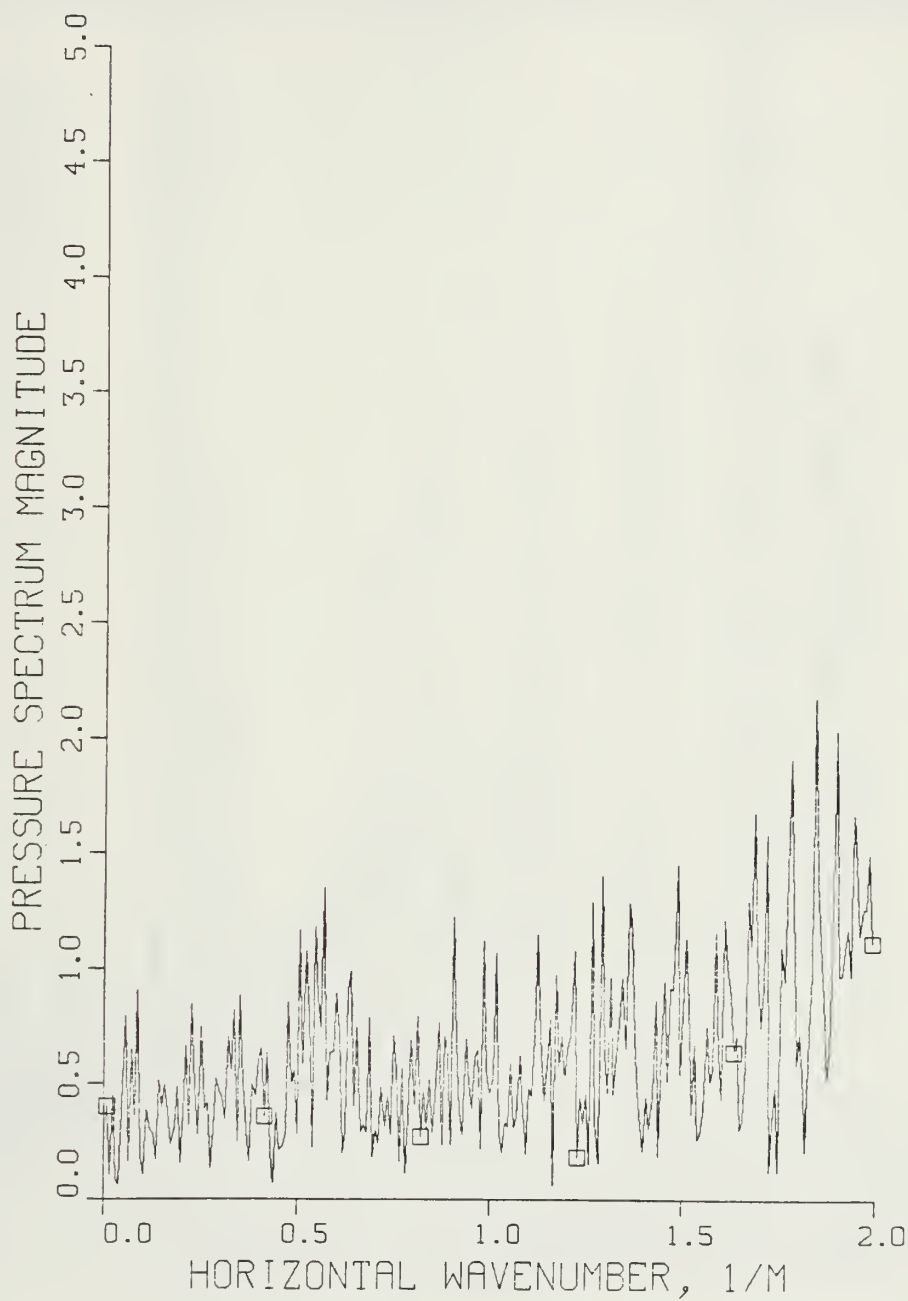
Figure 3.46   Pressure Spectrum vs. Gamma

91

PRESSURE SPECTRUM VS KZ

SOURCE DEPTH = 21.998 M, K = 2.0/M
RECEIVER DEPTH = 47.124 M, μ = 0.01
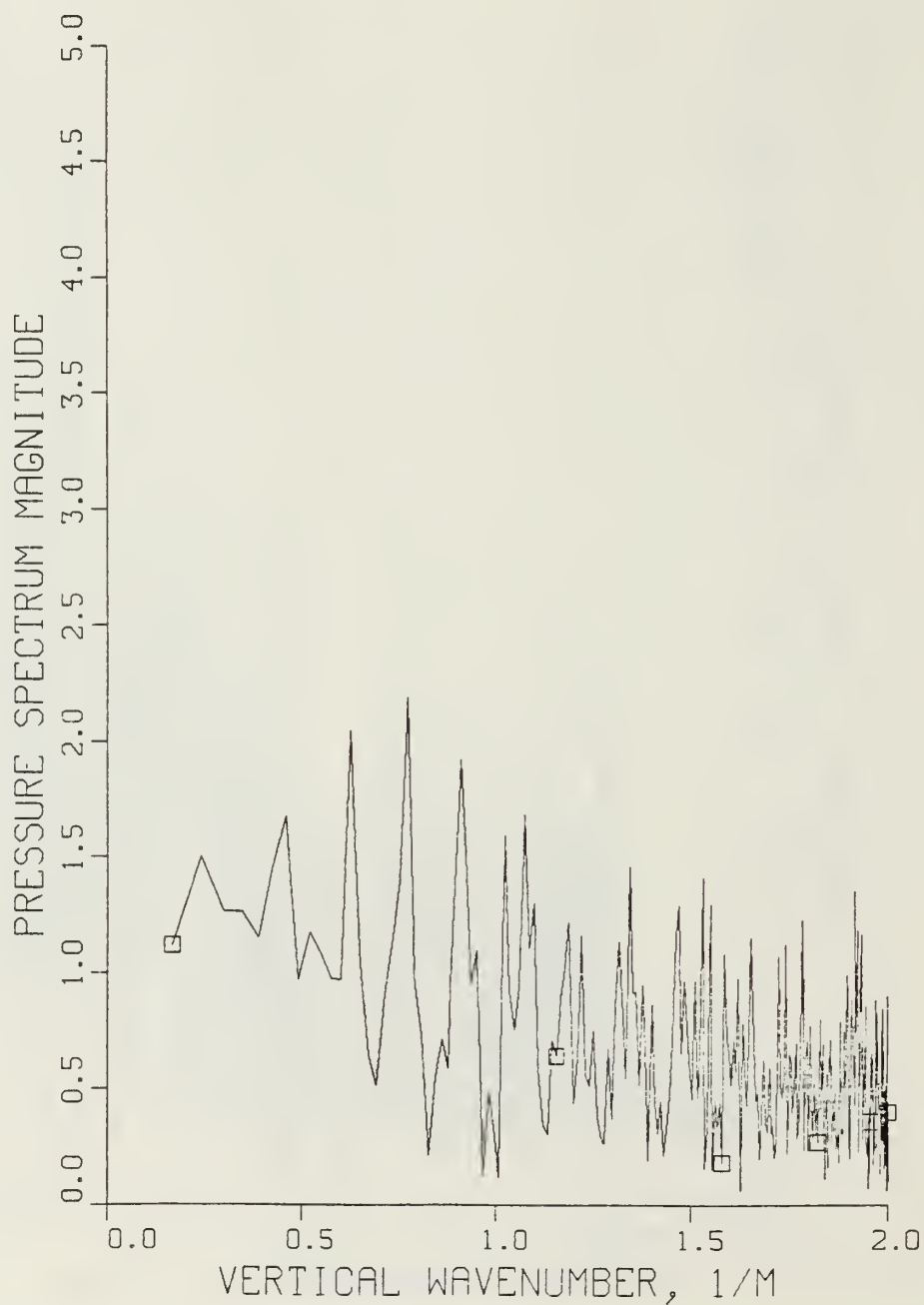
Figure 3.47   Pressure Spectrum vs. Beta

92

APPENDIX A: LLOYDS MIRROR PRESSURE FIELD SOURCE CODE

```
C***********************************************************************  TES00010
C***********************************************************************  TES00020
C     THIS PROGRAM WILL PLOT THE |P(R)| VS R CURVE STARTING AT THE ORIGIN TES00030
C     (I.E., THE SOURCE).                                                 TES00040
C                                                                         TES00050
C     THIS PROGRAM ALSO PLOTS THE SPECTRUM VS THE HORIZONTAL WAVENUMBER.  TES00060
C                       ALSO THE SPECTRUM VS THE VERTICAL WAVENUMBER.     TES00070
C                                                                         TES00080
C                                                                         TES00090
C     IT USES THE COOLEY-TUKEY FFT.                                       TES00100
C                                                                         TES00110
C***********************************************************************  TES00120
C***********************************************************************  TES00130
      DIMENSION DATA(8192),P(4096),CKM(4096),GM(4096),BE(4096),T(4096),  TES00140
     1U(4096),RNO1(4096),KNO1Z(4096),DADA(8192)                          TES00150
      DOUBLE PRECISION DSEED1,DSEED2                                      TES00160
      REAL LAMBDA                                                         TES00170
      DATA Y/'Y'/,ON/'ON'/                                               TES00180
      PIE = 4.0*DATAN(1.0)                                               TES00190
      EPS = 1.00E-6                                                       TES00200
C                                                                         TES00210
C     THE USER SELECTABLE VARIABLES ARE ENTERED                          TES00220
C                                                                         TES00230
      WRITE(6,2)                                                          TES00240
    2 FORMAT(1X,'ENTER THE SOURCE DEPTH IN METERS.')                      TES00250
      READ(5,*)ZS                                                         TES00260
      WRITE(6,4)                                                          TES00270
    4 FORMAT(1X,'ENTER THE RECEIVER DEPTH IN METERS.')                    TES00280
      READ(5,*)ZR                                                         TES00290
      WRITE(6,6)                                                          TES00300
    6 FORMAT(1X,'ENTER THE VALUE OF K, THE WAVENUMBER.')                  TES00310
      READ(5,*)AK                                                         TES00320
      WRITE(6,3)                                                          TES00330
    3 FORMAT(1X,'ENTER THE AVERAGE SURFACE WAVEHEIGHT, IN REAL METERS.')  TES00340
      READ(5,*)AICH                                                       TES00350
      WRITE(6,5)                                                          TES00360
    5 FORMAT(1X,'ENTER THE VALUE OF B (NAUGHT), BO.')                     TES00370
      READ(5,*)BO                                                         TES00380
      WRITE(6,7)                                                          TES00390
    7 FORMAT(1X,'ENTER N, THE NUMBER OF TRANSFORM POINTS.')               TES00400
      READ(5,*)IMAX                                                       TES00410
```

93

```
      IF(ZR.GE.ZS)GO TO 360
      GO TO 370
360   ZX = ZR
370   ZX = ZS
123   FORMAT(/,1X,'THE SHALLOWER DEPTH = ',F8.2)
C
      REALN = FLOAT(IMAX)
      REALM = ALOG10(REALN)/ALOG10(2.0) + 0.9
      IP2 = INT(REALM)
      JMAX = IMAX/4
      IMAX4 = IMAX/4 + 1
      KMAX = IMAX/2 + 1
      LMAX = IMAX + 3
      MMAX = IMAX + 4
      IMAX2 = IMAX * 2
      IMAX3 = IMAX2 + 1
      IMAX3 = IMAX2 + 2
      ELIMAX = FLOAT(IMAX)
      EJMAX = FLOAT(JMAX)
      IMAX3 = INT(FLIMAX/8.0)
C
      WRITE(6,8) FLIMAX,FJMAX,IMAX,IMAX8,JMAX,KMAX,LMAX,MMAX,NMAX
8     FORMAT(1X,2(2X,F7.2),7(2X,I4))
11    WRITE(6,9)
9     FORMAT(1X,'THE SELECTED PARAMETERS ARE:',/,10X,'SOURCE DEPTH IN METE
     *RS:',F8.2,/,10X,'RCVE DEPTH IN METERS:',F8.2,/,10X,'VALUE OF
     *THE WAVENUMBER IS:',F8.2,/,10X,'THE WAVEHEIGHT IS:',F8.2,/,5X,
     *'DO YOU DESIRE TO MAKE ANY CHANGES? (YES/NO)')
      READ(5,12)ANS
12    FORMAT(A1)
      IF(ANS.EC.ON)GO TO 122
      IF(ANS.NE.Y)GO TO 11
      GO TO 1
121
122   LAMBDA = 2.0 * PIE/AK
      WRITE(6,14) LAMBDA
14    FORMAT(1X,'THE WAVELENGTH IN METERS IS:',F12.,/,5X,'THE RANGE
     *INCREMENT MUST BE LESS THAN -LAMBDA/(2*PIE)- TO PREVENT ALIASING.
     *',/,10X,'ENTER THE RANGE INCREMENT.')
      READ(5,96)DR
96    DR = DR
      FMAX = RO + DR * JMAX
      FMIN = (-1.0) * FMAX/(2.0) + DR
      FAC = (-1.0) * RMAX/(2.0) * SQRT(2.0 * PIE))
15    WRITE(6,16)
16    FORMAT(1X,/,10X,'RANGE SELECTIONS ARE:',/,10X,'MINIMUM RANGE IN METERS
     *',F10.7,/,10X,'MAXIMUM RANGE IN METERS',F10.2,/,10X,'RANGE
     *INCREMENT IN METERS:',F10.7,/,10X,'FACTOR TERM IS:',F10.7,//,'RANGE
```

94

```
211   WRITE(6,211)
     3,5X,'DO YOU DESIRE TO MAKE ANY CHANGES? (YES/NO)')
      READ(5,121) GANS
      IF(GANS.EQ.ON)GO TO 211
      GO TO 15
C
212   WRITE(6,212)
10    FORMAT(//1X,'(YES/NO)')
      READ(5,121) GANS
      IF(GANS.EQ.ON)GO TO 320
      IF(GANS.NE.Y)GO TO 211
      GO TO 431
C
C************************************************************************
C*****                                                             *****
C*****      NOW WE GENERATE THE COMPLEX PRESSURE FIELD             *****
C*****                                                             *****
C************************************************************************
C
      WRITE(6,354)
354   FORMAT(4X,'I',8X,'GRE',17X,'GIM',10X,'WINDOW FACTOR',/)
320   DO 17 I=1,IMAX
      FLY = FLOAT(I)
      W = 0.5 * (1.0 + COS((FLY-1.0)*PIE/2JMAX))
C
      RSQ = SQRT(R)
      R1 = ((ZR-ZS)**2)
      R2 = ((ZR+ZS)**2)
      AINC = (Z+ZS)
      SSKAY = AICH * SIN(AINC)/LAMBDA
      SSKAY = (SSKAY**2)
      XMU = EXP(-SSKAY)
      GRE = (COS(AK*R1)/R1 - COS(AK*R2)/R2) * RSQ * FAC
      GIM = (SIN(AK*R1)/R1 - SIN(AK*R2)/R2) * RSQ * FAC
      DELTA = ...
      DATA(IMAX = ...
      DATA(IMAX = ...
      WRITE(6,100) I,GRE,GIM
100   FORMAT(2X,I5,3(3X,F10.7))
17    CONTINUE
C
C************************************************************************
C*****                                                             *****
C*****   THESE ARE THE PROGRAM ADDS A NORMALLY-DISTRIBUTED RANDOM  *****
C*****   NOISE FACTOR TO THE PRESSURE. IT CALLS UPON THE IMSL ROUTINE *
C*****   GGNML TO GENERATE THE MAGNITUDE AND PHASE RANDOM FACTORS, *****
C*****   R AND G. THIS ROUTINE SEEKS TO DUPLICATE THE GAUSSIAN DISTRIBUTION *
C*****                                                             *****
C************************************************************************
```

```
C**** DESCRIBED BY URICK ON PAGE 189 OF HIS "PRINCIPLES ...", 3RD ED.
C****
1100  WRITE(6,1110)
1110  FORMAT(/,2X,'DO YOU DESIRE TO ADD NOISE? (YES/NO)')
      READ(5,121)PANS
      IF(PANS.EQ.ON)GO TO 27
      IF(PANS.NE.Y)GO TO 1130
      GO TO 1120
C
1120  WRITE(6,1112)
1112  FORMAT(/,2X,'WHAT IS THE NOISE FACTOR? (A POSITIVE REAL NUMBER <=
     1 0.01)')
      READ(5,*)XNU
      XNU = XNU
      WRITE(6,1113)
1113  FORMAT(/,2X,'WHAT IS DSEED1?')
      READ(5,*)DSEED1
      DSEED1 = DSEED1
      WRITE(6,1116)
1116  FORMAT(/,2X,'WHAT IS DSEED2?')
      READ(5,*)DSEED2
      DSEED2 = DSEED2
      CALL GGNML(DSEED1,IMAX,R)
      CALL GGNML(DSEED2,IMAX,U)
      WRITE(6,1114)T(IMAX),U(IMAX)
1114  FORMAT(/,2X,'FINAL RANDOM NUMBERS, T AND U, ARE ',2(2X,F10.8))
C
      DO 28 I = 1,IMAX
      RNOIZ(I) = F(I) * XNU
      AINOIZ(I) = U(I) * XNU
28    CONTINUE
C
      DO 29 I = 1,IMAX
      DATA(2*I-1)= DATA(2*I-1) + RNOIZ(I)
      DATA(2*I) = DATA(2*I) + AINOIZ(I)
29    CONTINUE
C
C**** THIS PART OF THE PROGRAM ISOLATES THAT PART OF THE P(R) CURVE
C**** CORRESPONDING TO THE RANGE STARTING AT THE SOURCE AND MOVING
C**** IN A POSITIVE DIRECTION. ONE ENABLES ONE TO PLOT ONLY ONE-HALF THE |P(R)| VS R
C**** CURVE, WEIHCI IS DONE CONVENTIONALLY.
C****
27    DO 37 I = 1,JMAX
      DATA(2*I-1) = DATA(IMAX + (2*I-1))
```

```
      DADA(2*I) = DATA(IMAX + (2*I))
37    CONTINUE
C
C39   CALL EEPLOT(DADA,DE,IMAX,JMAX,RO)
C
      CALL FOUR2(DATA,IMAX,-1,1)
C
C352  WRITE(6,352)
C     FORMAT(/,5X,'I',4X,'SPEC DATA REAL',3X,'SPEC DATA IMAG',/)
C
      DO 18 I = 1,IMAX
C     WRITE(6,353)I,DATA(2*I - 1),DATA(2*I)
C18   CONTINUE
C353  FORMAT(2X,I4,2(4X,F13.7))
C
      DG = 2.0 * PIE/(ELIMAX * DK)
      WRITE(6,300)DG
300   FORMAT(/,2X,'DG = ',F12.8,/)
C
201   WRITE(6,201)
      FORMAT(/,5X,'I',6X,'CK4',10X,'G',10X,'KZ',/)
C
      DO 50 I=1,IMAX4
      FLY = FLOAI(I)
      GM(I) = FLY * DG
      IF(GM(I).GE.AK)GO TO 400
      GO TO 420
420   CONTINUE
C*************************************************************************
C*****IF GM(I) < AK, THEN BE(I) IS REAL AND REDUCES TO A FORM OF     *****
C*****THE SIN(A)/X FUNCTION, APPROXIMATELY. ACTUAL FORM IS GIVEN BELOW.****
C*************************************************************************
      BE(I) = SQRT(AK**2 - GM(I)**2) + EPS
      GE = ABS(SIN(BE(I)*ZX)*SQRT(GM(I))/BE(I))
      GO TO 450
400   CONTINUE
C*************************************************************************
C*****IF GM(I) >= AK, THEN BE(I) = SQRT OF A NEGATIVE NUMBER, AND THE *****
C*****THEORETICAL FUNCTION, P(X), REDUCES TO THE HYPERBOLIC SIN (SINH).****
C*************************************************************************
```

```
      BER = SQRT(GM(I)**2 - AK**2)
      QQ2 = EXP(-BER * (ZP - ZS)) - EXP(-BER * (ZR + ZS))
      QQ2 = ABS(QQ * SQRT(GM(I))/(2.0 * BER))
      GO TO 50
450   CONTINUE
C
      CKRE = DATA(2*I - 1)
      CKIM = DATA(2*I)
      CKM(I) = SQRT(CKRE**2 + CKIM**2)
50    CONTINUE
C
      IMAX5 = IMAX4 - 1
C
      CALL WEHPLT(IMAX5, GM, CKM, Q, AK, BE)
C
C
      CALL NTV2LT(IMAX5, CKM, Q, AK, BE)
      CALL DGNEPL
      STOP
431   END
C
      SUBROUTINE FOUR2(DATA,N,ISIGN,IFORM)
C     COOLEY-TUKEY FAST FOURIER TRANSFORM IN USASI BASIC FORTRAN.
C     MULTI-DIMENSIONAL TRANSFORM, EACH DIMENSION A POWER OF TWO.
C     COMPLEX OR REAL DATA.
C     TRANSFORM(K1,K2,...) = SUM(DATA(J1,J2,...)*EXP(ISIGN*2*PI*SQRT(-1)
C     *((J1-1)*(K1-1)/N(1)+(J2-1)*(K2-1)/N(2)+...))), SUMMED FOR ALL
C     J1 AND K1 FROM 1 TO N(1) AND K2 FROM 1 TO N(2), ETC.
C     FOR ALL SUBSCRIPTS.  N(1)*N(2)*... MUST BE A POWER OF TWO.
C     ISIGN IS +1 OR -1.
C     EACH DIMENSION MUST BE A POWER OF TWO.  ISIGN POSITIVE OR
C     NEGATIVE.  IF POSITIVE, DATA IS RETURNED TO DATA.  IFORM = 1 OR 0.
C     IF IFORM = 1, DATA IS COMPLEX.  AS INPUT, IF IFORM = 0, THEN THE
C     DATA ARE CONSIDERED TO BE REAL OR COMPLEX ARRAY.  TRANSFORM IS
C     NOT RETURNS AS COMPLEX ARRAY.  THE COMPLEX ARRAY DIMENSIONED 1 OR 0.
C     NOTE THAT IF IFORM = 0, THE COMPLEX ARRAY MUST BE
C     DIMENSIONED BY N(1) BY N(2) ... BY N(2), ENOUGH ROOM MUST BE
C     FOR ALL THE COMPLEX VALUES.  THEY ARE COMPLEX ARRAY DIMEN-
C     SIONED BY COMPLEX CONJUGA-
C     VALUES MAY BE HALVED BY SETTING IFORM/2+1.
C     THE TRANSFORM OF A REAL ARRAY (IFORM = 0) DIMENSIONED HALF COMPLEX
C     BY N(1)/2+1 EVEN BY N(1) ... IS ALSO COMPLEX.
C     RETURNED BY N(1) REAL ARRAY.  THE INPUT ARRAY IS NOT RATHER THAN
C     TO N(1) ... = LOG2(NTOT), LESS ERROR IS BUILT UP.
C     THE NAIVE NTOT*2.  FURTHERMORE, THE TRANSFORM IS SPLIT UP.
```

```
C     WRITTEN BY NORMAN BRENNER OF MIT LINCOLN LABORATORY, JANUARY 1969.
C     SEE--IEEE AUDIO TRANSACTIONS (JUNE 1967), SPECIAL ISSUE ON FFT.
      DIMENSION DATA(1), N(1)
      NDIM=1
      NTOT=1
      DO 10 IDIM=1,NDIM
10    NTOT=NTOT*N(IDIM)
      N(IFORM)=70,20,20
      DO 60 IDIM=1,NDIM
      NREM=NREM/(N(IDIM)*NFRM)
      NPREV=NTOT/(N(IDIM)*NREM)
      NCURR=NCURR/2...IFORM) 30,30,40
30    IF(IDIM-1+IFORM) 30,30,40
      NCURR=NCURR/2
      CALL BITRV(DATA,NPREV,NCURR,NREM)
40    CALL BITRV(DATA,NREEV,NCURR,NREM,ISIGN)
      IF(IDIM-1+IFORM) 50,55,60
50    CALL FIXRL(DATA,N(1),NREM,ISIGN,IFORM)
      NTOT=(NTOT/N(1))*(N(1)/2+1)
60    CONTINUE
      RETURN
      NTOT=(NTOT/N(1))*(N(1)/2+1)
      DO 100 IDIM=1,NDIM
      JDIM=1+IDIM
      IDIM=NDIM+1-IDIM
      N(IFORM)=30,80,90
80    NCURR=NCURR/2
      CALL FIXRL(DATA,N(1),NREM,ISIGN,IFORM)
      NTOT=(NTOT/(N(1)/2+1))*N(1)
      NPREV=NTOT/(N(IDIM)*NREM)
90    CALL BITRV2(DATA,NPREV,NCURR,NREM,ISIGN)
      NREM=NREM*N
100   RETURN
      END
      SUBROUTINE BITRV (DATA,NPREV,N,NREM)
C     SHUFFLE THE DATA BY BIT REVERSAL.
      DIMENSION DATA(NPREV,N,NREM)
      COMPLEX DATA
      EXCHANGE DATA(J1,J4REV,J3) WITH DATA(J1,J4,J5) FOR ALL J1 FROM 1
C     TO NPREV, J4 AND J4REV... WHICH MUST BE LOWERS OF TWO, AND
C     ALL J5. J4REV-1 IS THE BIT REVERSAL OF J4-1. E.G.
C     J4REV-1=32.... FOR J4-1=10011, J4REV-1=11001, ETC.
      DIMENSION DATA(1)
      IP0=2
```

99

```
      IP1=IP0*NPREV
      IP4=IP1*N
      IP5=IP1*NREM
      I4REV=1
      DO 30 I4=1,I4MAX,IP0
      I4REV=1+(J4REV-1)*IP1
   10 I4MAX=IP0+(J4-1)*IP1
      DO 20 I5=I4,I5MAX,IP4
      I4=I4+(J5-1)*IP1+(J5-1)*IP4
      TEMPR=DATA(I5)
      TEMPI=DATA(I5REV)
      DATA(I5)=DATA(I5REV)
      DATA(I5REV)=TEMPR
   20 DATA(I5REV+1)=TEMPI
C     ADD ONE WITH DOWNWARD CARRY TO THE HIGH ORDER BIT OF J4REV-1.
      IP2=IP4/2
   30 IF(I4REV-I4) 60,60,50
      I4REV=I4REV-IP2
   40 IP2=IP2/2
      IF(I4REV-IP2) 60,40,40
   50 I4REV=I4REV+IP2
   60 CONTINUE
      RETURN
      END
```

```
      SUBROUTINE COOL2(DATA,NPREV,N,NREM,ISIGN)
C     DISCRETE FOURIER TRANSFORM OF LENGTH N.  IN-PLACE COOLEY-TUKEY
C     ALGORITHM, DATA(NPREV,N,NREM), NORMAL ORDER, SANDE-TUKEY PHASE SHIFTS.
C     DIMENSION DATA(NPREV,N,NREM)
C     COMPLEX DATA
C        DATA(J1,J4,J5) = SUM(DATA(J1,J2,J5)*EXP(ISIGN*2*PI*I*(J4-1)*
C        (K4-1)/N)), SUMMED OVER J2 FROM 1 TO N FOR ALL J1 FROM 1 TO NPREV,
C        J4 FROM 1 TO N AND J5 FROM 1 TO NREM.
C     METHOD-- LET N=IFACT(1)*IFACT(2)*ETC.  THE FACTORING VALUES
C     ARE TAKEN FROM THE ARRAY IFACT.  DEPENDS ON WHETHER N IS
C     A POWER OF FOUR.  DEFINE IFACT=4, OR 3, THE NEXT FACTOR THEN--
C     IPREV MUST BE DEFINED AND LIKED, IFACT*IPREV, NREM
C     COMPLEX DATA(J1,J2,J3,J4,J5) = SUM(DATA(J1,J2,J3,J4,J5)*EXP(ISIGN*2*PI*I*
C        (IFACT*IPREV),(J4-1)*J2REV/(IFACT*IPREV)), SUMMED OVER J3 = 1
C        (K3-1 IFACT)  TO NREM, J2 FROM 1 TO NPREV, J2 FROM 1 TO IPREV, K3 FROM
```

TES03850
TES03860
TES03870
TES03880
TES03890
TES03900
TES03910
TES03920
TES03930
TES03940
TES03950
TES03960
TES03970
TES03980
TES03990
TES04000
TES04010
TES04020
TES04030
TES04040
TES04050
TES04060
TES04070
TES04080
TES04090
TES04100
TES04110
TES04120
TES04130
TES04140
TES04150
TES04160
TES04170
TES04180
TES04190
TES04200
TES04210
TES04220
TES04230
TES04240
TES04250
TES04260
TES04270
TES04280
TES04290
TES04300
TES04310
TES04320

```fortran
C  1 TO IFACT, J4 FROM 1 TO IREM AND J5 FROM 1 TO NREM.  THIS IS
C  A PHASE-SHIFTED DISCRETE FOURIER TRANSFORM OF LENGTH IFACT.  IFACT
C  FACTORING BY FOURS SAVES ABOUT TWENTY FIVE PERCENT OVER FACTOR-
C  ING BY TWOS.  DATA MUST BE BIT-REVERSED INITIALLY.  THIS SUBROUTINE-
C  NOTATION SO LONG NOT NECESSARY TO REWRITE THIS SUBROUTINE INTO COMPLEX
C  IMAGINARY PARTS IN ADJACENT STORAGE LOCATIONS.  IT MUST ALSO
C  STORE ARRAYS WITH THE FIRST SUBSCRIPT INCREASING FASTEST.
      DIMENSION DATA(1)
      TWOPI=6.283185307/2*FLOAT(ISIGN)
      IP0=2
      IP1=IP0*NPREV
      IP4=IP1*N
      IP5=IP4*NREM
      IP2=IP1*IPROD
      IP3=IP1*IPROD
      NPART=NPART/4
      NPART=(NPART-2)*0,30,20
   10 NPART=NPART/4
   20 IF (NPART-2) *0,30,20
      GO TO 10
C     A FOURIER TRANSFORM OF LENGTH TWO
   30 IF (IP2-IP4) 40,160,160
   40 IP3=IP2*2*IFACT
      DO 50 I1=1,IP1,IP0
      DO 50 I5=I1,IP5,IP3
      DO 50 I0=I5,I20,IP0
      I1=I0+(J4-1)*IP3+(J5-1)*IP4
C
   50 I1=I0+(J1-1)*IP0+(J2-1)*IP1+(J3-1)*IP2+(J4-1)*IP3+(J5-1)*IP4
      I3A=I5
      I3B=I3A+IP2
      TEMPR=DATA(I3B)
      TEMPI=DATA(I3B+1)
      DATA(I3B)=DATA(I3A)-TEMPR
      DATA(I3B+1)=DATA(I3A+1)-TEMPI
      DATA(I3A)=DATA(I3A)+TEMPR
      DATA(I3A+1)=DATA(I3A+1)+TEMPI
C     A FOURIER TRANSFORM OF LENGTH FOUR  (FROM EII REVERSED ORDER)
   60 IF (IP2-IP4) 70,160,160
   70 IP3=IP2*4*IFACT
C     COMPUTE THETA, WR AND WI IN DOUBLE PRECISION, IF AVAILABLE.
      THETA=TWOPI/FLOAT(IP2/IP1)
      SINTH=SIN(THETA/2.)*SINTH
      WSTPI=-2.*SINTH
      WR=1.
```

```
                                                                          TES04330
                                                                          TES04340
                                                                          TES04350
                                                                          TES04360
                                                                          TES04370
                                                                          TES04380
                                                                          TES04390
                                                                          TES04400
                                                                          TES04410
                                                                          TES04420
                                                                          TES04430
                                                                          TES04440
                                                                          TES04450
                                                                          TES04460
                                                                          TES04470
                                                                          TES04480
                                                                          TES04490
                                                                          TES04500
                                                                          TES04510
                                                                          TES04520
                                                                          TES04530
                                                                          TES04540
                                                                          TES04550
                                                                          TES04560
                                                                          TES04570
                                                                          TES04580
                                                                          TES04590
                                                                          TES04600
                                                                          TES04610
                                                                          TES04620
                                                                          TES04630
                                                                          TES04640
                                                                          TES04650
                                                                          TES04660
                                                                          TES04670
                                                                          TES04680
                                                                          TES04690
                                                                          TES04700
                                                                          TES04710
                                                                          TES04720
                                                                          TES04730
                                                                          TES04740
                                                                          TES04750
                                                                          TES04760
                                                                          TES04770
                                                                          TES04780
                                                                          TES04790
                                                                          TES04800

      WI=0.
   80 DO 15 I2=1,IP2,IP1
      IE=(I2-1)*IP1
      W2R=(90.,90.,30)
      W2I=W2R*WR-W2I*WI
   90 W3R=2.*W2R*WR-WR
      W3I=2.*W2R*WI+WI
      I1MAX=I1+IP0-1
      DO 14 I1=I2,I1MAX,IP0
      DO 14 I0=I1,I1,IP0
      DO 15 I5=I1,I1,IP5 IP3+(J2-1)*IP1+(J4-1)*IP3+(J5-1)*IP4
      I3A=I5+IP3A+IP2
      I3B=I3C+IP2
      I3C=I3C+IP2
      I3D=I3C+IP2             *IP0+(J2-1)*IP1+(J3-1)*IP2+(J4-1)*IP3+(J5-1)*IP4
C                            *IP5+(J2-1)*IP1+(J4-1)*IP3+(J5-1)*IP4
C                            *IP1+(J4-1)*IP3+(J5-1)*IP4
C                             +(J2-1)*IP1
C     APPLY THE PHASE SHIFT FACTORS
  100 TEMPR=DATA(I3B)-W2R*DATA(I3B)-W2I*DATA(I3B+1)
      DATA(I3B)=W2R*DATA(I3B+1)+W2I*TEMPR
      TEMPF=DATA(I3C)-W1R*DATA(I3C)-W1I*DATA(I3C+1)
      DATA(I3C)=W1R*DATA(I3C+1)+W1I*TEMPR
      TEMPR=DATA(I3D)-W3R*DATA(I3D)-W3I*DATA(I3D+1)
      DATA(I3D)=W3R*DATA(I3D+1)+W3I*TEMPR
  110 TOR=DATA(I3A)+DATA(I3B+1)
      TOI=DATA(I3A+1)+DATA(I3B+1)
      T1R=DATA(I3A)-DATA(I3B)
      T1I=DATA(I3A+1)-DATA(I3B+1)
      T2R=DATA(I3C)+DATA(I3D)
      T2I=DATA(I3C+1)+DATA(I3D+1)
      T3R=DATA(I3C)-DATA(I3D)
      T3I=DATA(I3C+1)-DATA(I3D+1)
      DATA(I3A)=TOR+T2R
      DATA(I3A+1)=TOI+T2I
      DATA(I3C)=TOR-T2R
      DATA(I3C+1)=TOI-T2I
      IF(ISIGN)120,120,130
  120 T3R=-T3R
      T3I=-T3I
  130 DATA(I3B)=T1R-T3I
      DATA(I3B+1)=T1I+T3R
      DATA(I3D)=T1R+T3I
  140 DATA(I3D+1)=T1I-T3R
```

102

TES04810
TES04820
TES04830
TES04840
TES04850
TES04860
TES04870
TES04880
TES04890
TES04900
TES04910
TES04920
TES04930
TES04940
TES04950
TES04960
TES04970
TES04980
TES04990
TES05000
TES05010
TES05020
TES05030
TES05040
TES05050
TES05060
TES05070
TES05080
TES05090
TES05100
TES05110
TES05120
TES05130
TES05140
TES05150
TES05160
TES05170
TES05180
TES05190
TES05200
TES05210
TES05220
TES05230
TES05240
TES05250
TES05260
TES05270
TES05280

```fortran
      TEMPR=WR
      WR=WSTPR*TEMPR-WSTPI*WI+TEMPR
      WI=WSTPR*WI+WSTPI*TEMPR+WI
      IE2=IP3
      GO TO 60
150   ...
160   RETURN
      END
      SUBROUTINE FIXRL (DATA,N,NREM,ISIGN,IFORM)
C     CONVERT THE TRANSFORM OF A DOUBLED-UP REAL ARRAY,
C     CONSIDERED COMPLEX, INTO ITS TRUE TRANSFORM. SUPPLY ONLY THE
C     FIRST HALF OF THE COMPLEX TRANSFORM, AS THE SECOND HALF HAS
C     CONJUGATE SYMMETRY. FOR IFORM = -1, CONVERT THE FIRST HALF
C     OF THE TRUE TRANSFORM INTO THE TRANSFORM OF A DOUBLED-UP REAL
C     ARRAY. COMPLEX NOTATION AND SUBSCRIPTS STARTING AT ZERO, THE
C     USING COMPLEX NOTATION
      DIMENSION DATA(N,NREM)
      ZSTP = EXP(ISIGN*2*PI*I/N)
      DO 10 I2=0,12,NREM
      DATA(0,I2) = CONJ(DATA(0,I2))*(1+I)
      DO 10 I1=1,N/4
      I1CNJ = 1+(2*IFORM+1)*I1*ZSTP**I1)/2
      DIF = DATA(N/2-I1,I2) -CONJ(DATA(I1CNJ,I2))
      TEMP = Z*DIF
      DATA(I1,I2) = (DATA(I1,I2)-TEMP)*(1-IFORM)
      DATA(I1CNJ,I2) = (DATA(I1CNJ,I2)+CONJ(TEMP))*(1-IFORM)
C     A SIMPLE CONJUGATION FOR THE CALCULATION FOR THAT VALUE COLLAPSES INTO
C     DIMENSION DATA(I1,I2).
      DIMENSION DATA(1)
      TWOPI=6.2831853071795*FLOAT(ISIGN)
      IP0=2
      IP1=IP0*(N/2)
      IP2=IP1*NREM
      IP3=IP2*2
C     PACK THE REAL INPUT VALUES (TWO PER COLUMN)
10    DATA(J1)=DATA(J1)
      I1=-1
      J1=J1+1
      DO 20 I2=1,NREM,IP2,I1
      DO 20 I1=I2,I2+IP1-IP2,IP1
      DATA(I1+1)=DATA(J1)
20    J1=J1+2
      ...
30    I1MAX=I2+IP1-IP0
```
```

103

```
      DO 40 I1=I1MIN,I1MAX,IP0                                       TES05290
      DATA(I1+1)=DATA(J1)                                            TES05300
      DATA(J1+IP0)=DATA(J1)                                          TES05310
   40 J1=J1+IP0                                                      TES05320
      DO 80 I2=1,IP2,IP1                                             TES05330
      TEMPR=DATA(I12)                                                TES05340
      DATA(I12)=DATA(I12)+DATA(I2+1)                                 TES05350
      DATA(I2+1)=TEMPR-DATA(I2+1)                                    TES05360
   80 THETA=TWOPI/FLOAT(N)                                           TES05370
      SINTH=SIN(THETA/2.)                                            TES05380
      ZSTPR=-2.*SINTH*SINTH                                          TES05390
      ZSTPI=SIN(THETA)                                               TES05400
   90 ZR=1.+ZSTPR                                                    TES05410
      ZI=ZSTPI                                                       TES05420
      IF(IFORM)100,110,110                                           TES05430
  100 I1MAX=IP0+1                                                    TES05440
  110 I1MIN=IE0+1                                                    TES05450
      I12=I12*IP1                                                    TES05460
      I2CN=N/4                                                       TES05470
      IF(ISIGN*I2+I12)120,120,130                                    TES05480
  120 I12CNJ=N/2+I2                                                  TES05490
      IF(IFORM)150,130,130                                           TES05500
  130 DIFR=DATA(I12)+DATA(I12CNJ)                                    TES05510
      DIFI=DATA(I12+1)+DATA(I12CNJ+1)                                TES05520
      TEMPR=DIFR+ZR                                                  TES05530
      TEMPI=DIFI+ZI                                                  TES05540
      DATA(I12)=DATA(I12)-TEMPI                                      TES05550
      DATA(I12+1)=DATA(I12+1)-TEMPR                                  TES05560
      DATA(I12CNJ)=DATA(I12CNJ)+TEMPI                                TES05570
      DATA(I12CNJ+1)=DATA(I12CNJ+1)-TEMPR                            TES05580
  150 DATA(I12)=DATA(I12)+DATA(I12CNJ)                               TES05590
      DATA(I12+1)=DATA(I12+1)+DATA(I12CNJ+1)                         TES05600
  160 TEMPR=ZR                                                       TES05610
      ZR=ZR*ZSTPR-ZI*ZSTPI+ZR                                        TES05620
  170 ZI=ZI*ZSTPR+TEMPR*ZSTPI+ZI                                     TES05630
      RECURSION SAVES TIME AT A SLIGHT LOSS IN ACCURACY.  IF AVAILABLE,  TES05640
      USE DOUBLE PRECISION TO COMPUTE ZR AND ZI.                    TES05650
```

104

```
C200   IF (IFORM) 270,210,210
C      UNPACK THE REAL TRANSFORM VALUES (TWO PER COLUMN)
 210   I2=IP2+1
       I1=I2
       J1=IP0*(N/2+1)*NREM+1
       GO TO 250
 220   DATA(J1)=DATA(I1)
       DATA(J1+1)=DATA(I1+1)
       I1=I1-IP0
       J1=J1-IP0
 230   IF (I2-I1) 220,240,240
 240   DATA(J1)=DATA(I1)
       DATA(J1+1)=0.
       I2=I2-IP1
 250   J1=J1-IP0
       DATA(J1+1)=DATA(I2+1)
       I1=I1-IE1
       DATA(J1+1)=0.
       I1=I1-IE0
       J1=J1-IE0
 260   IF (I2-I1) 260,260,230
       DATA(2)=0.
 270   RETURN
       END

       SUBROUTINE PRPLOT (DATA,DR,IMAX,JMAX,RO)
C  **********************************************************
C  *** THIS SUBROUTINE PLOTS THE IP(6,I) VS R CURVE, STARTING AT THE ***
C  *** SOURCE AND MOVING IN A POSITIVE DIRECTION OF RANGE. ***
C  **********************************************************
       DIMENSION DATA(4096),PLOD(2048),R(2048)
       IMARK = INT(IMAX/5.) + 1
       KMAX = JMAX - 1
       JMAX2 = JMAX - 2
       DO 30 I=1,JMAX
       FLY = FLOAT(I)
       R(I) = RO + FLY * DR
       R(JMAX-I) = -R(KMAX+I)
 30    CONTINUE
       RMIN = RO
       RMAX = R(JMAX)
       WRITE(6,100)
```

105

```fortran
100   FORMAT(/,3X,'I',6X,'RANGE',7X,'REALP',7X,'IMAGP',5X,'MODULUS OF P'
     1,/)
C
      DO 10 I = 1,JMAX
      PMOD(I) = SQRT((DATA(2*I-1))**2 + (DATA(2*I))**2)
      WRITE(6,200) I,F(I),DATA(2*I-1),DATA(2*I),PMOD(I)
1000  CONTINUE
C200  FORMAT(2X,I4,2X,F10.2,3(2X,F10.7))
C
      PMAX = -1.0
      DO 20 I = 1,JMAX
      IF(PMOD(I).GE.PMAX)PMAX = PMOD(I)
20    CONTINUE
C
      CALL COMPRS
C     CALL AREA2D(4.0,6.0)
C     CALL XNAME('RANGE(M)$',100)
C     CALL YNAME('MAGNITUDE OF PRESSURE, P(R)$',100)
C     CALL LINESP(0.5)
C     CALL HEADIN('MAGNITUDE OF PRESSURE AS A FN OF RANGE $',100,1.0,1)
C     CALL NOCHEK
C     CALL GRAF(RMIN,'SCALE',RMAX,0.0,'SCALE',PMAX)
C     CALL CURVE(R,PMOD,JMAX,IMARK)
C     CALL ENDPL(1)
      RETURN
      END
C
C*****************************************************************
C*****                                                       *****
C*****  THIS SUBROUTINE PLOTS THE ACOUSTIC PRESSURE SPECTRUM AS A FUNCTION
C*****  OF THE HORIZONTAL WAVENUMBER                         *****
C*****                                                       *****
C*****************************************************************
C
      SUBROUTINE WHELI(IMAX,G',CKM,Q,AK,BE)
C
      DIMENSION GM(4096),CKM(4096),Q(4096),BE(4096)
C
      IMARK = INT(IMAX/5.) + 1
      GMIN = GM(1)
      GMAX = -1.0
      PMAX = -1.0
      QMAX = -1.0
      DO 10 I = 1,IMAX
      IF(CKM(I).GE.PMAX)PMAX = CKM(I)
10    CONTINUE
C
      DO 15 I = 1,IMAX
```

```
      IF(Q(I).GT.QMAX) QMAX = Q(I)
15    CONTINUE
C
      IF(PMAX.GF.QMAX) SMAX = PMAX
      SMAX = QMAX
C **************************************************************
C **** GMAX IS THE MAXIMUM VALUE KH CAN TAKE ON BASED ON THE EQUATION
C ****     ((DELTA R)) = (2 * PI/IMAX)
C ****
C **** GMAX IS THE MAXIMUM VALUE KH CAN TAKE ON AND STILL PRODUCE "REAL"
C **** THEORETICAL Q AND ETA VALUES. KZ < SQRT(AK**2 + KH**2) => Q REAL.
C **************************************************************
C
C **** SCALE THE HORIZONTAL AXIS IN KH (GM)
C **************************************************************
      CALL COMPRS
      CALL AREA2D(4.0,6.0)
      CALL XNAME('HORIZONTAL WAVENUMBER 1/M$',100)
      CALL YNAME('PRESSURE SPECTRUM MAGNITUDE$',100)
      CALL LINESP(0.5)
      CALL HEADIN('PRESSURE SPECTRUM VS KH$',100,1.0,1)
      CALL NOCHEK
      CALL GRAF(GMIN,'SCALE',GMAX,0.0,'SCALE',SMAX)
      CALL CURVE(GM,CKM,IMAX,IMARK)
      CALL DOT
      CALL CURVE(GM,Q,IMAX,IMARK)
      CALL RESET('DOT')
      CALL ENDPL(2)
      RETURN
      END
C
      SUBROUTINE KTVPLI(IMAX,CKM,Q,AK,BE)
C **************************************************************
C **** THIS SUBROUTINE PLOTS THE PRESSURE SPECTRUM AS A FUNCTION OF THE
C **** VERTICAL WAVENUMBER (BE).
C **************************************************************
      DIMENSION CKM(4096),Q(4096),AK(4096),BE(4096)
      IMARK = INT(IMAX/5.) + 1
      GMAX = BE(1)
      GMIN = BE(IMAX)
      PMAX = -1.0
      QMAX = -1.0
```

107

BIBLIOGRAPHY

Bergland, G. D., "A Guided Tour of the Fast Fourier Transform," _IEEE Spectrum_, v.6, July 1969.

Blackman, R. B. and Tukey, J. W., _The Measurement of Power Spectra_, Dover Publications, Inc., 1958.

Brigham, E. O., _The Fast Fourier Transform_, Prentice-Hall, Inc., 1974.

DiNapoli, F. R. and Deavenport, R. L., "Numerical Models for Underwater Acoustic Propagation," _Ocean Acoustics_, v. 1, Springer-Verlag, New York, NY, 1979.

DiNapoli, F. R. and Deavenport, R. L., "Theoretical and Numerical Green's Function Field Solution in a Plane Multilayered Media," _Journal of the Acoustic Society of America_, v. 67(1), January 1980.

International Series of Monographs on Electronics and Instrumentation, v.9, Pergamon Press, Inc., 1960.

Naval Surface Weapons Center Report 75-18, _A Statistical Model for the Fluctuation of Sound Transmission in the Sea_, Urick, R. J., 11 February 1975.

Naval Underwater Systems Center Technical Memorandum 781054, _A Simplified Derivation of a Quadrature Subsampling Technique_, Lackoff, M. R., 14 March 1978.

Stanton, T. K. and Beyer, R. T., "The Interaction of Sound with Noise in Water," _Journal of the Acoustic Society of America_, v.64(6), December 1978.

Thomas, G. B. and Finney, R. L., _Calculus and Analytic Geometry_, 5th ed., Addison-Wesley Publishing Company, 1979.

Urick, R.J., "Models for the Amplitude Fluctuations of Narrow-Band Signals and Noise in the Sea," _Journal of the Acoustic Society of America_, v. 64(6), December 1978.

LIST OF REFERENCES

1. Lauer, R. B., Signal Transmission in the Wavenumber Domain, Technical Memorandum, Naval Underwater Systems Center, New London Laboratory, New London, CT, 5 June 1979.

2. Naval Underwater Systems Center Report 4103, Fast Field Program for Multilayered Media, by F. R. DiNapoli, 26 August 1977.

3. Stamey, B. B., Preliminary Investigation of the Environmental Sensitivity of Acoustic Signal Transmission in the Wavenumber Domain with Respect to Source Depth Determination, Masters Thesis, Naval Postgraduate School, Monterey, CA, 1982.

4. Blanchard, J., A Comparison of Two Acoustic Parabolic Equation Transmission Loss Models for Compatibility with the Wavenumber Technique in the Determination of Source Depth, Masters Thesis, Naval Postgraduate School, Monterey, CA, 1984.

5. Kinsler, L., and others, Fundamentals of Acoustics, 3rd ed., John Wiley and Sons, 1982.

6. Urick, R. J., Principles of Underwater Sound, 3rd ed., Mcgraw-Hill, 1983.

7. Officer, C. B., Introduction to the Theory of Sound Transmission, McGraw-Hill, 1958.

8. Coppens,A. B., Mathematical Derivation of the Acoustic Pressure Spectrum of the Lloyds' Mirror, Naval Postgraduate School, Monterey, CA, January 1985.

9. IMSL Library Reference Manual, 9th ed., v. 2, IMSL, 1982

10. Gabrielson, T., Mathematical Derivation of the Acoustic Pressure Spectrum for the Lloyds' Mirror, Naval Postgraduate School, Monterey, CA, February 1985.

INITIAL DISTRIBUTION LIST

		No.	Copies
1.	Defense Technical Information Center Cameron Station Alexander, VA 22314		2
2.	Library, Code 0142 Naval Postgraduate School Monterey, CA 93943		2
3.	Chairman (Code 55Fo) ASW Academic Group Naval Postgraduate School Monterey, CA 93943		1
4.	Prof. A. B. Coppens (Code 61Cz) Department of Physics Naval Postgraduate School Monterey, CA 93943		4
5.	Prof. C. R. Dunlap (Code 68Du) Department of Oceanography Naval Postgraduate School Monterey, CA 93943		3
6.	Prof. Suk Wang Yoon (Code 61Yo) Department of Physics Naval Postgraduate School Monterey, CA 93943		3
7.	Prof. T. Gabrielson (Code 61Gt) Department of Physics Naval Postgraduate School Monterey, CA 93943		1
8.	LCDR P. B. King 425 Pine Shadows Drive Slidell, LA 70458		3
9.	Commanding Officer Naval Ocean Research and Development Activity NSTL, MS 39522		1
10.	Commanding Officer Naval Ocean Research and Development Activity (ATTN: Code 223) NSTL, MS 39522		1
11.	Office of Naval Research ATTN: Mr. R. B. Lauer Naval Ocean Research and Development Activity 800 N. Quincy Street Arlington, VA 22217		1
12.	Commanding Officer Naval Eastern Oceanography Center ATTN: LCDR J. Blanchard McAdie Bldg. (U-117) Naval Air Station Norfolk, VA 23511		1

13. LCDR B. Stamey   1
     5508 Buskirk Street
     North Charleston, SC   29406

14. Ms Catherine Smith   2
     P. O. Box 58
     Carmel Valley, CA   93924